Selective Depression of Hexagonal Pyrrhotite from Pentlandite Using Starch

by

Caroline da Costa Gonçalves

A thesis submitted in partial fulfillment of the requirements for the degree of

Master of Science

in

Chemical Engineering

Department of Chemical and Materials Engineering

University of Alberta

Abstract

Pentlandite is very important to the mining industry since it is the main source of metallic nickel. However, its separation from hexagonal pyrrhotite is a challenge for processing engineers due to the similar floatabilities of these sulfide minerals. An inefficient separation of these minerals generates serious environmental issues caused by the emissions of sulfur oxide gases during the pyrometallurgy of final concentrates. Although successful, the current depressant used, diethylenetriamine (DETA), is also harmful to the environment when disposed. Due to stringent environmental policies being implemented, the mining industry is under the obligation of researching/developing alternative reagents which are non-toxic and biodegradable. Therefore, new flotation strategies must consider the use of reagents such as polysaccharides. Three non-toxic starch depressants for hexagonal pyrrhotite were used in this study. They include a paste starch with higher molecular weight distribution, a paste starch with lower molecular weight distribution, and a crosslinked starch formed using the paste starch with lower molecular weight distribution and copper ions. We hypothesize that the presence of crosslinking agents such as copper would provide a "driving" effect towards the main gangue mineral. The performance of depressants was investigated in single and binary mineral systems. For single minerals, comparing paste starches, the higher molecular weight paste starch was more detrimental to the recovery of pentlandite and hexagonal pyrrhotite than the lower molecular weight paste starch. In addition, the crosslinked starch further reduced the recoveries of both minerals. A better result for the binary mineral systems considering Ni recovery and Ni grade was achieved by using $9.66x10^{-6}$ M of PIBX (equivalent to 240 g/t) and 5 mg/L of starch depressants (equivalent to 660 g/t). Whereas the lower molecular weight paste starch almost did not affect Ni recovery (91.2%) comparing with the collector baseline (92.5%), the higher molecular weight paste starch and the crosslinked starch had a Fe recovery no

greater than 31.0%. The choice of the best starch depressant showed to be complex since pentlandite and hexagonal pyrrhotite were able to chemically interact with the starch depressants as verified via XPS. The hydroxyl groups present on the α-D-glucose units of starch bound with the metal hydroxylate species. Moreover, the crosslinked starch also interacts with the mineral surfaces by electrostatic attraction due to the presence of weakly electronegative copper center. Kinetics and equilibrium adsorption tests allowed a more direct comparison of the effect of the starch depressants, regarding the mechanism of depression. It has been proven the importance of a balance of hydrophobic/hydrophilic species on both mineral surfaces. This was further as confirmed by contact angle measurements (Washburn method), QCM-D, and AFM tests. For the paste starches, it has been proposed that the mechanism of depression is related to the hydration levels of the adsorbed depressant layer. The amount of water molecules held by the polysaccharide structure is directly related the packing density (conformation). Furthermore, the latter is a function of the starch molecular weight, showing the importance of this parameter for mineral depression. For the crosslinked starch, however, the distribution of depressants across both mineral surfaces, given in terms of surface coverage, is the most relevant parameter dictating its depressing effect. The findings of this research will contribute with the advancement of topics related to the use of polysaccharides as depressants for sulfide minerals. The utilisation of non-toxic depressants can benefit the industry regarding the mitigation of safety and environmental problems.

Acknowledgement

First, I would like to express my gratitude to my supervisor Dr. Qingxia Liu for the opportunity of being part of the nickel group at the University of Alberta. He trusted in my work, supported, and guided me throughout my master's degree. This will never be forgotten! I extend my acknowledgment to Laurie Kachmaryk for her assistance and patience, and to the other members who are/were part of the nickel group, especially Dr. Jing Liu, Jonathan Malainey, Han Wang, Jean Han, and Chao Qi. Their friendship was essential to complete this journey.

I am also grateful for all lab support received from Jim Skwarok, Ni Yang, Shiraz Merali, and nanoFAB staff members especially Peng Li, Nancy Zhang, and Shihong Xu. I would like to give a special acknowledgment to Mark Labbe from the Earth and Atmospheric Science Department; Gareth Lambkin from the Chemistry Department; Dr. Garima Chauhan for her unmeasurable aid with all ICP-OES analysis; Mohammad Taghi Amiri for his availability in helping me with the McCrone mill, and Dr. Tom Etsell for authorizing its use; Daniel Dixon for the GPC analysis and Dr. Joao Soares for authorizing it; Monir Khan for training me with the Autosorb instrument; Bailin Xiang for the QCM-D training; Liyuan Feng for the AFM images; Dr. Hongbo Zeng for always authorizing me to use his lab facilities; and Dr. Rogerio Manica for his insightful contributions to the proofreading and editing parts of this thesis.

An acknowledgement to XPS - Expert Process Solutions and the National Sciences and Engineering Research Council of Canada (NSERC) for their financial support. I also extend an acknowledgment to Dominic Fragomeni, Dr. Gregg Hill, Mika Muinonen, Liz Whiteman, and Tony Deng from XPS for their valuable suggestions. I am tankful to Dr. Manqiu Xu and Dr. Zongfu Dai from Vale for proving the pentlandite sample.

I am also grateful for all support and friendship received since the beginning of my journey in the mineral processing field from Dr. Paulo Fernando Almeida Braga, Dr. Daniela Gomes Horta, Dr. Silvia Cristina Alves Franca, Tio, Amanda Soares de Freitas, Bruna Trampus, Samantha Grisol, and Guilherme Moreira. A special thank you to Dr. Paul Bédard at the Université du Québec a Chicoutimi who supported my return to Canada.

I must say that I am very grateful for meeting my fiancé Aaron during this time. His immense heart and kindness held me strong and optimistic every single day. His love, patience, and support are priceless. I cannot thank you enough!

Finally, I do not have enough words to express my gratitude to my family for their unconditional love and continuous encouragement. Mãe, Paizinho e Gabi, vocês são a minha vida! Thank you for trusting me, sacrificing, understanding, and staying strong for me. Our physical distance is big but our love makes it insignificant. To you three, I dedicate this work.

Table of Contents

List of Tables

List of Figures

List of Abbreviations

MW – molecular weight;

LP – lower MW paste starch;

LC – lower MW crosslinked starch;

PP – higher MW paste starch;

PC – higher MW crosslinked starch.

Chapter 1 Introduction

Although 60% of the world's nickel resources are concentrated in lateritic deposits (1), pentlandite [$(Fe,Ni)_9S_8$] is still the primary source of nickel (2). This valuable mineral is found in magmatic deposits with enormous amounts of pyrrhotite ($Fe_{(1-x)}S$, $0 < x \leq 0.125$), a gangue mineral. Their separation via froth flotation aims to reduce the emissions of sulfur oxide gas (SO_x) during the metallurgical processing of nickel concentrates. The association of hexagonal pyrrhotite (Fe_9S_{10} - 5C), one of the two polymorphic structures of pyrrhotite, and pentlandite becomes a challenge for processing engineers due to their similar floatabilities. To improve this separation, polyamines such as diethylenetriamine (DETA) and combinations with sulfur-bearing regents have been successfully used for over 25 years as pyrrhotite depressants (3–8). Nevertheless, the waste of these reagents consists of an environmental problem (9). The recent adoption of stringent environmental policies requires that the mining industry performs research to develop eco-friendly reagents, hence polysaccharides-based depressants can provide a greener alternative to the conventionally used toxic reagents.

Polysaccharides are usually applied as depressants for naturally hydrophobic minerals such as talc (10) and graphite (11). A limited number of studies using polysaccharides as depressants for complex sulfide minerals have been reported (12–16), and to the best of my knowledge, a study related to the differential separation of high hexagonal pyrrhotite-pentlandite ratios using starch still remains absent. The chemical complexity of starch and its mechanism of adsorption on mineral surfaces may be the limiting factors to its application. The control of starch gelatinization, for instance, will influence starch properties and functions, and impact its performance as a depressant (17,18), e.g. short chains starches are used as depressants, whereas the long chains ones as flocculants (19).

Generally, polysaccharides depressants act to prevent collector adsorption on the mineral surface by occupying adsorption sites and creating a hydrophilic layer on the mineral surface (20). Mechanisms of starch adsorption on mineral surfaces are still in debate, even though extensive studies can be found regarding the adsorption of starch on the surface of hematite (21–23), for instance. According to the literature (24–26), the adsorption in sulfide mineral surfaces seems to include polysaccharide-metal hydroxide interaction. More specifically, some authors also

suggested chemical complexation between polysaccharides and metal ions based on co-precipitation tests (27).

The conformational and chemical characteristics of polysaccharides highly affect the floatabilities of minerals (28). Attempts to use a modified polysaccharide may show an improvement in selectivity towards a gangue mineral. However, the polysaccharide modification must consider factors such as substituted groups, additives, impurities, and the molecular weight (MW) distribution. Impurities are usually present in insufficient amounts to be considered as a major contribution to the depressant behavior (29). On the other hand, non-reacted hydroxyl groups in a polysaccharide with high (or noncontrolled) molecular weight distribution might hinder the interactions between the mineral surface and substituted groups (29). Therefore, narrowing molecular weight distributions can contribute to an enhancement in selectivity. More recently, Yue and Wu (30) produced a series of caustic gelatinized starch complexed with different metal ions, called metallic starch, for depressing hematite ore. The authors found that colloidal particles were formed, and were responsible for improving adsorption on the surface of hematite due to a stronger electrostatic interaction with the mineral surface as well as hydrogen bonding and chemisorption. The metal ions added to the starch solution acted as a crosslinking agent, reacting with the starch hydroxyl groups and bridging its macromolecules (31,32).

In this context, the main objective of this study is to use a series of non-toxic and biodegradable starches to depress hexagonal pyrrhotite, improving the separability of this gangue mineral from pentlandite. Three gelatinized starch depressants were used, including two paste starches free of metal ions and a crosslinked starch with copper ions. The mixture of pure hexagonal pyrrhotite-pentlandite intends to mimic a target ore known by its moderate to high pyrrhotite-pentlandite ratio, similar to that found in the Sudbury deposit, Ontario, Canada.

The following questions are the basis for this study:

- Can paste starch/crosslinked starch be selectively adsorbed on the surface of hexagonal pyrrhotite?
- How does the molecular weight distribution of a starch depressant affect the floatabilities of hexagonal pyrrhotite and pentlandite?
- How additives such as copper ions can impact the interaction of starch on the surfaces of hexagonal pyrrhotite and pentlandite?

I hypothesized that the metal ions added to the gelatinized starch would have a role as "drivers" towards the main gangue mineral surface. The idea that a crosslinked starch with metal ions could work as a selective depressant is based on the difference of surface reactivity between pyrrhotite and pentlandite when in a mixed mineral pulp. Due to galvanic interactions, the transfer of electrons between those minerals "catalyzes" direct chemisorption of metal ions. Additionally, the control of the molecular weight distribution was used to increase the depressant selectivity.

Additional objectives are:

1) To synthesize a crosslinked starch depressant (s);
2) To understand the role of copper ions added to the starch structure;
3) To evaluate the conformation and coverage density of starch depressants on the aforementioned mineral surfaces.

1.1. Thesis scope

This thesis is composed of six chapters (Figure 1):

- Chapter 1 introduces the main challenges, questions, and objectives to support this study;
- Chapter 2 consists of a literature review covering the fundamental aspects of sulfide mineral flotation; the reactivity of pyrrhotite and pentlandite surfaces; pyrrhotite depression strategies using polyamines and sulfur-bearing regents; and polysaccharides used as depressants in mineral processing. Additionally, a short introduction to starch gelatinization/modification is provided;
- Chapter 3 includes the production and characterization of paste starches and crosslinked starches. The main differences among the depressants are their molecular weight distributions and the presence of copper ions;
- In Chapter 4, micro-flotation tests of single and binary minerals systems are shown. A short discussion about the effect of controlled oxidation on the metallurgical recoveries for binary minerals systems is also included;
- Chapter 5 is divided in two main axes: the mechanism of depression and the mechanism of adsorption of the starch depressants. Based on the kinetics and equilibrium adsorption measurements, the described mechanism of depression is also confirmed by contact

angle, QCM-D, and AFM tests. Finally, the mechanism of adsorption is given by electrokinetic and XPS measurements, and supported by earlier research works;

- Chapter 6 synthesizes the main conclusions of Chapters 3-5, and provides recommendations for future works.

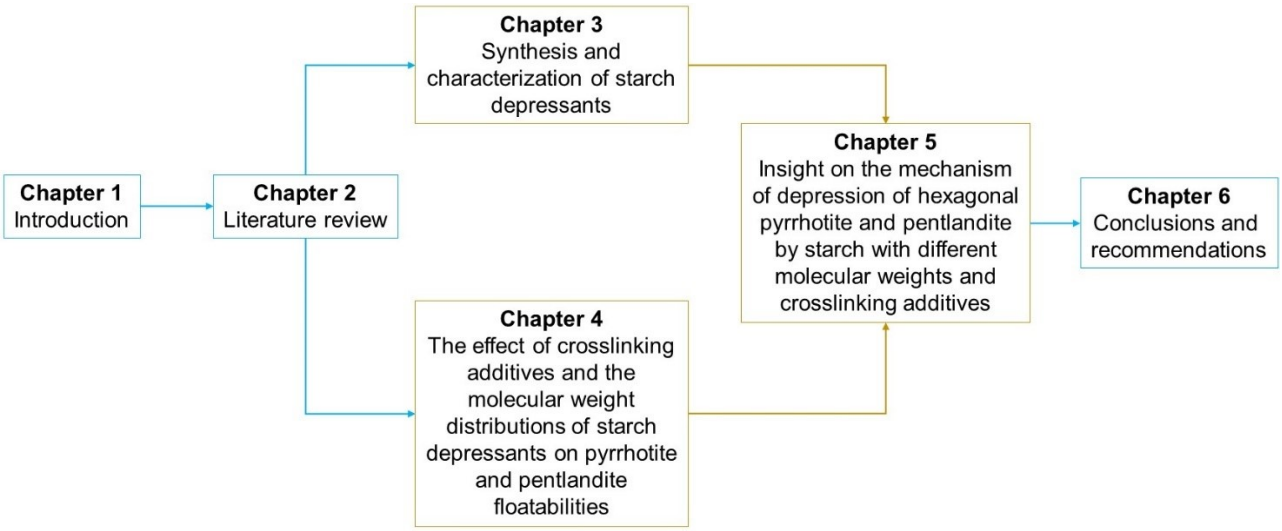

Figure 1: Thesis scope.

Chapter 2 Literature Review

2.1. Flotation overview

Froth flotation is a well-established mineral processing technique (33) designed to recover valuable minerals by their selective attachment to air-bubbles. Hydrophobic minerals are collected with the froth (concentrates) while the hydrophilic ones are depressed (tailings). Many factors can affect the optimal performance of the flotation process such as those of ore genesis and the machinery used (i.e. cell size, geometry, air flow, etc.) (34). However, the surface chemistry is one of the main factors influencing air bubbles-mineral particles attachment. This parameter correlates with the hydrophobic/hydrophilic aspect of a surface. The hydrophobicity of a mineral particle can be natural or induced. When induced, it accounts for the use of collectors such as thiol collectors, namely xanthate. Conversely, depressants, classified as a flotation regulators (34), may render the mineral surface hydrophilic by either replacing or removing collector molecules and hydrophobic species.

2.1.1. Flotation of sulfide minerals

The flotation of sulfide minerals is a complex topic since it involves electrochemical reactions on the surfaces of a mineral particle. One of the main examples of the electrochemical reactions is the interaction between the mineral surface and the collector molecules which is explained by the mixed potential model (34–37). In the mixed potential model, two or more electrochemical reactions take place on the same mineral surface. This process is sustained by the fact that sulfide minerals are semi-conductors (38) and, consequently, able to transfer electrons.

Therefore, during xanthate adsorption, the mineral can host an anodic site in which xanthate will be oxidized. This reaction is written as

$$X^- \rightarrow X_{ads} + e^- \quad (1)$$

where X^- represents the xanthate ion, and X_{ads} the adsorbed xanthate molecule. The mineral can also host a cathodic site where the oxygen reduction occurs, which is given by

$$\frac{1}{2}H_2O + \frac{1}{4}O_2 + e^- \rightarrow OH^- \quad (2)$$

Equation 2 demonstrates the significance of parameters such as dissolved oxygen (DO) and pH in the flotation/depression of sulfide minerals (34). Moreover, even though the mechanism of xanthate adsorption (Equation 1) is specific for each sulfide mineral (36,37,39), the sulfur atom usually interacts with the metal ion present on the mineral surface (34), forming metal-xanthate species. Further xanthate oxidation may generate hydrophobic species called dixanthogen, written as

$$2X^- \rightarrow X_2 + e^- \quad (3)$$

which depends on the mineral pulp potential (37).

2.2. Flotation of nickeliferous sulfide minerals

The processing strategies for an efficient separation of pentlandite from other sulfide minerals (gangue) are associated with the geological characteristics of a particular deposit. However, in Sudbury, Canada, nickeliferous sulfide minerals are separated via froth flotation using xanthate as a collector, and DETA as a depressant. According to Rao (38), two flotation steps are normally carried out: first, the generation of a bulk concentrate of all sulfide minerals, followed by the concentration of chalcopyrite/pentlandite after pyrrhotite depression. The presence of other sulfide minerals such as pyrrhotite and chalcopyrite ($CuFeS_2$) may detrimentally impact the nickel (Ni) content in the final concentrate. Differential separation of pentlandite from pyrrhotite requires further attention and studies, especially those involving hexagonal pyrrhotite and pentlandite due to their similar floatabilities. The separation of chalcopyrite from pentlandite requires other methods, which are not considered in this thesis.

2.2.1. Reactivity of pyrrhotite and pentlandite surfaces

The considerable reactivity of sulfide mineral surfaces causes their flotation to be a challenge. This includes electrochemical interactions among different minerals in the presence or absence of oxygen. These interactions are called galvanic interactions, which is one of the crucial parameters in sulfide mineral flotation determining which mineral will act as a cathode or as an anode. They cannot be supressed and exist during the entire processing, including comminution (Figure 2) (40,41). The higher the mineral's rest potential, the more cathodic (noble) it is considered.

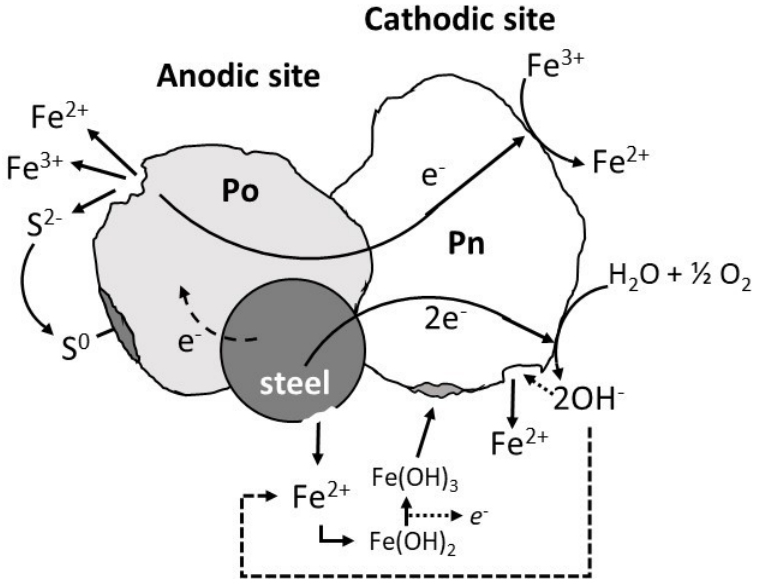

Figure 2: Simplified galvanic interaction model among pyrrhotite (Po), pentlandite (Pn), and grinding media in the absence of xanthate. Modified from (42).

Overall, in the presence of oxygen, it is possible to determine which mineral might be preferentially oxidized. For individual pyrrhotite and pentlandite, measured rest potentials at pH 9.2 are 60 and 100 mV (SCE), respectively (36). Consequently, it is possible to infer that, in a collectorless scenario, anodic reactions (oxidation) may occur on the pyrrhotite surface (43) such as

$$Fe_{1-x}S + (2 - \left(\frac{1}{2}\right)x)O_2 + xH_2O \rightarrow (1-x)Fe^{2+} + SO_4^{2-} + 2xH^+ \qquad (4)$$

while oxygen reduction (cathodic reaction) occurs on the pentlandite surface (36,44). The presence of xanthate switches the anodic and cathodic sites due to collector oxidation on pentlandite surface (See Equation 3) (36).

Surface oxidation of sulfide minerals is a largely studied topic because of its influence on mineral flotation by forming new surface species. The floatability differences of distinct crystallographic forms of pyrrhotite, i.e. monoclinic (Fe_7S_8 – 4C) and hexagonal (45) might be related to their dissimilar rate of oxidation (46). These surface species may benefit or hinder pyrrhotite floatability as well as their iron-sulfur ratio, and ferrous (Fe^{2+})/ferric (Fe^{3+}) species ratio on its surface (14).

Mycroft et al. (47) also refined a model to explain the sequence of pyrrhotite oxidation, in which they identified only ferric oxyhydroxide species during the initial stages of oxidation. In the presence of air, iron ions are released from the lattice and bind to oxygen [Fe(III)-O], forming a sulfur-rich subsurface. This subsurface is then reorganized as marcasite/pyrite (FeS_2). This model may be applied for pyrrhotite oxidation in the presence of water and air (normal conditions in flotation), suggesting the formation of iron hydroxides on the upper layer. Therefore, after oxidation, pyrrhotite surface could have the following species: metal-deficient subsurface ($M_{1-x}S$), elemental sulfur (S), hydrate iron oxides [FeO(OH)], ferrous hydroxide [$Fe(OH)_2$], ferric hydroxides [$Fe(OH)_3$)], and remaining iron ions at the solid/liquid interface.

In the case of pentlandite, three oxidation processes can arise. According to Buckley and Woods (48), in a low oxidation environment, ferric ions (Fe^{3+}) are removed from the lattice (Figure 3a step 1), leaving a metal-deficient pentlandite surface (Figure 3a step 2). The ferric ions in solution will then precipitate on pentlandite surface as hydrate iron oxides [FeO(OH)] (Figure 3a step 3). In the case of releasing of ferrous irons (Fe^{2+}) from the lattice, $Fe(OH)_2$ can be formed, which will later be oxidized to $Fe(OH)_3$. At high oxidation conditions, nickel ions from the lattice (Figure 3b step 1) are also precipitated as hydroxides (Figure 3b step 2).

In addition, Thornber (49) identified violarite ($FeNi_2S_4$) after pentlandite oxidation (Figure 3c). This process also releases nickel and iron ions to the solution in a process similar to

$$Fe_{4.5}Ni_{4.5}S_8 \rightarrow 2FeNi_2S_4 + 0.5Ni^{2+} + 2.5Fe^{2+} + 6e^- \quad (5)$$

These metals ions can then activate other sulfide minerals, altering their floatabilities. For instance, in a mixed pentlandite/pyrrhotite system, nickel ions may interact with pyrrhotite surface forming violarite as given by

$$Fe_7S_8 + 4Ni^{2+} \rightarrow 2FeNi_2S_4 + 5Fe^{2+} + 2e^- \quad (6)$$

Finally, after oxidation, pentlandite surface could have the following species: $M_{1-x}S$, elemental sulfur (S), $FeNi_2S_4$, FeO(OH), $Fe(OH)_3$, nickel hydroxide [$Ni(OH)_2$)], and remained nickel and iron ions at the solid/liquid interface.

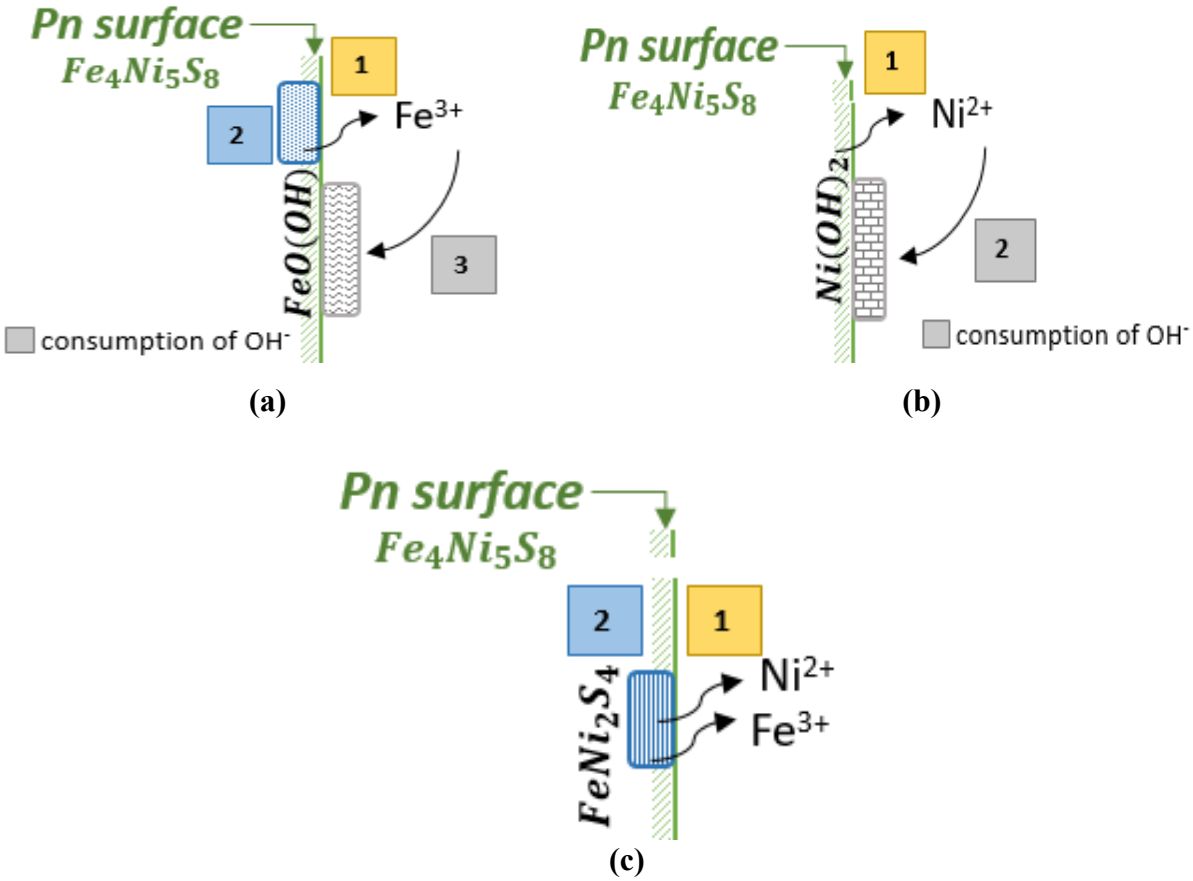

Figure 3: Low (a) and high (b) oxidation of pentlandite, and violarite formation (c).

When in aqueous media, minerals can also acquire surface charges by four different mechanisms: surface ionization, surface dissolution, adsorption of ions from the solution, and defects on the mineral lattice (50). Those charges can be responsible for the interactions of mineral surfaces with the flotation reagents. As described by Salopek et al. (51), most minerals ionize when

in contact with a polar medium. Conversely, sulfide minerals undergo dissolution by releasing metal ions in solution (Figure 3), which may precipitate as hydroxides on the same mineral surface and/or activate another mineral surface. Rao (37) also mentioned that sulfide mineral hydrolysis reactions as follow

$$S^{2-}_{(surface)} \leftrightarrow S^{2-}_{(solution)} \quad (7)$$

$$S^{2-}_{(surface)} + H_2O \leftrightarrow HS^-_{(aq)} + OH^- \quad (8)$$

$$S^{2-}_{(solid)} + 2H_2O \leftrightarrow H_2S + 2OH^- \quad (9)$$

$$S^{2-}_{(solid)} + H^+ \leftrightarrow HS^-_{(aq)} \quad (10)$$

Therefore, a more general schematic of sulfide mineral surface hydrolysis (considering also metal ions) is given in Figure 4 (34,52). In a free surfactant system, potential determining ions governing sulfide mineral hydrolysis are H^+ and OH^-.

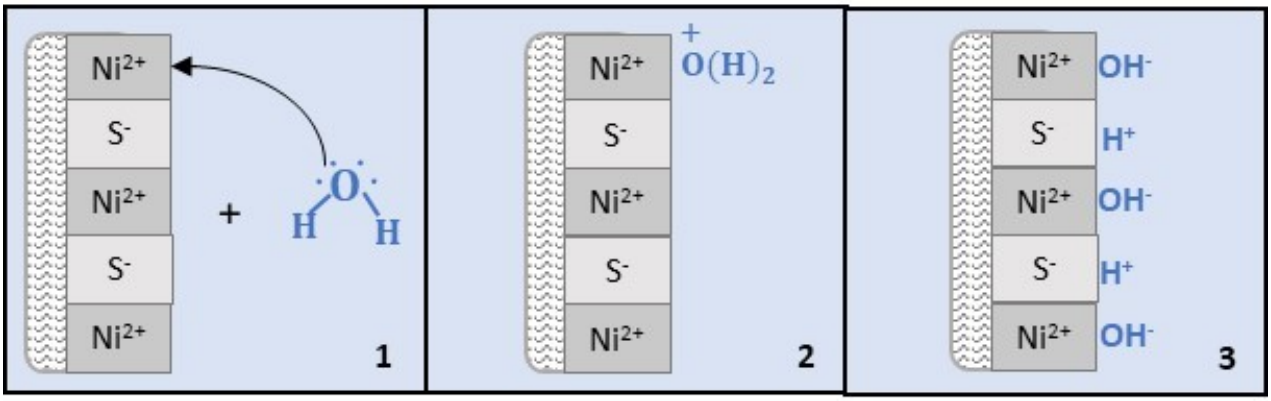

Figure 4: Example of the hydrolysis of a nickel sulfide mineral.

Tajadod described that ions of opposite charge are adsorbed on the mineral surface to balance metals ions in solution, moving towards electrical neutrality (53). This process results in the generation of an electrical double layer (Figure 5), defined originally by Helmholtz. Later, Gouy and Chapman proposed the concept of the diffuse electric double layer, which was thereafter refined by Stern. One of the greatest Stern contributions was the combination of the previous

models which considered the effects of specific adsorptions, in other words, by including that the ions could also be adsorbed by forces other than those of electrostatic nature (50).

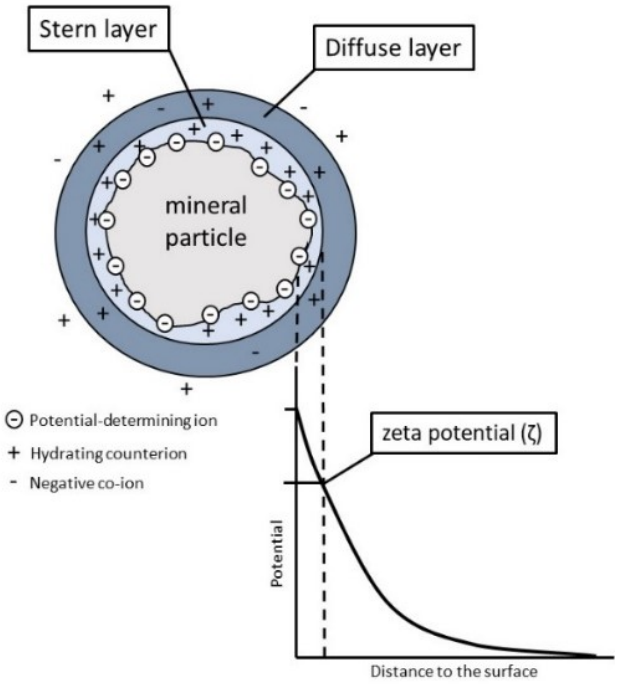

Figure 5: Schematic representation of the electric double layer. Modified from (14,53).

This surface potential variation as a function of the distance from the mineral surface can be measured in terms of the zeta potential (ζ). By definition, the zeta potential is the potential obtained on the shear plane between the particle and the solution when both are in movement relative to each other, in the presence of an electric field (50). As also explained by Montes and Peres (50), some authors consider the Stern plane (Figure 5) as the shear plane. The zeta potential measurement and calculation is widely used in flotation because it gives a representation of some mineral/liquid interface properties such as surface electric characteristics, wetting of solids as well as solution characteristics (51). The zeta potential ζ has Volts (V) units and is calculated from

$$\zeta = 4\pi \times \left(\frac{\mu}{D}\right) \times \left(\frac{V}{E}\right) \times 9 \times 10^4 \quad (11)$$

where μ is the solution viscosity (poise), D is the dielectric constant, V is the particle velocity (cm/s), and E is the potential gradient (V/cm).

2.2.2. Metal ion activation of pyrrhotite and pentlandite surfaces

The influence of metal ions in froth flotation is dependent on parameters such as the pulp chemistry (pH, Eh, metal ion concentration), and the mineral geology (54). In the context of pyrrhotite-pentlandite flotation, the presence of metal ions in the pulp is well known for interfering in the process (5,55,56). The presence of metal ions can be either a consequence of the oxidation of other minerals or added during the conditioning stage (34). Generally, the type of resulting surface species after metal ion adsorption dictates the mineral floatability. When the mineral surfaces are activated by those ions, their recovery usually improves. The recovery improvement is due to the increased interaction of collector with metal ion species, resulting in a hydrophobic surface. As explained by Gerson (56), in the case of copper activation, Cu (I) species are expected to interact with the sulfur atoms present in xanthates, and Cu (II) species forms hydrophilic precipitates (Figure 6).

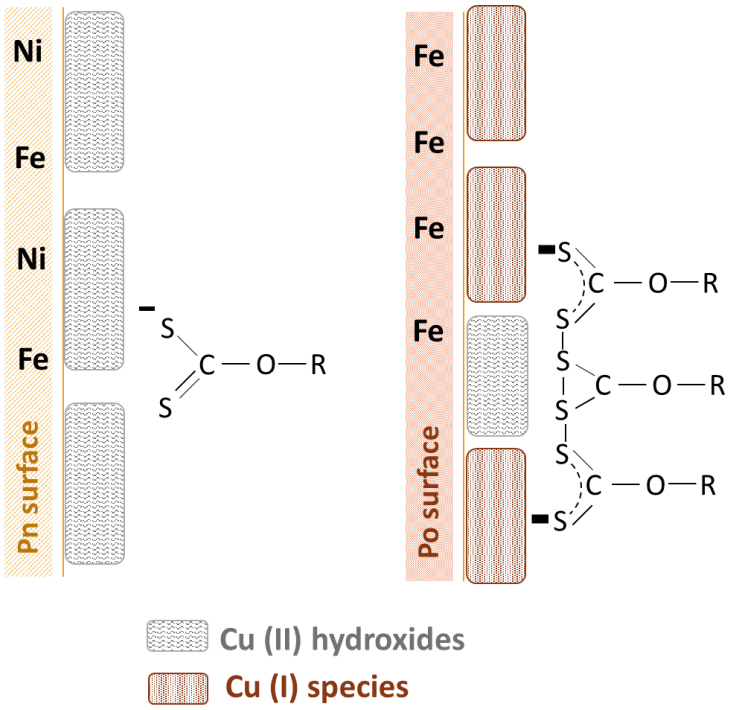

Figure 6: Simplified mechanism of xanthate interaction with species formed on pentlandite (Pn) and pyrrhotite (Po) surfaces after the addition of copper sulfate ($CuSO_4$). On the left side, the xanthate molecule does not interact with copper (II) hydroxide species, while dixanthogen and/or metal-xanthate species are formed on the right after interaction with copper (I) species.

Pyrrhotite surface activation is highly detrimental to the concentrates' purity since those heavy metal sites increase xanthate adsorption even in a reducing and low collector dosage environment (5,8). The addition of copper ions, for instance, does not always promote a better mineral recovery. Pyrrhotite flotation is considerably higher in the presence of copper sulfate ($CuSO_4$) whereas pentlandite recovery remains unchanged for particle size interval from 10 to 100 μm (55). Moreover, high dosages of $CuSO_4$ can depress minerals such as pentlandite (54).

2.3. Pyrrhotite depression

The choice of depressants in sulfide minerals flotation is especially attributed to the characteristics of the material such as liberation size, solubility, and previous mineral activation (57). Therefore, the depressant should affect only a particular mineral, i.e. the gangue minerals. Its depressing performance should not require excessive additions during the next flotation stages (28). The choice of depressant and the understanding of its activity mechanism (depression and adsorption) define the failure or success of the entire process. Historically, one of the first studies using exclusively DETA as pyrrhotite depressant was published by Marticorena et al. (7). At that point, even though the mechanism of depression was not clear, 75-80% of pyrrhotite was rejected during the flotation tests and little pentlandite was lost. DETA still remains the main depressant for pyrrhotite for the treatment of nickeferous sulfide mineral deposits.

2.3.1. Pyrrhotite depression by DETA and sulfur-bearing reagents

In order to improve mineral depression in flotation systems, some reagents may be used individually or combined. Activity mechanisms of combined depressants could be a result of a synergetic effect or just a summation of two distinct processes. Since the 90's, blends of polyamines such as DETA with sulfur-bearing depressants such as sulfur dioxide (SO_2) or sodium metabisulfite (SMBS) have been proved efficient for pyrrhotite depression either in collectorless or collector scenarios (4,6,8,58). Their mechanism of depression addresses several problems associated with pentlandite-pyrrhotite flotation.

One of the first challenges concerning pentlandite-pyrrhotite separation is the inadvertent activation of pyrrhotite surface during flotation (4,59,60) by heavy metal ions (e.g. Cu^{2+} and Ni^{2+})

(5) due to the oxidation of other sulfide minerals. Therefore, DETA appears to act via removal of adsorbed metal ions on the pyrrhotite surface by readily chelating with them (7,60), generating colloidal complexes (5,59,61). Mendiratta et al. (8) observed a reduction of the contact angle at pH 6.8 after DETA addition on Ni-activated and inactivated pyrrhotite in the presence of potassium ethyl xanthate.

The basic condition for DETA chelation with metal ions appears to be the presence of oxidized species (5,7,59) because oxidation products are more easily solubilized than their relative heavy metal sulfides (e.g. CuS pK_{sp} = 35.20 and $Cu(OH)_2$ pK_{sp} = 19.66) (62). Impacts on the chelation between DETA and metal ion species based on their solubilities was proved to be relevant. Xu et al. (59) showed that, in a single mineral system for activated pyrrhotite samples with copper, nickel and ferric ions, DETA virtually resolubilized all copper hydroxide [$Cu(OH)_2$], some $Ni(OH)_2$ but no $Fe(OH)_3$. DETA: metal ion molar ratio for complexes formation is 2:1. The coordination can happen with either two or three of their nitrogen pairs of electrons with the metal ions (61) (Figure 7). Therefore, this chelation can be considered selective, and pyrrhotite surface is left with a hydrophilic film of iron hydroxides (59,61), hindering its flotation. A similar mechanism is not verified on pentlandite and chalcopyrite surfaces, although these minerals have nickel and copper ions on their surface most likely as a result of steric hindrance (4,7).

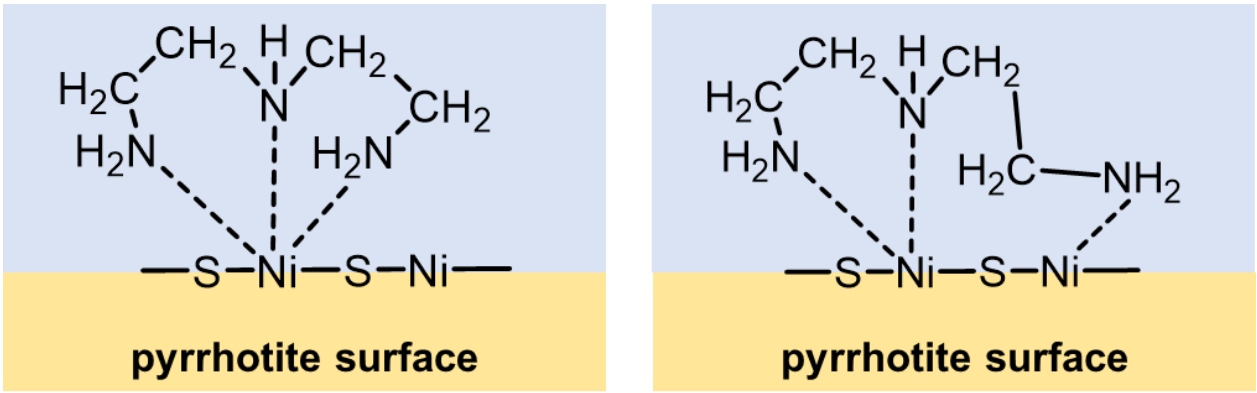

Figure 7: Simple schematic showing complexation of nickel ions by DETA on an activated pyrrhotite surface. Note that the dash lines represent the coordination of electron pairs. Modified from (59).

In addition, some studies have investigated DETA's effect on the formation of xanthate hydrophobic species such as dixanthogen. It has been recognized that DETA blends with sulfur-

bearing reagents might contribute to the reduction of pulp potential and retardation of collector oxidation (34). At low pulp potential, xanthate oxidation to dixanthogen (Equation 3) is hindered. The combination of DETA with sulfur-bearing reagents also promotes the formation of new complexes with heavy metal ions (4,59–61). In fact, $S_2O_4^{2-}$ and $S_2O_6^{2-}$ have been recognized to form hydrophilic precipitates such as $[Ni(DETA)_2]S_2O_6$ (4,59). Other specific effects are the easier solubilisation of some hydrophobic sulfide species such as elemental sulfur (S) (7), covellite (CuS), destruction of collector coatings (34), and reduction of dissolved ferric ions (Fe^{3+}) to ferrous ions (Fe^{2+}) (45). The latter consequence is important once DETA can associate with Fe^{2+} due to its lower product of solubility.

Overall, several mechanisms by which DETA or DETA-sulfur reagents promote pyrrhotite depression can be considered. DETA is responsible for reducing xanthate surface adsorption by chelating with surface activated metal ions, especially nickel and copper ions. The chelation is more effective upon metal hydroxide species due to their lower solubilities. Sulfur reagents appear to remove hydrophobic coatings via their solubilisation, helping to create a reducing environment. A lower pulp potential (reducing) environment hinders xanthate oxidation to dixanthogen, also favoring mineral depression.

2.4. Polysaccharide depressants applied to mineral depression

A few studies using polysaccharide as depressants for sulfide minerals have been reported (14,29,63,64). Examples of depressants are starch, guar gum, and carboxymethyl cellulose (CMC), and also their modified products such as dextrin, polyamines-modified starches, amine-modified starch, soda ash-dextrin, soda ash-CMC. Dextrin, for instance, has been extensively used in the depression of sulfide minerals (26,27,29,65,66). Recently, researchers (10) tested guar gum and CMC to depress naturally floatable minerals from two Merensky, a deposit of platinum group elements (PGE) in South Africa, both containing around 0.31-0.53% of pentlandite, and 0.44-0.62% of pyrrhotite. Tests were performed at 300 g/t of depressant, and demonstrated that almost all gangue minerals were rejected, and an improvement in Ni grade was verified. These studies are often performed to improve the depression of naturally floatable gangue minerals such as talc, while raising the sulfur content in the concentrate. Therefore, those do not account for the separation of two sulfide minerals such as pentlandite from pyrrhotite.

According to Laskowski et al. (20), depressants in general have two functions for depressing minerals: to prevent collector adsorption on mineral surface by occupying adsorption sites, and to form of a hydrophilic surface. Starch, for instance, retains water molecules between its chains, forming a hydrophilic interface and preventing the attachment between mineral particles and air bubbles (Figure 8) (12).

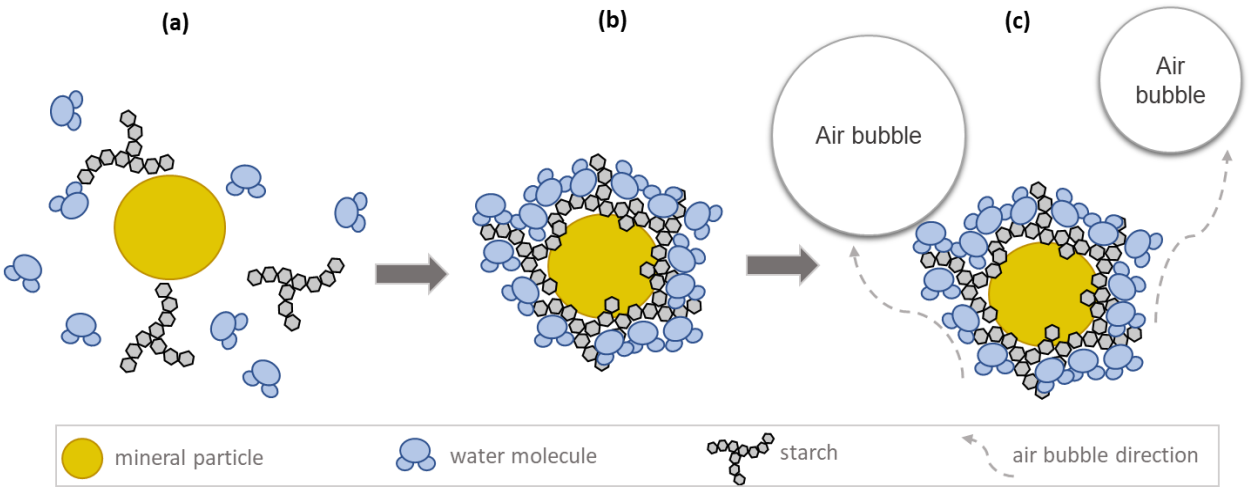

Figure 8: Illustration of the depression mechanism of dispersed starch molecules (a) forming a hydrophilic coating on the mineral surface (b), and preventing air-bubble attachment during flotation (c).

In terms of the mechanisms of adsorption of polysaccharides on mineral surfaces, Liu (63) listed five possibilities, namely hydrogen bonding, chemisorption, salt linkage, hydrophobic bonding and electrostatic interaction. The hydrogen bonding considers the interaction between the hydroxyl groups (OH^-) of the polysaccharide structure and the oxygen present on the mineral surface (10) in the case of natural hydrophobic minerals. Guar gum appears to adsorb via hydrogen bonds. This may not be thermodynamically favorable due to the necessity of breaking two hydrogen bonds (63). Moreover, some research with starch and hematite confirmed chemical adsorption (23), reporting surface changes on the mineral. Other reagents such as CMC might need a divalent metal cation to interact (Lewis acid-base interactions).

The interactions of sulfide minerals with the polysaccharides depressants seem to be associated with metal ions receiving electrons from the polysaccharide species (e.g. hydroxyl groups of a D-glucose unit), configuring an acid-base interaction (29). According to Liu (63) and

Laskowski et al. (66), these metal ions form “bridges” between mineral surface and the polysaccharide hydroxyl-groups. In fact, the idea that the addition of metal ions into the mineral pulp is a technique used to improve starch adsorption was confirmed by Bogusz et al. (65). These added metal ions might form oxidation species on the mineral surface, which appears to be the main adsorption site for polysaccharides such as dextrin (24) (Figure 9). Consequently, the more oxidized the mineral surface, the more dextrin is adsorbed (63,65). The preferential oxidation of pyrrhotite in the presence of pentlandite due to galvanic interactions may be a point to support the use of polysaccharides depressants.

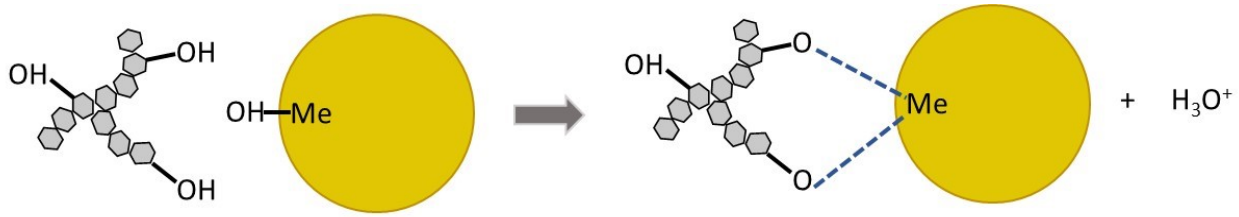

Figure 9: Non-balanced mechanism of adsorption of dextrin on metallic mineral surfaces. Note: Me corresponds to a metallic site. Modified from (24).

The aforementioned adsorption mechanism has been proven for a variety of polymetallic minerals (25–27,29). The isoelectric point (iep) of the metal hydroxylated species contributes with the mineral surface-polysaccharide interaction, demonstrating the significance of the pH during flotation. The mineral surface-polysaccharide interaction is further enhanced at the isoelectric point (iep) of the specific metal hydroxylated species.

The chemical and conformational characteristics of the polysaccharides is highly related to their effect on minerals floatability (28). Additional parameters to the success of polysaccharides adsorption and selectivity include the presence of specific substituted functional groups and the (MW) distribution. In fact, considering that the hydroxyl groups in a D-glucose monomer interacts with the mineral surface, in a polysaccharide with a high (noncontrolled) MW distribution, the non-reacted hydroxyl groups may hinder the specific interactions between the mineral surface and substituted groups (29). The manipulation of polysaccharide characteristics can be carried out via chemical, physical, and enzymatic modification processes (31). For starch (non-ionic depressant), simple modification processes include caustic gelatinization (digestion) and crosslinking reactions. Starch is an exceptional carbohydrate due to its particular physical properties and relatively low

detrimental impact in the natural environment. Innumerable industrial applications make it a valuable supply for food, paper, textile, and mineral processing industries. Example of its extensive use is the application in the reverse flotation of iron oxides (hematite) in Brazil (67). Quartz is floated using amines while hematite is depressed by gelatinized starch.

2.4.1. Starch chemistry

Fundamental information about starch chemistry can support the understanding of future modifications on its structure. Despite the fact that starch properties vary according to their botanical origin, some characteristics are common to all kinds. Starch is a polysaccharide that is composed by α-D-glucose units which may be found as open-chain (Fisher projection) with a terminal aldehyde group. The open chain can fold and generate a D-glucopyranose ring (Harworth projection) (Figure 10), which is more energetically stable.

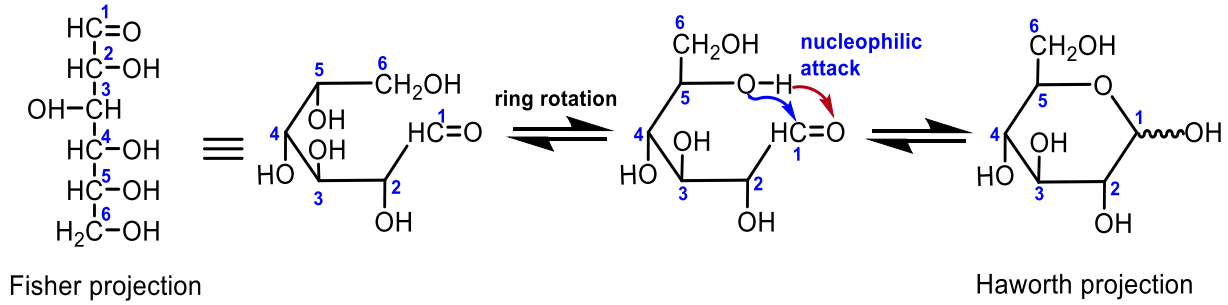

Figure 10: Formation of the pyranose ring from D-glucose molecule. Note that there is no distinction about the stereochemistry of the shown structure. Modified from (68).

Native starch granules have defined structures (Figure 11a), consisting of crystalline rings bound to amorphous areas (69,70). Ring thickness varies from nanometers to few micrometers according to the distance from the core (70). These amorphous areas are mainly composed of amylose (flexible chain segments) (69) and the core size is associated with this linear molecule content in starch (70). The D-glucopyranose mers bound to each other through bonds known as glycosidic bonds. Their linkage can be on the α-1,4 and/or α-1,6 carbon positions as can be seen in Figure 11b. These structures are named amylose (linear chain) and amylopectin (branched chain), and their distinct properties highly influence starch processing/modification.

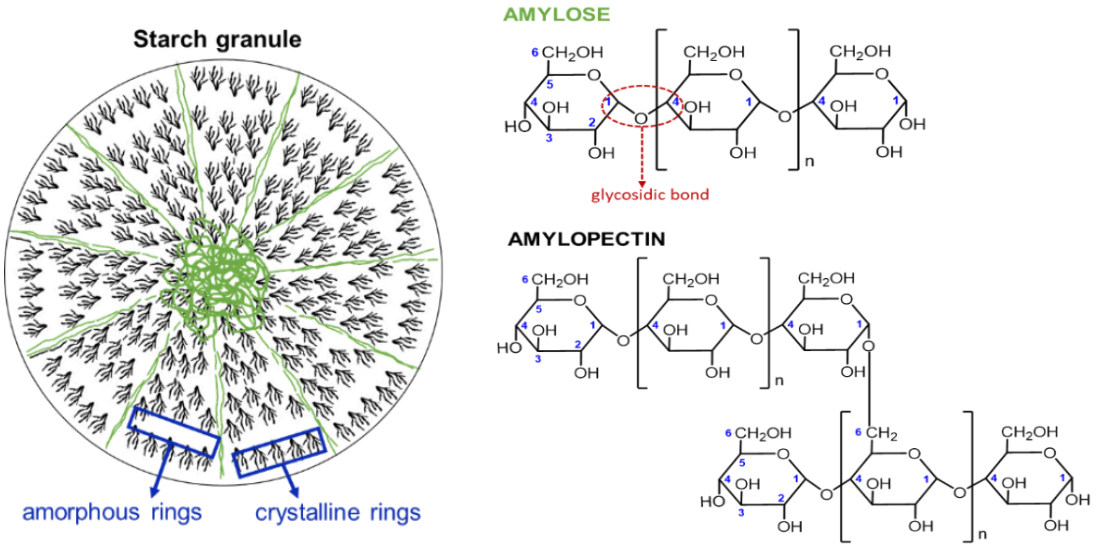

(a) **(b)**

Figure 11: Structure of starch granules (a), and detailed structures of amylose and amylopectin (b). Modified from (70).

2.4.2. Modification reactions with starch

Despite the high chemical complexity of starch molecules, a lot of information can be found about the gelatinization process due to its importance to the industry (68–72). Independently of the final application, the control of starch gelatinization will influence starch properties and functions (72). Since starch granules are not reactive, a process to release those amylose and amylopectin chains is necessary, extending the use of starches to new applications.

By definition, gelatinization is a process performed to disrupt the crystallinity of starch granules (68), altering their physicochemical structure (69). Although starch gelatinization seems to be a simple process, it is influenced by many factors such as granule type, reagents/ingredients added, water content, degree of granular heterogeneity, temperature, time, and mechanical stress (69). Small changes in those parameters define the final product.

The first step is the swelling of starch granules when in water (about 30% w/w moisture) (71). With continuous heating, their soluble constituents, i.e. amylose, are leached (69,70). This leaching process can be improved by applying shear forces, leading to a total disruption of starch granules as illustrated in Figure 12.

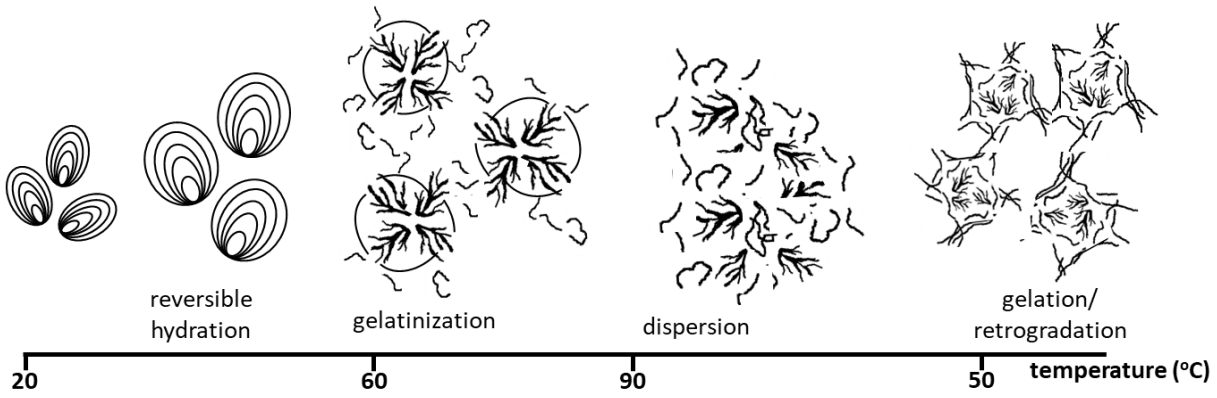

Figure 12: Thermo modification of starch granules in water. Modified from (68–70).

The presence of sodium hydroxide (NaOH) improves this process. The result is a viscous fluid composed of released amylose and amylopectin chains as well as some remaining granules called "ghosts". After gelatinization, the process of cooling down is called gelation, and the final product is a gel with viscoelastic semisolid properties (68). In the absence of a caustic reagent, differences between gelatinization temperatures of starches are related to their botanic origin (69). Specifically, potato starch has a low gelatinization temperature at about 62.6±0.1 ºC (71) due to the presence of phosphate-monoester which is responsible for improving the breakage of the crystalline structure due to repulsion.

Further chemical modifications can be performed with starch. In mineral processing, a major example is the production of dextrin. Dextrin is a low MW depressant produced by the hydrolysis of starch. Esterification and crosslinking reactions are other examples. The latter refers to the formation of side bonds connecting two free starch chains (31).

Chapter 3 Synthesis and characterization of starch depressants

Since the use of polysaccharides in mineral flotation is always attributed to low selectivity, considerable attention has been given to the preparation and characterization of the depressants. Although potato starch was used, similar depressants might be prepared using starches from different botanic sources. The lack of information in this area could be considered a limiting factor for their use. In this study, the main characteristics of 28 successful synthesis of crosslinked starch are discussed.

3.1. Experimental

For the following tests, all reagents used were analytical grade and can be seen in Table 1.

Table 1: Description of reagents used for crosslinked starch production and characterization.

Compound	Formula	CAS	Purity	Supplier
Copper (II) chloride anhydrous	$CuCl_2$	7447-39-4	99%	Fisher Scientific
Copper (II) sulfate	$CuSO_4$	7758-98-7	≥99%	Sigma-Aldrich
Potassium bromide	KBr	7758-02-3	≥99%	Fisher Scientific
Potato starch powder	$(C_6H_{10}O_5)_n$	9005-25-8	Extra pure	Across Organics
Reagent Alcohol	Ethyl alcohol, methyl alcohol and isopropyl alcohol	64-17-5, 67-63-0, 67-56-1	90%	Fisher Scientific
Sodium hydroxide	NaOH	1310-73-2	98%	Macron Fine Chemicals

Raw potato starch (moisture 18-21%) was chosen due to its considerable amount of phosphorus (P) in comparison with other starches (73). The presence of phosphorus may enhance metal ion coordination.

3.1.1. Production of different starch depressants

Two procedures of gelatinization were employed in order to produce the starch depressants. The first one is similar to the preparation of depressants for hematite ores (67), called thermo-caustic gelatinization (or digestion). The second relies on food chemistry works (74–77), and it is called thermo gelatinization. Two different copper salts were used to assess the influence of anions on the stability of complexes between starch groups and copper ions. Peres et al. (78) noted that for some metal ions, with exception of Cr (III) and Fe (III), the counter ions used influences the amount of metal ions complexed, especially chloride. A Rushton impeller was used in both procedures to promote a better stir, hence granules disruption.

Both methodologies consisted of preparing a 2% w/w starch suspension in deionized (DI) water, and heating the system (heating plate Thermo-Scientific Super-Nuova Multi-Place set up at 300 ºC) until reaching 90 ºC (usually in 30-40 minutes). The system was kept under vigorous mixing for an additional 20 minutes (external stirrer IKA RW 20 digital). All details for batch tests with 20.0 g of potato starch are given in Table 2. Temperature and pH values discussed in Section 3.2 are from an average of 14 tests of the paste starch and 14 testes of the crosslinked starch. In the case of thermo-caustic gelatinization, 1 g of NaOH was added for each 4 g of raw potato starch, i.e. a 1:4 ratio which is considered optimal (18). The transparent gel produced is called the higher MW paste starch (PP) since there was no molecular weight distribution control.

Once PP cooled down to 22 ºC, around 150 ml of deionized water (DI) was added due to evaporation. To PP, an amount of 0.1 M copper salt solution equivalent to 12.70 mg of Cu (II) for each gram of potato starch was added, and mixed for another 20 minutes under magnetic agitation (380 rpm with the CORNING PC 4200 plate). In this experiment, 12.70 mg Cu (II) for each gram of potato starch was calculated since the average metal coordination amount is 10.0 mg of metal ion per 1 g of starch (77).With that, the higher MW crosslinked starch (PC) was prepared. The total process takes around 1 hour and 40 minutes.

The low MW paste starch (LP) was obtained from PP. The 2% w/w starch suspension was centrifuged at 4,000 rpm (Centrifuge Hettich Rotanta 460R) using an Amicon® Ultra-4 Centrifugal Filter Unit 3,000 g/mol for 7 hours. The concentration of the centrifugation pellet (passing material) was compared with PP by total organic carbon (TOC) using a Shimadzu TOC-L CPH Model Total Organic Carbon Analyzer with an ASI-L and TNM-L at the Department of Renewable Resources

at the University of Alberta. PP and LP solutions were acidified with 1 M HCl, then sparged to remove purgeable organic and inorganic carbon. The liquid samples were placed in a combustion tube at 720°C which contains platinum catalyst beads. A redox reaction of the samples with carbon dioxide gas (CO_2) was detected by a non-dispersive infrared (NDIR) detector, and quantification was obtained by calibration of the instrument with potassium hydrogen phthalate. Finally, copper sulfate solution was mixed with LP in order to form the lower MW crosslinked starch (LC) as described before.

Table 2: Gelatinization processes employed for batches of 20 g of raw potato starch.

Thermo gelatinization	*Time (min)*	Thermo-caustic gelatinization
Starch grains are swelled in DI water at room temperature (19.1 – 20.0 °C). Stir 750 rpm.	*0*	Starch grains are swelled in DI water at room temperature (19.1 – 20.0° C). Stir 750 rpm.
Heating the system. Stir 750 rpm.	*6*	Adding NaOH. Stir 750 rpm.
Keeping stir at 750 rpm.	*7*	Heating the system. Stir 750 rpm.
Keeping stir at 750 rpm.	*10*	Increasing stir to 1100 rpm.
Keeping stir at 750 rpm.	*20*	Keeping stir at 1100 rpm.
Starting count 20 min of gelatinization at 90.0° C. Increasing stir to 1100 rpm.	*30 - 40*	Starting count 20 min of gelatinization at 90.0° C. Stir 1100 rpm
Keeping temperature at 90.0° C and stir at 1100 rpm.	*50 - 60*	Keeping temperature at 90.0° C and stir at 1100 rpm.

3.1.2. Characterization of raw potato starch, paste starch and crosslinked starch

Small aliquots of the starch gel were precipitated with reagent alcohol for analytical tests. The ratio used was 1:1 starch suspension:reagent alcohol. Precipitates were filtrated under vacuum.

Paste starch and crosslinked starch precipitates were frozen for 24 hours, and then dried using a freeze dryer (Labconco Lyph-Lock 12) for 24 hours (temperature around -52 ºC and $430x10^{-3}$ MBar). The final product (Figure 13) was ground for 10 min using an Agatha mill Retsch RM 200 resulting in a very fine powder.

To determine the phosphorus amount in the raw potato starch and the amount of copper (Cu) complexed in the crosslinked starch, Inductively Coupled Plasma Mass Spectrometry (ICP-MS) was performed in the Earth Science Department using a Perkin Elmer's Elan 6000. About 0.2 g of sample was digested with 10 ml nitric acid (HNO_3) at 130º C until it was completely clear. This clear solution was diluted to 15 ml with deionized water. In 1 ml of this diluted solution, 0.1 ml HNO_3, 0.1 ml of internal standards (In, Bi, and Sc) and 8.8 ml deionized water were added. The samples were ready for analysis after being well shaken. For the instrument running conditions, the flow rate was about 1 ml/minute, ICP RF power was 1300 W, and dual detector mode activated. The final results are the average of three replicates.

(a) **(b)**

Figure 13. Crosslinked starch precipitates dried in a freeze-dryer for 24 hours. (a) Thermo-caustic and (b) thermo gelatinized.

DRIFTS measurements were carried out with a Cary 670 FTIR Spectrometer (Agilent Technologies). All spectrums were collected using the Agilent Resolution Pro software version 5.2.0 CD 846. 25 mg of PP or PC sample (powdered samples) was mixed with 0.5 g of potassium bromide (KBr), ground using a small Agatha mortar, and then placed in a sample cup from Pike Technologies EasiDiff accessory. Pure KBr was employed as the background spectrum. Raw starch

spectrum was also collected under the same conditions. Spectrums were recorded ranging from 400 – 4000 cm^{-1}, resolution 4 cm^{-1}, totalizing 35 scans.

The amylose contents of native potato starch, and produced paste starch samples (PP and LP) were determined by a colorimetric method according to Williams (79). 20 g of potassium iodide (KI) and 2 g of iodine (I) were mixed and diluted in a 100 ml volumetric flask (Solution 1). Solution 1 was diluted 10 times (Solution 2). For 20 mg of starch, 10 ml of 0.5 KOH solution was added and the suspension dispersed for 5 min, then further diluted in a 100 ml volumetric flask (Solution 3). 10 ml of Solution 3 was mixed with 5 ml HCl and 0.5 ml of solution 2. The final solution was again diluted in 50 ml, and the absorbance read at 560 and 620 nm. All readings were performed with a UV-3600 Shimatdzu UV-VIS-NIR spectrophotometer. Error bars show the standard error. Amylose and amylopectin complexes with iodine have the greatest absorbance at 560 and 620 nm, respectively (80). The concentrations of amylose [A] are calculated by

$$[A] = \frac{(a_{AP560})(A_{620}) - (a_{AP620})(A_{560})}{(a_{A620})(a_{AP560}) - (a_{AP620})(a_{A560})} \quad (12)$$

while the amylopectin [AP] is given by

$$[AP] = \frac{(a_{A620})(A_{560}) - (a_{A560})(A_{620})}{(a_{A620})(a_{AP560}) - (a_{AP620})(a_{A560})} \quad (13)$$

where a is the unit absorptivity and A_{XXX} is the absorbance at 560 or 620 nm.

With the concentration of amylose and amylopectin, the amylose percentage (A%) is calculated (81) as follow

$$A\% = \frac{[A]}{[A]+[AP]} \quad (14)$$

The molecular weight distributions of paste starch samples (PP and LP) were obtained via Gel Permeation Chromatography (GPC). Previously, samples were immersed in distilled water at room temperature and then heated to 70 °C for 6 hours with gentle agitation. The samples were then sonicated for 10 minutes and agitated overnight at room temperature, yielding transparent

solutions with a small amount of insoluble material. Samples were filtered with 0.2 µm nylon filters before injection. For the GPC test, samples were monitored using an Agilent 1260 refractive index detector, equipped with a column PL aquagel OH. Data acquisition and handling were made with the Jordi GPC software. Experimental data were obtained under the following conditions: 100 mM $NaNO_3$ in water as a solvent; flow rate of 1.0 mL/min; injection volume of 100 µL for sample, and 50 µL for standards (standards polyethylene glycol 1511K, 1039K, 545K, 117.9K, 68.9K, 28.23K, 16.1K and 3.86K g/mol); column temperature at 45 °C; and concentration of injection of around 3 mg/mL for sample, and 0.5 mg/mL for the MW standard samples.

With this analysis, two values can be determined: the number average molecular weight ($\overline{M_n}$), and the weight average molecular weight ($\overline{M_w}$). $\overline{M_n}$ can be defined as (82)

$$\overline{M_n} = \sum x_i M_i \tag{15}$$

where x_i is the mole fraction and the molecular weight of a specific fraction (M_i). x_i can be calculated as follow

$$x_i = \frac{n_i}{N} \text{ and } N = \sum n_i \quad \rightarrow \quad \overline{M_n} = \frac{\sum n_i M_i}{\sum n_i} \tag{16}$$

using the number of polymer molecules per unit volume (n_i).

Similarly, $\overline{M_w}$ could be determined as

$$\overline{M_w} = \sum w_i M_i \tag{17}$$

using the weight fraction w_i and M_i, and further simplified to

$$\overline{M_w} = \frac{\sum n_i {M_i}^2}{\sum n_i M_i} \tag{18}$$

Additionally, the polydispersity index (PDI) shows how heterogeneous is the molecular weight distribution of a polymer. PDI is calculated by dividing $\overline{M_n}/\overline{M_w}$ (83).

Moreover, small aliquots of precipitated LP and LC were analyzed by X-ray photoelectron spectroscopy (XPS). XPS experiments at room temperature were performed using a Kratos Axis (Ultra) spectrometer with monochromatized Al Kα (hυ = 1486.71 eV) at nanoFAB. Calibration was performed with a binding energy (84.0 eV) of Au 4f7/2 referencing the Fermi level. The analysis chamber had a pressure greater than 5×10^{-10} Torr for the experiments. The core-level spectra were collected with a hemispherical electron-energy analyzer (pass energy of 20 eV) and the survey spectrum (binding energies from 0 to 1100 eV) was obtained at an analyzer pass energy at 160 eV. The C 1s peak at 284.8 eV was used to adjust any charge effects. A Shirley background was applied to the core-level peaks. Peak positions, widths, and peak intensities were determined using a non-linear optimization (Marquardt Algorithm). The XPS core-level lines was a product of Gaussian and Lorentzian functions [GL(30)]. UPS (power 3kVx20mA and 60 W) was carried out using the same spectrometer and measured with He I source (hv =21.2 eV). The sample was -10 V bias on. The survey spectra analysis provided the calculation and identification of peaks as well as the composition of the sample surface. CASA XPS was used to fit all spectrums with their peaks, analyzing the chemical bonds.

Finally, the radius of gyration (R_g) measurement showed the influence of Cu (II) ions as crosslinking agent. This parameter provides the size of the polymer which can assume different shapes such as a coil. As explained by Rudin and Choi (84), R_g is directly related to the molecular weight, composition (e.g. amylose and/or amylopectin), and interaction of the polymer with the solvent. It is defined as the root-mean-square distance of the fragments of a polymer molecule from its center of mass (84). The analysis of PP and PC was performed using Static Light Scattering (SLS) Postnova AF2000 instrument (refractive index increment dn/dc equals to 0.15 for potato starch, detector flow rate 0.50 ml/min, spacer 350 μm, run time 74, and solvent 55.7 ml). Zimm model was used to fit the data points.

3.2. Results and discussions

3.2.1. Synthesis of paste starch and crosslinked starch

Several challenges were faced during the production of crosslinked starch production. More details can be consulted in Appendix 1. It is relevant to notice that the results and characteristics of

the synthesis tests showed below are related only to PP and PC synthesized via thermo-caustic gelatinization and thermo gelatinization (Table 2). The differences in the use of different copper ions sources (i.e. $CuCl_2$ vs $CuSO_4$) are also discussed.

The 2% w/w raw potato starch suspension in the beginning of the gelatinization had an average pH of 6.81±0.08. In the thermo-caustic digestion, after NaOH addition, the pH ranged from 12.40 to 12.85, and slightly reduced during the entire gelatinization process (varied from 10.90 to 12.00). In other words, the final paste starch has a lower pH than in the beginning of the gelatinization when NaOH is added, suggesting the release of protons from the starch structure. The release of protons generates sites for the sodium cations (Na^+) which creates a repulsion of the starch components, promoting an easier swell and disruption of the granules (Figure 11) (85). In fact, the NaOH presence promotes a change in the hydroxyl groups(-OH) in the starch structure similar to

$$\text{starch—OH} \xrightarrow[\text{90 °C}]{\text{NaOH, 4:1}} \text{starch—O}^-\text{Na}^+ \quad (9)$$

This might reduce the gelatinization temperature. Upon heating, the dissolution is again intensified. The release of protons also exposes $-O^-$ groups that are more likely to coordinate with metal ions. However, independently of the digestion procedure for those tests, the final gel obtained (Figure 14) was very liquid and almost transparent. The gel was formed due to the amylopectin part since amylose is completely soluble in water.

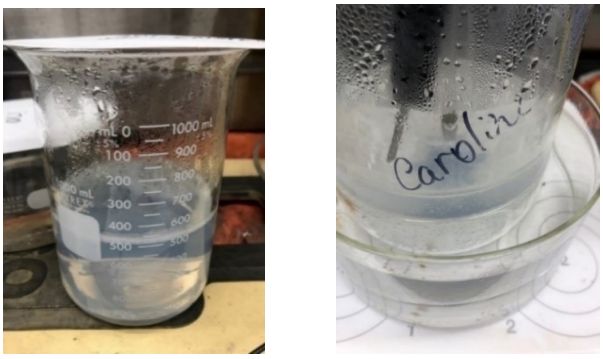

(a) **(b)**

Figure 14: Comparison between final paste starch gel, showing that the (a) thermo-caustic gel has a similar aspect to the (b) thermo gelatinized starch.

Differences between the gelatinization processes appeared after the addition of the copper solution (Figure 15). Similar colors were observed when either $CuCl_2$ or $CuSO_4$ were added. Thermo-caustic crosslinked starch has an intense blue color (Figure 15a), whereas the thermo digested vary from light blue to light green (Figure 15b). The color of their precipitates showed a similar trend (see Figure 13).

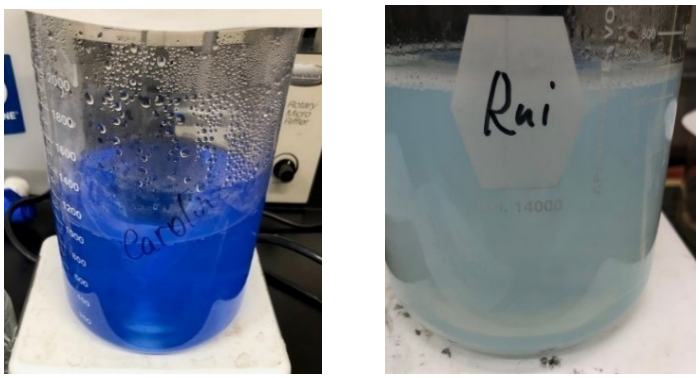

(a) **(b)**

Figure 15. Crosslinked starch gel color differences after the addition of copper sulfate solution. (a) Thermo-caustic, (b) thermo digested.

The filtration of thermo-caustic gelatinized starch after precipitation with alcohol was a challenge since small flocs were formed, inferring that the presence of NaOH during gelatinization directly influenced the chain sizes (molecular weight) of the final product. The precipitates dried using the freeze-dryer also had different hardness. The thermo-caustic digested crosslinked starch was more friable and very easy to grind.

3.2.2. Main characteristics and structure of paste starches and crosslinked starches

Similarly to 3.2.1, this section shows the main characterization tests performed with paste starch (PP) and crosslinked starch (PC), unless mentioned otherwise. The LP was analyzed in terms of the molecular weight distribution and the amylose content. All changes promoted by the addition of copper as a crosslinked agent were considered to be adequately applied to LC.

The amount of copper complexed with starch was determined by ICP-MS for the precipitates. A comparison between thermo-caustic and thermo crosslinked starches obtained using

$CuCl_2$ and $CuSO_4$ can be seen in Table 3. In terms of the crosslinked starches, the amount of Cu (II) complexed varied according to the counter ions used as well as the gelatinization method. Greater complexation was achieved for thermo-caustic digested starch mixed with $CuSO_4$. 10.173 mg of copper was bound to 1 g of potato starch, showing that chloride anions were detrimental to copper ion coordination in polysaccharide structures. This value also agreed with the average given by the literature (77). Very low amounts of copper were complexed with the paste starch produced via thermo gelatinization. It is likely that this route promotes the breakage of the starch granules but can only partially disrupt the starch chains. It is considered that a greater metal ion complexation would lead to a better "driver" depressant. For this reason, no further investigations were carried out for thermo gelatinized products and for those mixed with copper chloride.

Table 3: ICP-MS results with main elements for raw potato starch and crosslinked starches produced with copper chloride and copper sulfate salts equivalent to the amount of the element per gram of potato starch (mg/g).

		$CuCl_2$		**$CuSO_4$**	
	Raw potato starch	**Thermo-caustic**	**Thermo**	**Thermo-caustic**	**Thermo**
B	0	0.015	0.005	0.015	0
Na	0.012	41.304	0.013	49.944	0.0195
Mg	0.018	0.027	0.006	0.026	0.007
Al	0.002	0.026	0.031	0.027	0.0169
P	0.435	0.438	0.467	0.45	0.438
K	0.334	0.103	0.021	0.084	0.037
Ca	0.167	0.145	0.037	0.143	0.081
Fe	0.0985	0.118	0.225	0.188	0.196
Mn	$1.5x10^{-4}$	$5.3x10^{-4}$	$2.9x10^{-4}$	$4.7x10^{-4}$	$1.7x10^{-4}$
Cu	$2.0x10^{-4}$	5.783	0.929	10.173	1.846
Zn	$2.9x10^{-4}$	0.005	0.003	0	0

Additionally, the phosphorus (P) content is an essential parameter since it can also dictate certain physical behaviors of starch during and after gelatinization such as temperature of gelatinization and viscosity. The presence of P in starch structure can assist with a greater

complexation of metal ions as well as an easier adsorption on mineral surfaces. The phosphorus content found for the raw potato starch was lower than that described in the literature since this value can vary from 510 to 1334 mg/L (86). However, the starch purchased is a purified one (Table 1).

With DRIFT results (Figure 16), it was possible to identify peaks from different regions of the spectrum. The evaluation of raw potato starch, paste starch, and crosslinked starch were based on literature values as described in Table 4. Most of C-C, C-O, C-H bond vibrations, stretching, and bending have pronounced peaks in the region 500-2000 cm^{-1}, and some of them show a shift compared with the literature values. After the thermo-caustic gelatinization, peaks were either intensified or created. One example is the peak at 975 cm^{-1} corresponding to the glycosidic linkage, while raw potato starch does not demonstrate a C-C stretching at 753 cm^{-1}. Other peaks are at 1150 cm^{-1} which is characteristic of the pyranose ring while 1333 cm^{-1} corresponds to C-C-H and C-O-H deformations. A relevant distinction between paste starch and raw potato starch is the presence of carboxylic acid groups (Figure 16).

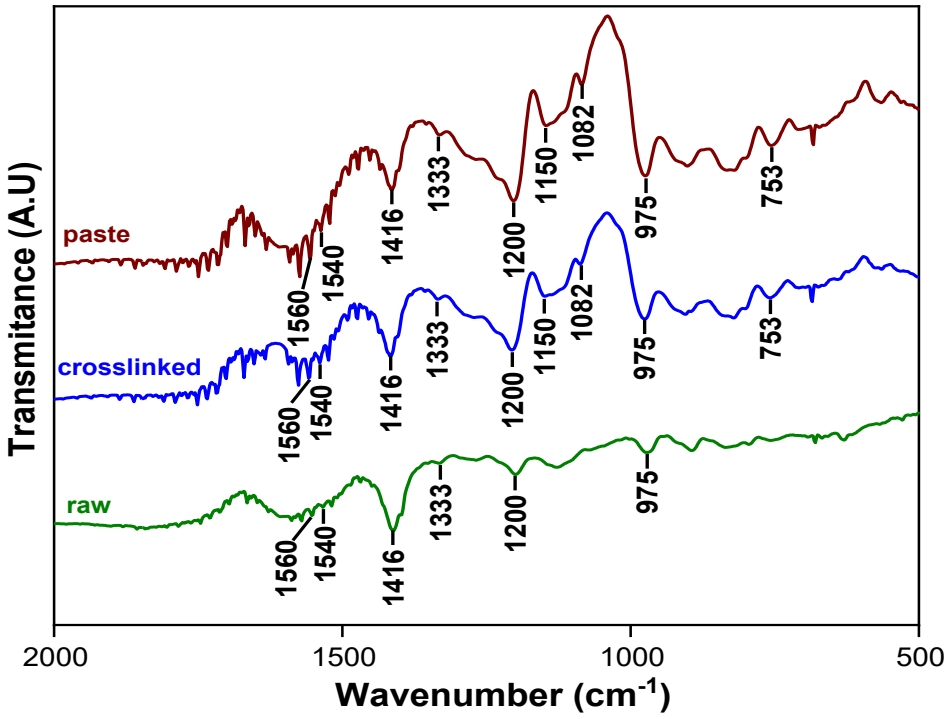

Figure 16: DRIF spectrums from 2000 cm^{-1} to 500 cm^{-1} of the higher MW starches (PP and PC) compared with raw potato starch.

Table 4: Description of peaks assignment using DRIFT for starch.

Frequency (cm^{-1})	Assignment	Reference
537	Skeletal modes of the pyranose ring	(87) and their references
577-581	Skeletal modes of the pyranose ring	(88), (87) and their references
627	Skeletal modes of the pyranose ring	(87) and their references
711	Skeletal modes of the pyranose ring	(87) and their references
764-780	C-C stretching	(88), (87) and their references
860	C^1-H, CH_2 deformation	(87) and their references
930	Skeletal vibrations of α-1,4 glycosidic linkage, C-O-C	(88), (87) and their references
995	Glycosidic linkage	(89)
1050-1020	Starch retrogradation	(89)
1022	Amorphous regions of starch	(88)
1030	Typical C^4-OH vibration	(89)
1048	Crystalline regions of starch	(88)
1067	C^1-H bending	(87) and their references
1094	C-O-H bending	(87) and their references
1110	CO ring, C^4-O, C^6-O	(89)
1150	Characteristic pyranose ring	(89)
1163	C-O and C-C stretching	(87) and their references
1164	Vibrations of the glycosidic C-O-C bond and the entire glucose ring	(88)
1242	CH_2OH side chain	(87) and their references
1344	C-O-H bending, CH_2 twisting	(87) and their references
1412/1415	CH_2 bending, C-O-C stretching	(88), (87) and their references
1340/1460	C-C-H and C-O-H deformations	(89)
1642/1650	Water absorbed in the amorphous regions	(88), (87) and their references
2100	If the presence of free water content	(88)
2800-3000	CH_2 deformation	(88), (87) and their references
3000-3600	O-H stretching	(88), (87) and their references

As described by Tang et al. (19), those groups appear at 1540 and 1560 cm^{-1} wavenumbers. The paste starch shows very intense peaks for those groups, which may enhance its adsorption on

mineral surfaces (19). No differences in the carboxylic acid groups intensity or shifting was verified between crosslinked starch and paste starch, suggesting that those groups may not react with the added copper ions. Nevertheless, the peak at 1082 cm^{-1} referring to a C-O-H bending is inexistent in the raw potato starch, and it had its intensity slightly reduced in the crosslinked starch. This may indicate a drop due to copper complexation. A similar change can be seen at 1200 cm^{-1} which is associated with the deformation of an O-H group coupled with a deformed C-H group. Therefore, the copper added is most likely bound to the alcohol groups in the amylose/amylopectin structures.

Another parameter that may affect polysaccharide depressant effect is the amylose content (Figure 17). It has been proved that the use of either pure amylose or pure amylopectin may distinctly interfere in the floatability of minerals such as quartz and hematite (90). Amylose and amylopectin have unsimilar structures which can be responsible for different conformations and hydration levels. The raw potato starch is composed of 26.06±0.14% of amylose, which agrees with the literature (73). However, after gelatinization, amylose content of PP was 65.99±4.29% whereas for LP it was 31.59±3.01%. Comparing PP with the raw potato starch, it can be seen that the gelatinization process promoted a powerful disruption of the granules, releasing the amylose structure. However, this process of disruption seems to have generated small amylopectin structures which are present in LP. This is given by the lower amylose content on LP than PP (Figure 17).

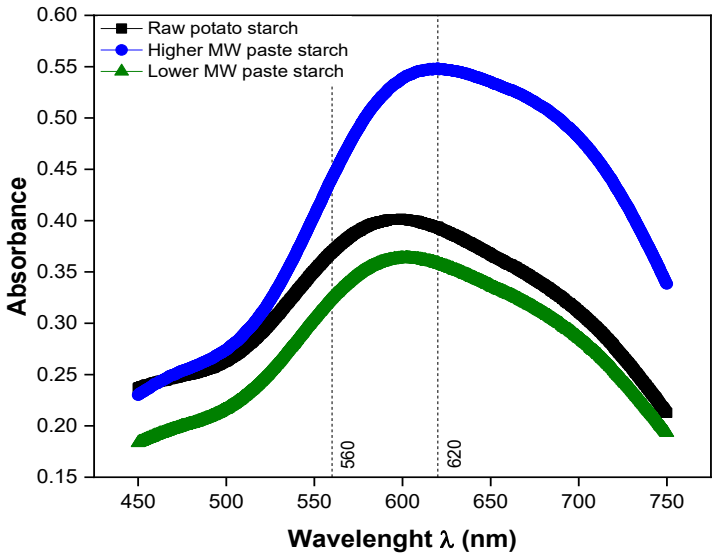

Figure 17: Amylose content of raw potato starch, higher MW paste (PP), and lower MW paste (LP) determined by colorimetric method at 0.04 mg/ml.

As discussed by Liu and Laskowski (24), the size of starch chains impacts the depressant selectivity, and it should be controlled to avoid external and undesired interactions. The MW distribution of paste starches is considered extremely relevant to this study. The GPC results of PP and LP are shown in Figure 18.

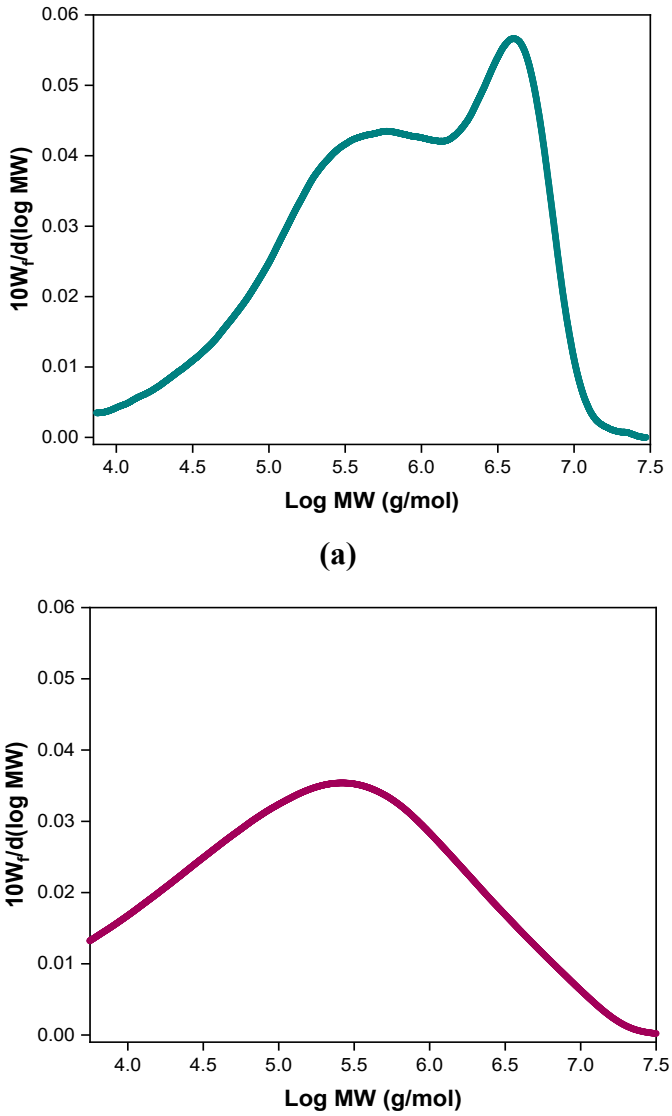

Figure 18: Molecular weight distribution of PP (a), and LP (b) measured by GPC. Note that W_f on the y-axis stands for weight fraction.

PP produced (Figure 18a) has a bimodal MW distribution. The $\overline{M_w}$ of PP is 1,702,226 g/mol while the $\overline{M_n}$ is 139,399 g/mol. No MW control was employed during PP synthesis, and a

high $\overline{M_w}$ value was expected. The use of a 3,000 g/mol membrane was necessary in order to narrow PP's MW distribution. Since the gelatinized starch chains are flexible, LP is composed of macromolecules weighting above 3,000 g/mol (log MW > 3.5). In fact, LP has a $\overline{M_w}$ of 773,138 g/mol which is fairly smaller than commercially available high MW guar gum and CMC depressants. LP $\overline{M_n}$ is 23,122 g/mol with the majority of chains weighting around 316,000 g/mol. LP is considered a low MW depressant in this study but commercially available depressants such as dextrin and maltodextrins have smaller chains than the aforementioned paste starches.

Although XPS is a surface analysis technique, it can provide information about the species formed between copper and starch. It also complements the XPS data of starch depressants on the mineral surfaces that will be presented in Chapter 5. The scan survey of powdered LP and LC are given in Figure 19. Both survey spectra seem identical, with the exception to the presence of a minor Cu 2p peak highlighted. This corroborates that the added copper became part of the starch structure.

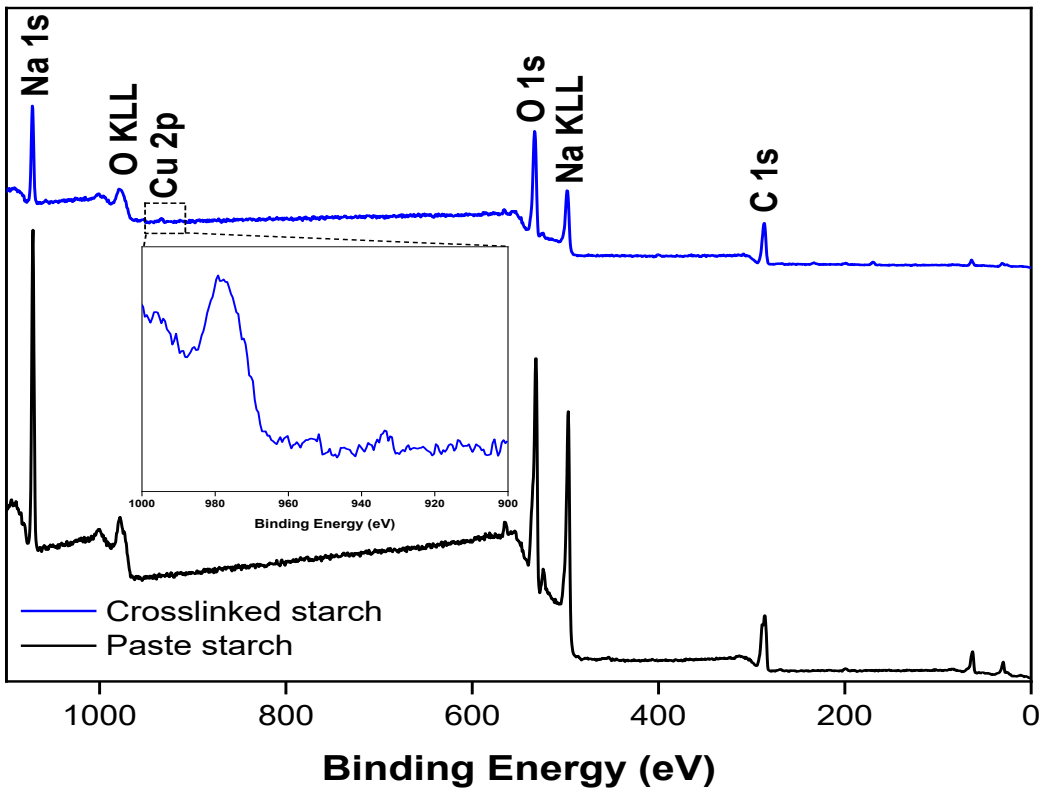

Figure 19: Survey spectra comparison between paste starch (black line) and crosslinked starch (blue line). Note that the Cu 2p part is zoomed out to allow its visualization.

The high-resolution spectrums in the region of binding energy for carbon 1s (C 1s) (282-292 eV), oxygen 1s (O 1s) (527-238 eV), and copper element (Cu 2p) (926-968 eV) are shown in Figure 20. Those better illustrate the different species that compose paste starch and crosslinked starch. All information after the Gaussian analysis is given in Table 5.

Table 5: XPS of paste starch and crosslinked starch assigned according to the literature (23,91–95).

			Figure label	Position	FWHM	Area (%)	Residual STD
Paste starch	C 1s	-C-C-/-C-H-	C_1	284.80	1.15	43.98	1.58
		-C-O-	C_2	286.30	1.15	24.11	
		-O-C-O-	C_3	287.80	1.15	7.96	
		-O-C=O	C_4	289.00	1.15	23.94	
	O 1s	C=O	O_1	530.94	1.30	58.31	1.08
		-C-O-	O_2	532.70	1.74	26.00	
	Na KLL	Na_{Auger}		535.56	2.06	15.69	
Crosslinked starch	C 1s	-C-C-/-C-H-	C_1	284.80	1.26	31.47	0.86
		-C-O-	C_2	286.30	1.26	47.34	
		-O-C-O-	C_3	287.60	1.01	9.75	
		-O-C=O	C_4	288.80	1.64	11.44	
	O 1s	C=O	O_1	531.19	1.64	32.60	0.76
		-C-O-	O_2	532.70	1.63	57.34	
	Na KLL	Na_{Auger}		535.96	2.23	10.06	
	Cu 2p 3/2	Cu (II) oxide		932.99	1.84	100	0.80

Two of the components of C 1s remained unchanged while the C_3 and C_4 decreased their binding energy 0.20 eV (Table 5 and Figure 20). The changes in FWHM and area also demonstrated that the electronic distribution around the carbon atom in the crosslinked starch were altered compared to paste starch. It is understood that the oxygen atom of the hydroxyl groups of the glucose unit directly interacts with metal ions (92,96). Nevertheless, contrarily to other works (92,96), no additional peak in the O 1s spectra was verified.

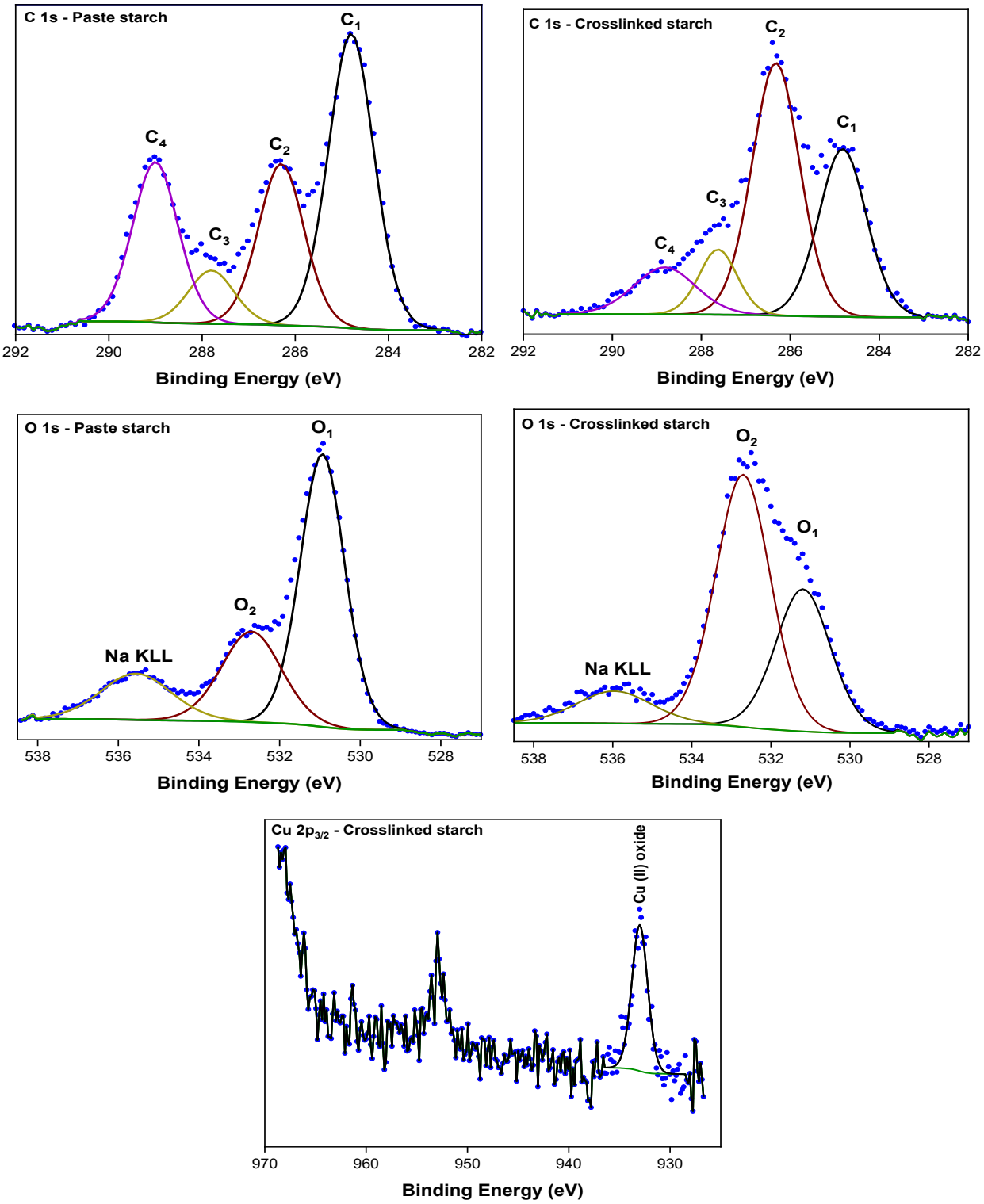

Figure 20: High-resolution C 1s, O 1s, and Cu 2p spectrums of paste starch and crosslinked starch.

The increase in binding energy of the O_1 peak from 530.94 eV (paste starch) to 531.19 eV (crosslinked starch) suggested a reduction of charge on the oxygen atom, most likely due to electron donation. Coincidentally, the binding energy of Cu (II) oxide is close to 531 eV, suggesting that the CuO peak may have been masked by the C=O peak. In fact, the amount of copper added is 100 times smaller than the amount of gelatinized starch. The small concentration of copper also influenced the analysis of the Cu 2p peak. The assessment of Cu 2p spectrum may be considered only as an indication of the formation of Cu-O.

The measured average R_g of PP is 53.8 nm. After $CuSO_4$ addition this value increased to 148 nm, suggesting that the copper center is able to bridge, on average, to two to three starch macromolecules.

3.3. Summary

The chain sizes of the synthesized paste starches were indirectly given by the difficulties encountered during the filtration of starch precipitates and visual assessment. Thermo digested starch produced bigger flocs, hence bigger amylose and amylopectin chains. The use of NaOH enhanced the breakage of starch granules, generating smaller chains. This gelatinization also had influence on the amount of copper present on the crosslinked starch (Table 3). Paste starches reacted with $CuSO_4$, instead of $CuCl_2$, yielded crosslinked starches with a greater amount of copper, demonstrating the detrimental effect of chlorine ions to copper complexation within the starch structure. Based on these results and considering the copper species present in solution at pH 12 (Figure 21a), it has been proposed that the copper hydroxylated species loses the hydroxyl groups, and the copper can be bound with the exposed oxygen present in the α-D-glucose unit (Figure 21b). The oxygen is likely to be exposed due to the gelatinization process (Equation 19), forming a Cu-O specie as suggested by XPS (Figure 20 and Table 5). Additionally, because Cu (II) can assume different geometries when bonding with chemical species due to its coordination number flexibility (97), the copper center might coordinate as well with unreacted alcohol groups (Figure 21b) as proposed in the DRIFT results (Figure 16). It is considered that the crosslinking reaction is independent of the MW distribution of the paste starch. Therefore, a similar structure is formed for LC. After separation with a 3,000 g/mol membrane, the $\overline{M_w}$ of LP is 2.20 times smaller

than PP. Their influence on the floatabilities of hexagonal pyrrhotite and pentlandite is further investigated on the following chapter.

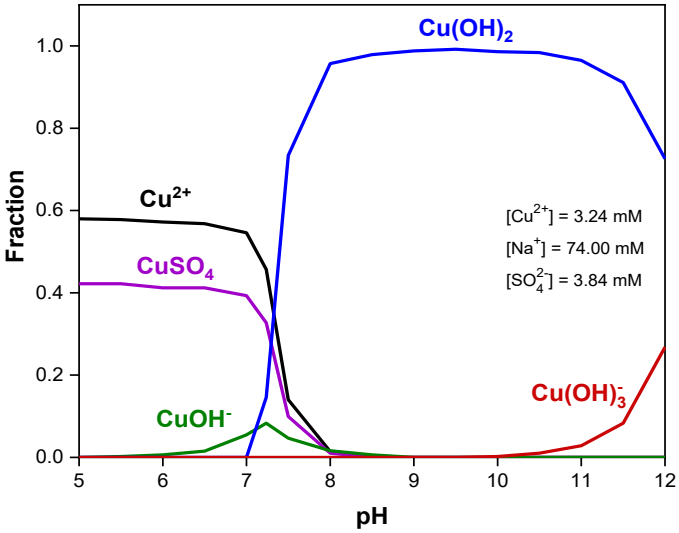

(a)

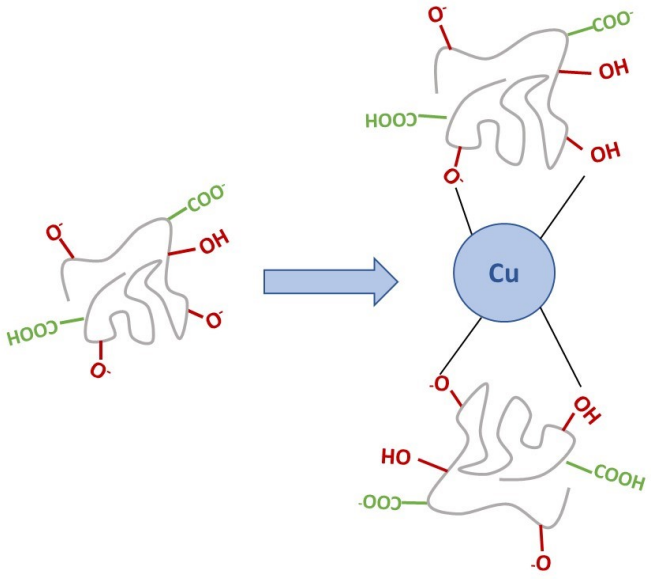

(b)

Figure 21: (a) Speciation diagram of copper species in solution during PC production (fractions were calculated using HYDRA and MEDUSA). (b) Schematic view of PC structure based on DRIFT, XPS, and R_g measurement. Note that a solid line is used to represent the chemical bonds between the oxygen and copper, and the dative bonds between the hydroxyl groups and the copper.

Chapter 4 The effect of crosslinking additives and the molecular weight distributions of starch depressants on pyrrhotite and pentlandite floatabilities

Although sulfide mineral flotation has an enormous impact on diverse economies, this domain still needs fundamental understanding, especially topics related to the use of polysaccharides depressants. The efficiency of DETA for pentlandite-pyrrhotite separation, and the complexity of polysaccharides depressants might be some of the reasons for their restricted applications. In order to investigate the effects of starch depression on hexagonal pyrrhotite and pentlandite floatabilities, in this chapter, single and binary micro-flotation results using the synthesized starch depressants are shown.

4.1. Experimental

For the following tests, all reagents used were analytical grade and can be seen in Table 6, except for potassium isobutyl xanthate (PIBX). Those not mentioned here can be seen in Table 1.

Table 6: Description of reagents for xanthate purification and micro-flotations tests.

Compound	Formula	CAS	Purity	Supplier
Potato dextrin	$(C_6H_{10}O_5)_n$	9004-53-9	Extra pure	Sigma-Aldrich
Acetone	C_3H_6O	67-64-1	≥99.5%	Fisher Scientific
Benzene	C_6H_6	71-43-2	99.8%	Fisher Scientific
Petroleum ether	C_6H_{14}	8032-32-4	-	Fisher Scientific
Sulfuric acid	H_2SO_4	7664-939	95-98%	Fisher Scientific
PIBX	$C_5H_9KOS_2$	6791-12-4	-	Prospec Chemicals

PIBX was purified according to the method described in Dewitt et al. (98). The first step consisted of solubilizing 10 g of PIBX in 100 ml of warm acetone (40 ºC) in a water bath to remove insoluble materials. The solution was then filtered using a Büchner funnel, and the filtrate carefully stirred with 400 ml of benzene. The precipitated material was again filtered in a Büchner funnel, and resolubilized in 50 ml of acetone. Subsequently, it was quickly re-precipitated in 500 ml of petroleum ether with no stirring. The final precipitate was filtered as mentioned before, and washed several times with warm petroleum ether fractions (40 ºC). The solid material was dried in a freeze dryer for 24 hours. The final product was stored in a sealed container in a freezer to avoid oxidation.

4.1.1. Mineral sample preparation and characterization

Pentlandite (Pn) from Sudbury, Canada, was provide by Vale and used as received after being dry classified. A hexagonal pyrrhotite (Po) sample from Virginia, United States, was purchased from Boreal Science. The sample was crushed in an Agatha mill Retsch RM 200 and dry classified. 92.9 % pure hexagonal pyrrhotite was obtained after two magnetic separation steps using a Frantz magnetic separator model LB-1operated at 0.01 A and 0.03 A with 15º slope. All samples were vacuum sealed, and stored in a vacuum desiccator at room temperature (around 19.8 ºC) to avoid any contact with oxygen.

4.1.1.1. X-ray fluorescence (XRF) and X-ray diffraction (XRD)

Elemental composition of the mineral samples was obtained using an Orbis PC MicroEDXRF Elemental Analyzer. In this study, -10 μm mineral samples were placed in a plastic cup, and covered with a plastic film before measurements were taken. Instrument specifications for all tests were 40 kV, 350 μA, Live Tm 30, Resolution 135.8, and Dtm 39%. Three measurements for each sample were taken and the average considered as the final value. Mineral phases were determined using a Rigaku Ultima IV instrument at the Earth Science Department. Sample powders were top packed in an aluminum Rigaku sample holder for analysis. The instrument running conditions were: radiation source cobalt tube at 38 kV and 38 mA; focusing geometry Bragg Brentano Mode; detector D/Tex Ultra with Fe Filter (K-beta filter); slit sizes used were divergence slit (2/3 degrees), divergence height limiting slit (10 mm), scattering slit (open), receiving slit

(open); scan information ranging from 5 to 90°; scan axis 2Θ/Θ; scan mode was continuous; sampling width (step size) was 0.0200°; and scan speed 2.00 deg/min ~45 min. Data interpretation was done using JADE 9.6 software with the 2019 ICDD Database PDF 4+, and 2018-1 ICSD databases.

4.1.2. Micro-flotation tests

Micro-flotation tests were carried out in a 165 ml Hallimond tube for single and binary (artificial mixture 1:1) mineral systems. In these tests, approximately 1.25 g of mineral sample (-75+38 μm) was sonicated for 5 min in 150 ml of deionized water in order to deslime. The supernatant was discharged and the remaining part was conditioned under magnetic agitation in 50 ml of pH 9.2 deionized water. This pH was chosen due to the poor pyrrhotite recovery at this pH (55), and based on industrial flotation practices. In the first minute no reagent was added. PIBX was added and conditioned for 2 min, followed by the starch depressant, which was conditioned for 5 min, totalizing 8 min conditioning. Only those thermo-causticized starch depressants were used for micro-flotations.

It is important to notice that a comparison between paste starch, crosslinked starch, and copper ions with paste starch (Cu+PP and Cu+LP) was made for single mineral flotations. The latter depressants mean that an aliquot of $CuSO_4$ solution was added at the concentration equivalent to that present in the same amount of crosslinked starch before adding paste starch. In this case, the conditioning times for Cu (II) ions and paste starch were 2 and 3 min, respectively. NaOH and H_2SO_4 were used as pH regulators. The flotation was conducted for 5 min running with nitrogen (N_2) as the flotation gas at flow 20 mL/min with continuous magnetic stirring (100 rpm CORNING PC 4200 plate). For binary minerals, concentrate and tails were collected and analyzed by XRF (see 4.1.1.1). All tests were repeated three times with fresh reagents, and error bars show the standard error.

4.2. Results and discussions

4.2.1. Characterization of hexagonal pyrrhotite and pentlandite samples

Analysis of XRF showed a purity greater than 82.8% for pentlandite, with small amounts of Si, Ca, Cu, Co, and Rh (Table 7). In fact, with X-ray diffraction (XRD) analysis no silicate mineral was determined, while hexagonal pyrrhotite and pyrite are the main gangue minerals (Figure 22). On the other hand, according to X-rays fluorescence (XRF), hexagonal pyrrhotite sample presents low Si, Mn, Ca, and Zn contents (Table 7), being sphalerite [(Zn,Fe)S] the main sulfide gangue mineral (Figure 22b). This sample did not contain any trace of monoclinic pyrrhotite.

Table 7: Chemical composition of the micro-flotation samples used by XRF.

Pentlandite				**Pyrrhotite**			
Element	*%*	*Std deviation*	*Std error*	*Element*	*%*	*Std deviation*	*Std error*
Si	0.38	0.04	0.02	*Si*	0.24	0.01	0.00
S	35.25	0.11	0.07	*S*	39.52	0.02	0.01
Ca	0.29	0.03	0.02	*Ca*	0.90	0.04	0.03
Fe	33.53	0.07	0.04	*Mn*	0.15	0.01	0.01
Ni	28.33	0.07	0.04	*Fe*	57.91	0.04	0.02
Cu	0.33	0.03	0.02	*Cu*	0.49	0.02	0.01
Rh	0.70	0.07	0.04	*Zn*	0.80	0.00	0.00
Co	1.18	0.03	0.02				

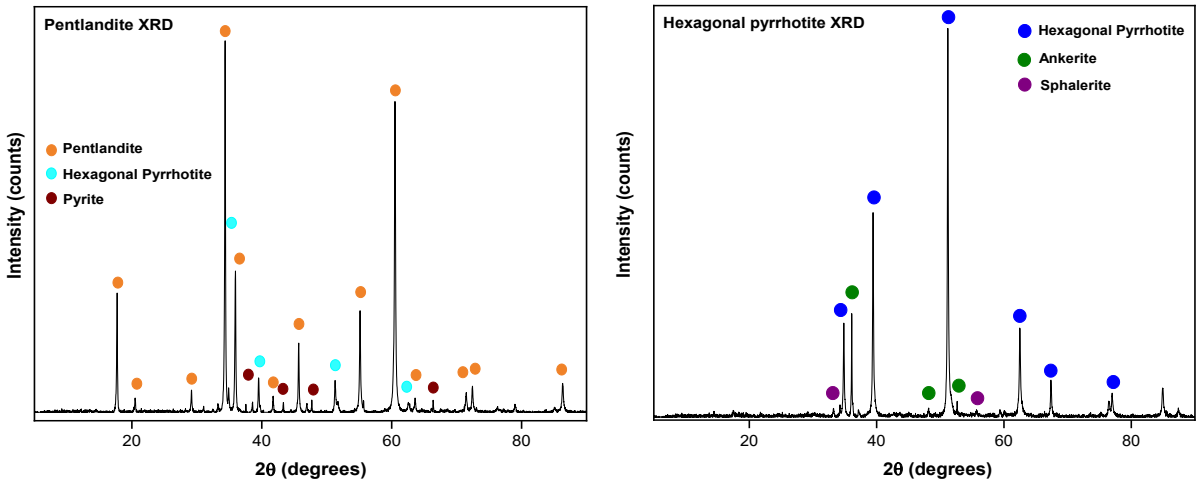

(a) **(b)**

Figure 22: XRD for pentlandite (a) and hexagonal pyrrhotite (b) samples used in this study.

Note: Ankerite is a carbonate mineral with the chemical formula $Ca(Fe,Mg,Mn)(CO_3)_2$.

4.2.2. Micro-flotations of single minerals

Hexagonal pyrrhotite and pentlandite single micro-flotations at pH 9.2 using paste starches, crosslinked starches, and copper ions with paste starches were assessed at 5 mg/L. Figure 23 shows that starch, in general, is a very strong depressant for both sulfide minerals and significantly interferes on their flotation kinetics.

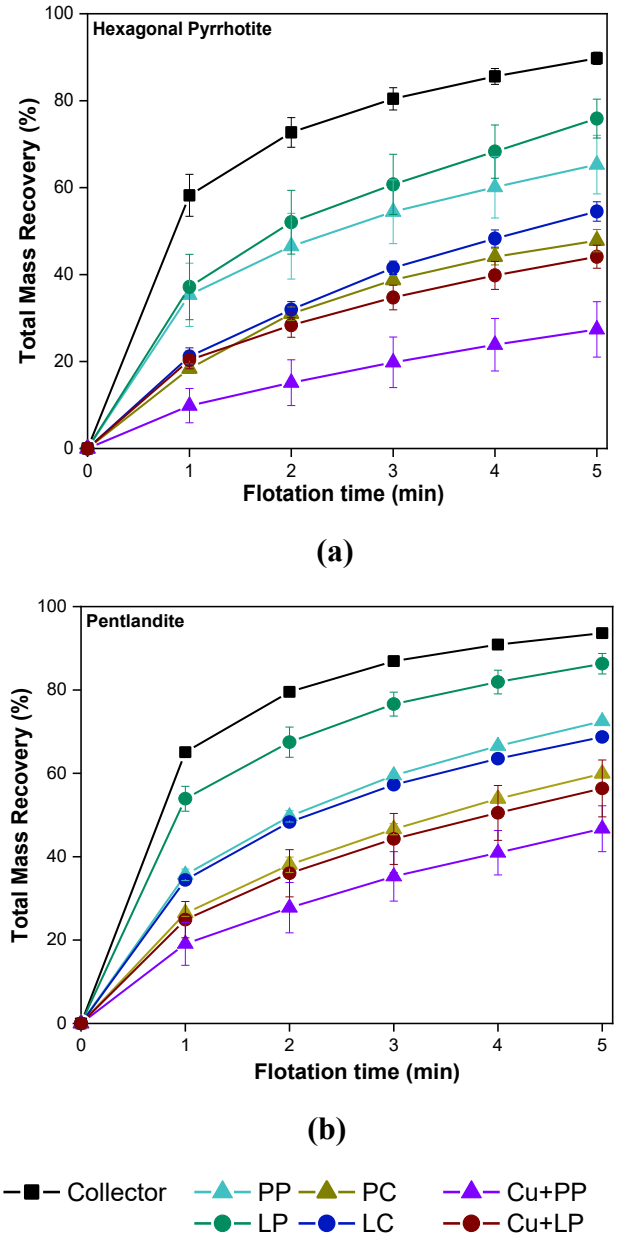

Figure 23: Kinetics micro-flotation results of single hexagonal pyrrhotite, and single pentlandite. All flotations were performed with 9.66×10^{-6} M PIBX, and 5 mg/L starch depressant.

Important differences can be seen for depressants with distinct molecular weight distributions. In fact, low MW depressants (i.e. LP, LC, and Cu+LP) have a reduced adverse effect on pentlandite recovery. Comparing the recovery with the baseline case (collector) for each mineral, hexagonal pyrrhotite depression can be 6.5-15.4% greater than pentlandite depending on the depressant used (Figure 23a). The floatabilities of both minerals may be hindered by the formation of a hydrophilic layer on the mineral surface, impairing their attachment to air bubbles. This is further discussed in Chapter 5.

The depressing effect was further enhanced when copper ions were added, either before (crosslinked starch) or during conditioning (Cu+LP or Cu+PP). According to the calculated speciation diagram for $CuSO_4$ (Figure 24), the copper ions added previously to LP or PP precipitate as $Cu(OH)_{2(s)}$ on the mineral surface at pH 9.2, increasing the density of metal hydroxide species on both mineral surfaces. The copper hydroxide species interaction with starch is further enhanced due to the isoelectric point (iep) of $Cu(OH)_2$ (25) which is at pH 9.2-9.3 (99). According to the literature (24), polysaccharide adsorption is improved by the presence of metal-hydroxide species on the mineral surface. Therefore increasing the number of oxidation species at the mineral surface should increase the amount of starch adsorbed (63,65).

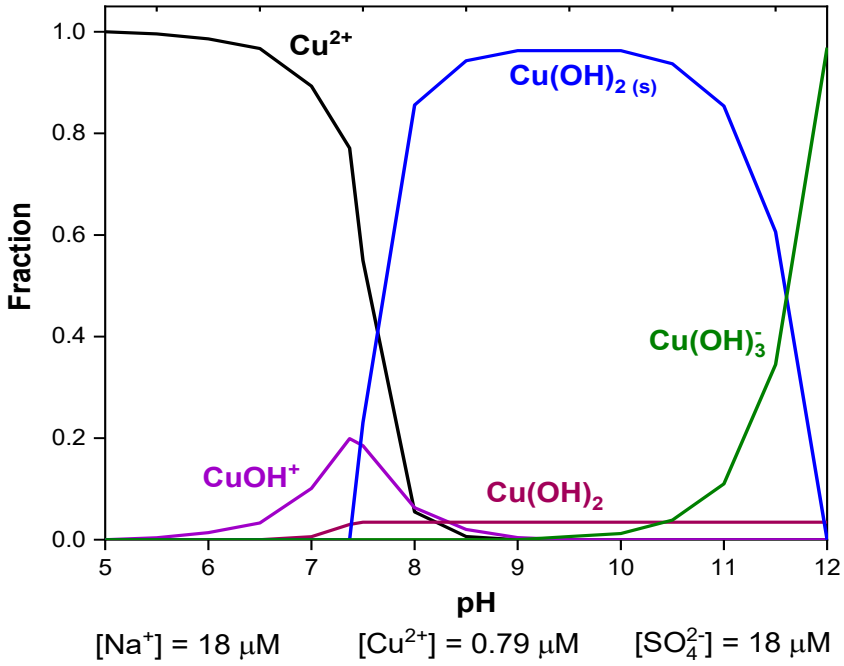

Figure 24: Speciation diagram of copper species during micro-flotation tests using $CuSO_4$ and paste starch (Cu+PP and Cu+LP). Fractions were calculated using HYDRA and MEDUSA.

Nevertheless, the addition of metal ions is random and both minerals showed the ability to adsorb copper ions on their surface (54), increasing the number of interaction sites with the depressants, and consequently, the hydrophilic characteristic of their surface. The use of metal ions in the flotation of nickeliferous sulfide minerals has been extensively studied (54–56) and it can have an activating or depressing effect depending on the dosage used. As additional information, single and mixed micro-flotation results using copper or nickel ions can be consulted in Appendix 2.

The depressing effect is also directly related to the dosage and not only the molecular weight distribution and presence of copper. At 10 mg/L (Figure 25), the differences between PP and LP become insignificant for pentlandite recovery, and their depressing effects are similar. This may infer that above a certain concentration, the hydrophilicity generated by the starch depressants is the same on pentlandite surface and is independent of the molecular weight distribution.

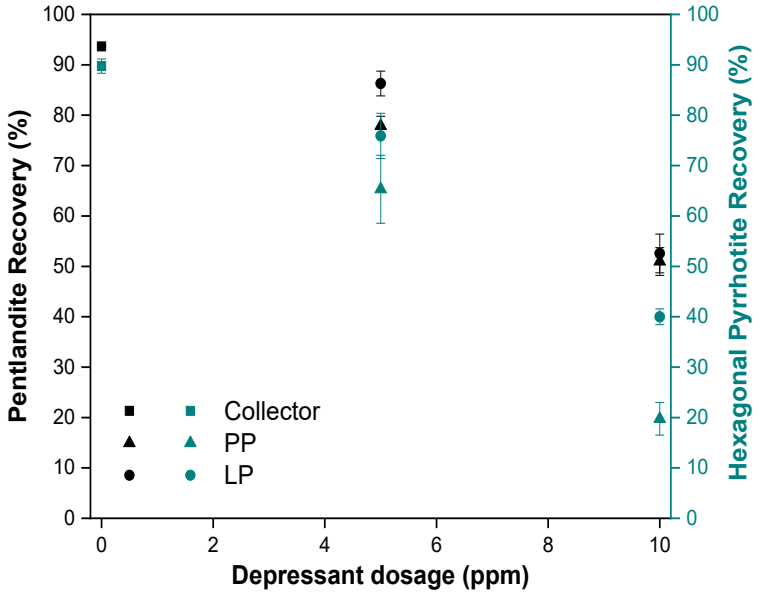

Figure 25: Effect of paste starch dosage on single pentlandite and hexagonal pyrrhotite mass recoveries. All flotations were performed with 9.66×10^{-6} M of PIBX.

In addition, this similar flotation data is most likely related to the mineral surface density coverage with hydrophobic/hydrophilic species. In other words, the fact that PIBX adsorption on pentlandite is greater than on hexagonal pyrrhotite (36) results on a faster saturation of available adsorption sites. Since xanthate adsorbs preferentially on the Ni sites of pentlandite lattice (36,39),

they may not be the main point to improve depressant adsorption. Furthermore, due to the pH used for the micro-flotations (pH 9.2), only a partial interaction with nickel sites occurs since the iep of $Ni(OH)_2$ is above 11 (100).

Considering the LP chain sizes (Figure 18b), after Cu (II) addition, LC weights two to three times bigger (Figure 21b). In this context a comparison between LC and potato dextrin (Table 6) was made (Figure 26a). The reason for a comparison with a commercially available product is to assess whether the molecular weight distribution of a depressant is the main reason for its depressing capability as suggested by Figure 23 (see PP and LP results), and/or whether starch additives such as metal ions can modify the depressing mechanism.

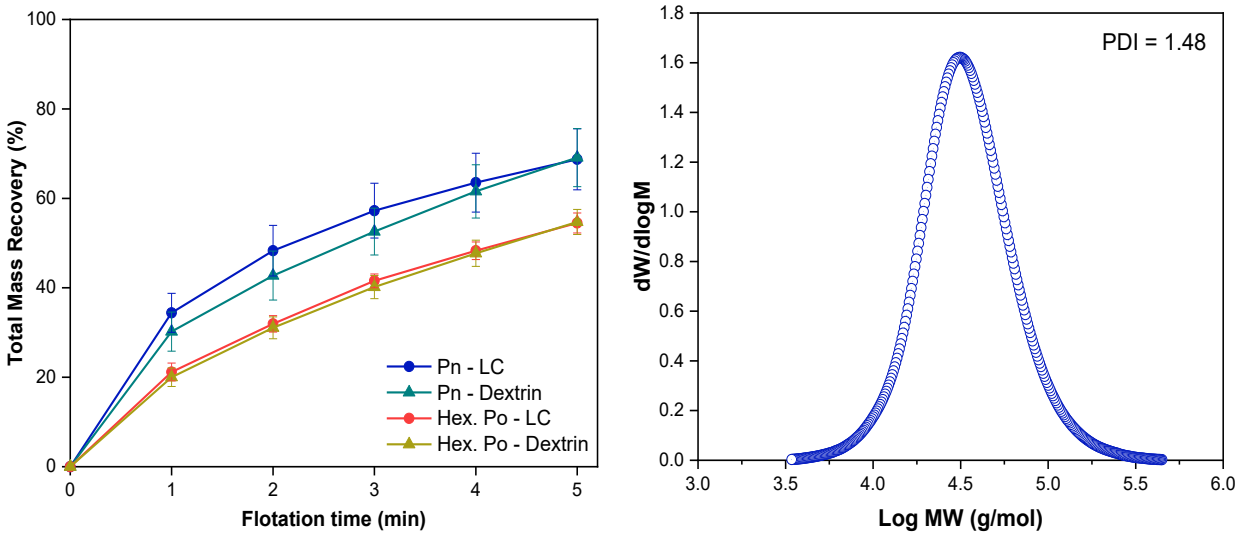

Figure 26: (a) Comparison of the kinetics single micro-flotation results between LC and potato dextrin, and (b) the potato dextrin MW distribution obtained by GPC. All flotations were performed with 9.66×10^{-6} M of PIBX, and 5 mg/L of depressant.

The molecular weight distribution of potato dextrin (Figure 26b) was also determined by GPC. A GPC Agilent 1260 Infinity equipped with two detectors (viscosity and refractive index), and two columns (TKS gel G6000PW XL-CP, designed for cationic polymers) connected in series for higher resolution. The instrument was calibrated using PEO standards provided by Agilent Technologies. An aqueous solution of 0.2 M sodium nitrate ($NaNO_3$) in deionized water was used as the mobile phase, and sample concentration was 1-2 mg/mL. The weight average molecular

weight of potato dextrin ($\overline{M_w}$=42,190 g/mol) is around 18 times smaller than LP. The single mineral micro-flotations results (Figure 26a) for pentlandite and hexagonal pyrrhotite show that the flotation kinetics and mass recovery of both minerals for LC and potato dextrin are identical. This indicates that the depression mechanism of polysaccharides depressants is not only dependent on the molecular size of the depressant but likely on its conformation/distribution on the mineral surface.

4.2.3. Micro-flotations of binary minerals

The efficiency of starch depressants was demonstrated by single mineral micro-flotation results (Figure 3). However, the complexity of sulfide minerals involves other factors, for instance, galvanic interactions, species within the pulp, and mineral surface oxidation rates (60). A better picture of the effect of starch depressants is achieved with binary mineral micro-flotations (Figure 27). Since hexagonal pyrrhotite and pyrite, both Fe-sulfide minerals, are the main gangue minerals in the pentlandite sample, the recovery values are given in terms of Ni recovery and Fe recovery (Fe present in the gangue minerals only). Similar trends to single mineral micro-flotations (Figure 23) are found in terms of the depression impact of the starch depressants but an improved separability is verified. Three different PIBX dosages were used: 3.22×10^{-6} M, 9.66×10^{-6} M, and 12.88×10^{-6} M.

A better result considering Ni recovery and Ni grade was achieved by using 9.66×10^{-6} M of PIBX (equivalent to 240 g/t). While the lower MW paste starch almost did not affect Ni recovery (91.2%) compared with the collector baseline (92.5%), the higher MW paste starch and the crosslinked starch had a Fe recovery no greater than 31.0% (Figure 27). The higher MW paste starch and the crosslinked starch also achieved the highest Ni grades of 19.0% and 20.4%, respectively, whereas the lower MW paste starch did not attain 17.5%. This shows that even though the higher MW paste starch and the crosslinked starch reduced pentlandite recovery, they may be considered as more selective. The Fe recovery vs Fe grade (Figure 27b) also had the best results with 9.66×10^{-6} M of PIBX and did not exceed 42.5% of Fe grade.

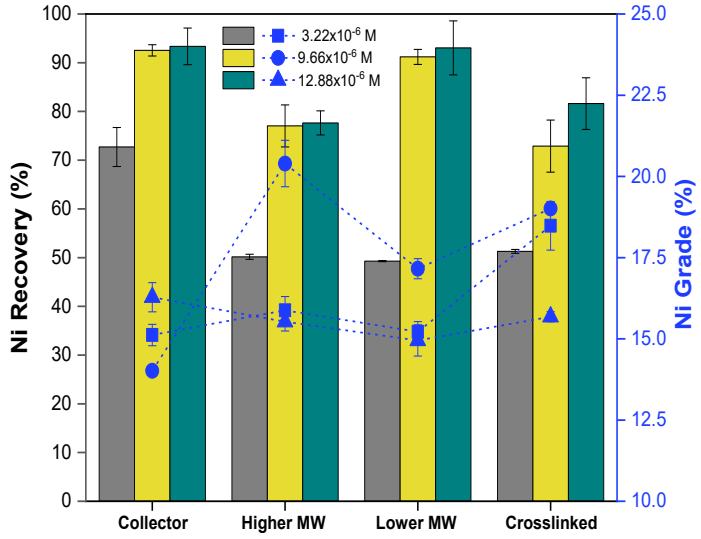

(a)

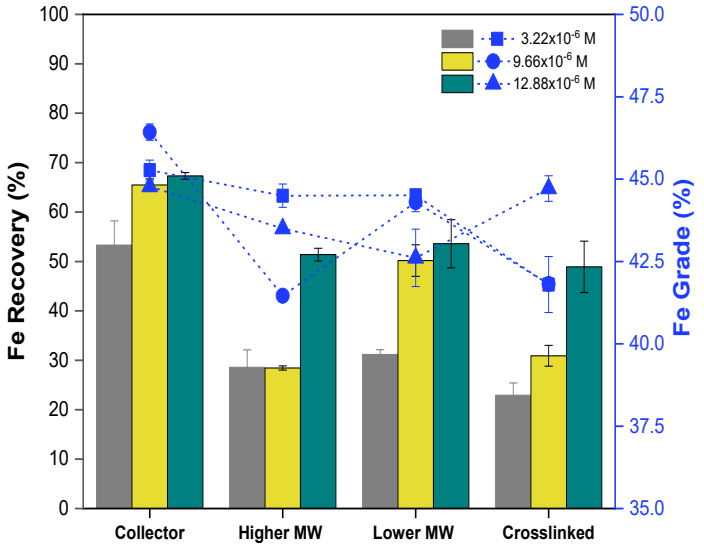

(b)

Figure 27: Ni recovery (a) and Fe recovery (b) results of mixed mineral micro-flotations with 3.22x10^{-6} M, 9.66x10^{-6} M, and 12.88 x10^{-6} M of PIBX. All flotations were performed with 5 mg/L of starch depressant.

The increased amount of collector to 12.88x10^{-6} M as an attempt to boost pentlandite recovery was detrimental in terms of Ni grade even though Ni recovery was slightly larger. A three times lower PIBX concentration (3.22x10^{-6} M is equivalent to 80 g/t) did not promote the necessary mineral particle hydrophobicity hence both minerals were poorly recovered. As hexagonal pyrrhotite and pentlandite have similar floatabilities, and surface charge density at alkaline pH, the

selectivity by using starch can be very challenging. Therefore, this shows the importance of a balance between the surface density of hydrophobic and hydrophilic species which are promoted by PIBX and starch depressants, respectively.

Ni recovery was negatively impacted when starch dosage was increased to 10 mg/L (Figure 28). For those, only higher PIBX dosages were employed, i.e., $9.66x10^{-6}$ M and $12.88x10^{-6}$ M. Ni recovery using 10 mg/L of LP dropped more than 20% when compared with 5 mg/L (Figure 27). However, there are few interesting points about this data: (1) Fe recovery of PP and LC were kept at similar values to those of 5 mg/L; (2) LP achieved the lowest Fe recovery for $9.66x10^{-6}$ M of PIBX; (3) the rise in collector dosage was a more critical parameter to increase Ni recovery than when 5 mg/L of depressant was used; 4) among the three depressants used, LC presented the best Ni recovery, especially when high PIBX dosages were utilized. The fourth point suggests that LC may be prevented from adsorbing on the mineral surface in the presence of high PIBX dosages and/or its interaction with the mineral surfaces is distinct from the paste starches. LC molecules may be removed and/or replaced in a competitive environment.

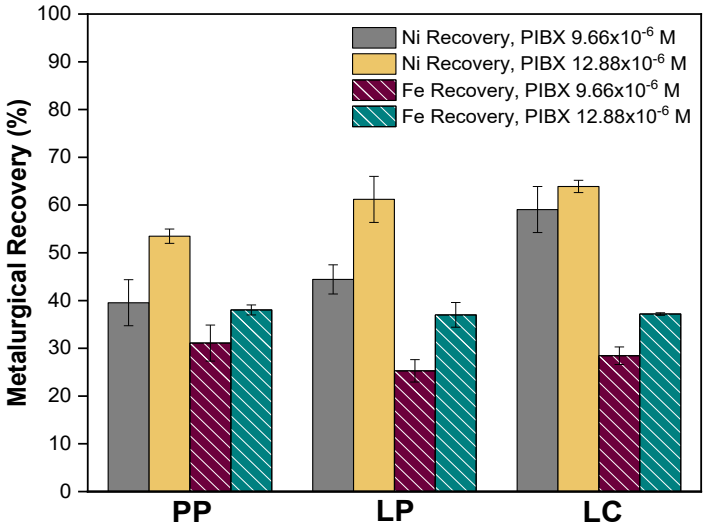

Figure 28: Metallurgical recovery results of mixed mineral micro-flotations. All flotations were performed with 10 mg/L starch depressant.

Nonetheless, in general, the data exposed in Figure 28 reinforce that there is a hydrophobic/hydrophilic balance which dictates the floatability behavior of pentlandite and hexagonal pyrrhotite. The significant Ni recovery seems to be a synergistic result of the preferential

xanthate adsorption on pentlandite over hexagonal pyrrhotite (36) associated with the starch improved selectivity when lower MW depressants are employed. Additionally, the hexagonal pyrrhotite oxidation in the presence of pentlandite due to galvanic interactions (see 2.2.1) may be a point to justify the greater interaction of hexagonal pyrrhotite with starch depressants in a mixed binary system scenario.

4.2.4. Micro-flotations of binary minerals after controlled oxidation

Considering that polysaccharides will adsorb on oxidation species (24,65), a sequence of micro-flotations were carried out after a controlled oxidation (Figure 29) using PP, LP, and LC. The same procedure was followed as described in Section 4.1.2. However, during conditioning, the mixed mineral pulp was purged with oxygen gas 4.3 purity (Praxair) for 30 min (101) either before or after xanthate addition. The set of micro-flotations with xanthate added before were intended to diminish the impact of oxidation on the collector adsorption. Dissolved oxygen (DO) concentration was measured before and after conditioning using an Orion Versa Star Pro as well as the pulp potential (vs SHE) using a TPS meter. The DO value of deionized water (8.12±0.05 mg/L, temperature 21 ºC, and pressure 709.2 mmHg) was considered as the baseline for all tests. During oxygen purging, the DO concentration was on average 31.45±0.37 mg/L.

The impact of oxidation on the floatability of hexagonal pyrrhotite and pentlandite is evident compared to the collector and collectorless results with no oxygen purging (Figure 27). Although a certain degree of oxidation can provide the formation of hydrophobic species in sulfide minerals (102) and help with dixanthogen formation (Equation 3), its excess generates hydrophilic species on the mineral surface such as metal hydroxides (see section 2.2.1). Those species impair the floatabilities of both minerals. Therefore, it seems that the oxidation species on the surface of both minerals were responsible for the greater depression, and no selectivity was achieved (Figure 29). In fact, for collector tests in Figure 27 using 9.66×10^{-6} M of PIBX, Ni recovery was above 90% while after oxidation it dropped to below 75%. Similarly, Fe recovery reduced around 20% after oxygen purging. It is difficult to evaluate whether the dramatic impact on the metallurgical recovery was a result of a more significant adsorption of starch or due to the formation of hydrophilic oxidation species.

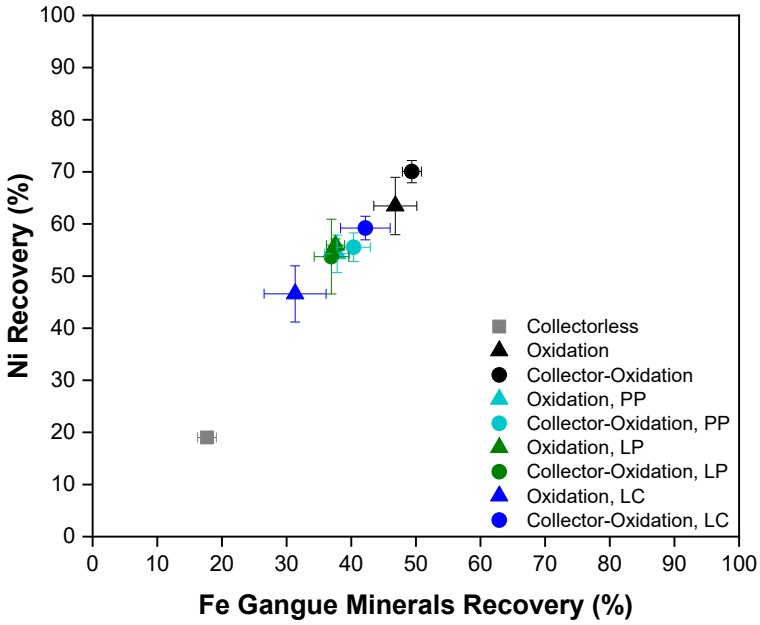

Figure 29: Metallurgical recovery results of mixed micro-flotations after 30 min of oxidation. All flotations were performed with 9.66×10^{-6} M of PIBX and 5 mg/L of starch depressant.

The floatability of sulfide minerals is not only controlled by pH changes but also dependent on the oxidation-reduction potential (Eh) (102). The presence of dissolved oxygen highly impacts the values of pulp potentials (Figure 30).

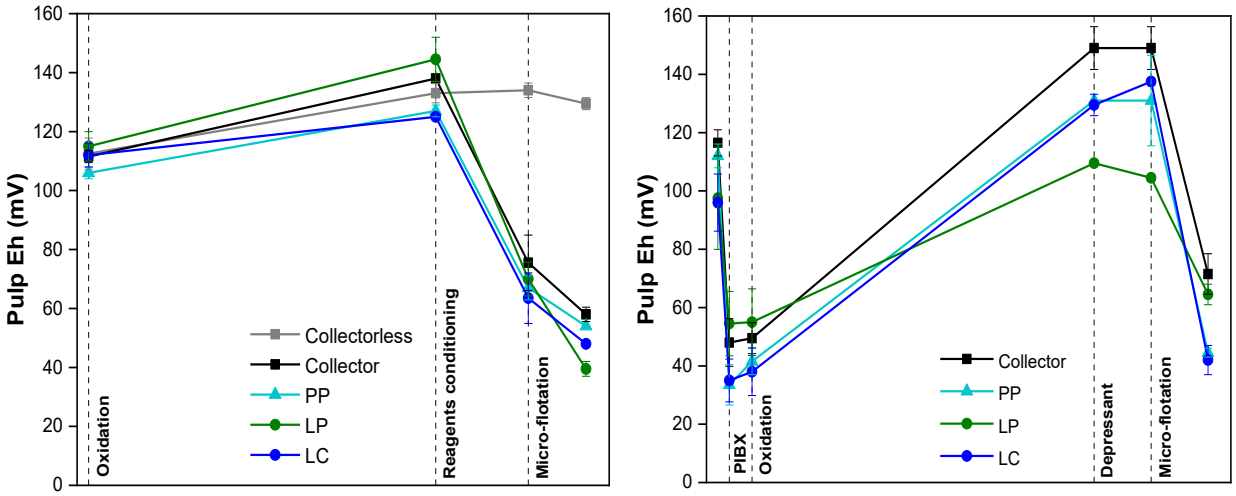

(a) **(b)**

Figure 30: Pulp potential changes during conditioning with oxygen purging (a) before and (b) after PIBX addition.

It is confirmed that the oxygen purging increases the pulp potential (Figure 30), as expected. This is valid even when PIBX is conditioned before the controlled oxidation (Figure 30b). The addition of xanthate drops the pulp potential to around 70 mV as discussed elsewhere (34–36). The variations in pulp potential upon starch depressant conditioning were minimal, suggesting that polysaccharides depressants cannot contribute to changes in the pulp potential. This result agrees with studies that mentioned that polysaccharides can passivate mineral surfaces (11). Therefore, polysaccharides' mechanism of depression is very distinct from DETA and/or DETA-SMBS combination, since polyamines and sulfur-bearing reagents can provide a more reducing environment, hindering further xanthate oxidation (see Equation 3).

4.3. Summary

Differences on the floatabilities of hexagonal pyrrhotite and pentlandite were observed for depressants with different molecular weight distributions and crosslinking additives, demonstrating the importance of those parameters for mineral recovery. For single minerals, comparing paste starches, the higher MW distribution was more detrimental to the recovery of both minerals. The crosslinked starch further reduced the recoveries of hexagonal pyrrhotite and pentlandite. Even though the use of the lower MW paste starch did not affect the Ni recovery of the binary mineral systems (5 mg/L of depressant and 9.66×10^{-6} M of PIBX), the highest Ni:Fe ratios are given by the higher MW paste starch and crosslinked starch at 2.7 and 2.4, respectively. The use of higher dosages of collector as an attempt to boost the mineral particle hydrophobicity such as 12.88×10^{-6} M, however, diminished Ni grades to up to 2.5-5.0%. Therefore, the choice of the best starch depressant for complex sulfide ores such as pyrrhotite/pentlandite mixtures is difficult since pentlandite and hexagonal pyrrhotite seem able to interact with the starch depressants.

Lastly, an attempt to promote a greater polysaccharide adsorption on hexagonal pyrrhotite by further oxidizing its surfaces was carried out. This strategy turned out to be very adverse for the metallurgical recovery of both minerals. Therefore, the assessment on whether the most substantial depression effect was due to the formation of hydrophilic metal hydroxides species or starch was unattainable. All starch depressants presented no (or very small) influence on the pulp potential during the conditioning step.

Chapter 5 Insight on the mechanism of depression of hexagonal pyrrhotite and pentlandite by starch with different molecular weights and crosslinking additives

The adsorption of polymers such as starch on solid surfaces is a complex phenomenon. Conversely to other reagents such as collector or metal ions, their adsorption is dependent not only on the affinity between the polymer and the surface but also on the solvent-polymer interaction (103). Therefore, good solvents will decrease the polymer adsorption. Kronberg (103) also listed eight factors that can contribute to the polymer adsorption, i.e. temperature, surface to volume ratio, ionic strength, multivalent ions, other additives, polymer charge density, pH, and the molecular weight. In this chapter, a distinction between the mechanism of depression of PP, LP, and LC is shown. This is complemented with the mechanism of adsorption of all starch depressants on hexagonal pyrrhotite and pentlandite surfaces. The mechanisms of depression and adsorption are based on the results of the kinetics and equilibrium adsorption measurements, XPS, QCM-D, zeta potential, contact angle, and AFM tests.

5.1. Experimental

For the following tests, all reagents used were analytical grade and can be seen in Table 8. Those not mentioned here, can be consulted in Tables 1 and 6.

Table 8: Description of reagents used in Chapter 5.

Compound	Formula	CAS	Purity	Supplier
D-glucose	$C_6H_{12}O_6$	50-99-7	≥99.5%	Sigma-Aldrich
Phenol	C_6H_6O	108-95-2	≥99 %	Fisher Scientific
n-heptane	C_7H_{16}	142-82-5	≥99 %	Fisher Scientific

5.1.1. Kinetics adsorption measurements

The first set of batch adsorption tests was performed to evaluate the amount of starch depressants adsorbed by hexagonal pyrrhotite and pentlandite in a certain period of time. For each test, 0.3 g of hexagonal pyrrhotite or 1.0 g of pentlandite was placed into a 250 mL beaker containing 100 mL of DI water. The beaker was sealed and kept under magnetic stir for 121 min. Nitrogen gas (N_2) was purged throughout the process to avoid excessive oxidation. A low depressant concentration (25 mg/L) was used to try to mimic the flotation data shown in Chapter 4. When used, PIBX (50 mg/L) was added at 1 minute (step 3), and the depressant after 30 minutes (step 5). During the test, the pH was maintained constant at 9.0-9.5 with NaOH/ H_2SO_4. 5 mL fractions were taken at 31, 61 min, 91 min and 121 min for analysis (steps 4, 6, 7, and 8) (Figure 31).

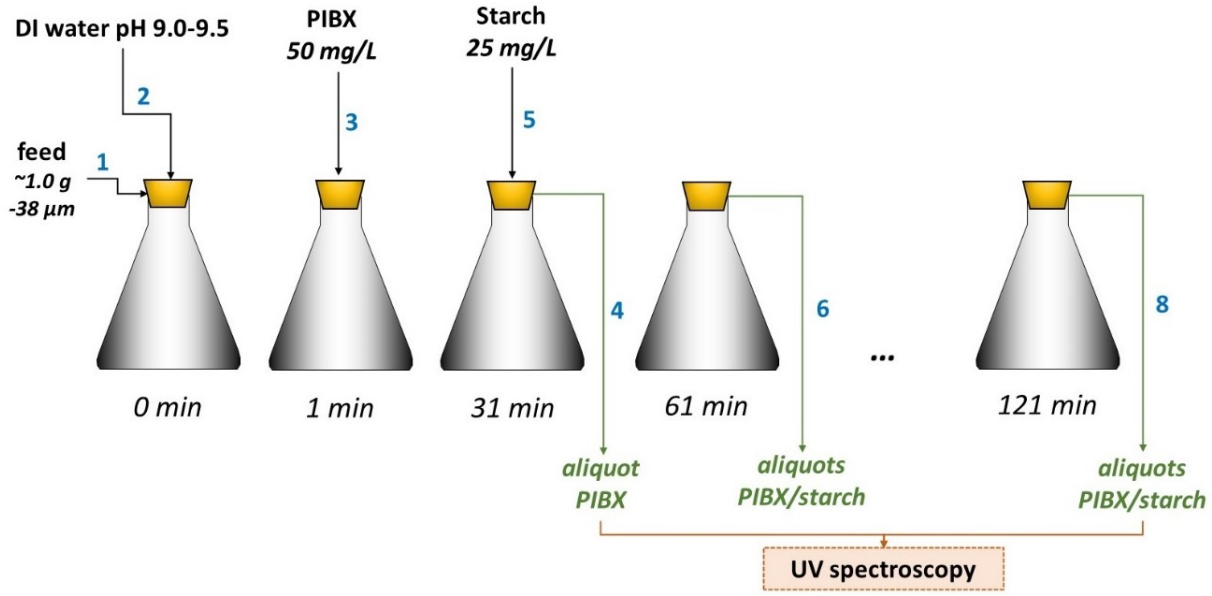

Figure 31: Procedure of the kinetics adsorption tests performed for single minerals (-38 µm) at pH 9.0-9.5. In the absence of collector, a starch depressant at 25 mg/L was added (31 min), and aliquots were taken every 30 min for total carbohydrates analysis. For the co-adsorption tests, collector was added at 50 mg/L (1min), and conditioned for 30 min before the starch depressant addition (25 mg/L). The total time for the abovementioned tests was 120 minutes.

The amount of collector and/or depressant depleted from the solution was considered as absorbed by the mineral phase over time (q_t in mg/m^2), and calculated by

$$q_t = \left(\frac{C_0 - C_t}{A}\right) V \quad (20)$$

in which C_t is the D-glucose concentration at time t (mg/L), C_o is the initial concentration of D-glucose (mg/L) present in a 25 mg/L of starch solution, A is the mineral surface area (m^2) determined by Brunauer–Emmett–Teller (BET) analysis (see section 5.1.4), and V (L), the volume of solution in contact with the mineral. Those were separately analyzed by UV–vis spectroscopy (UV-3600 Shimatdzu UV-VIS-NIR Spectrophotometer) for PIBX content at $\lambda = 300$ nm, and also for carbohydrate content in the remaining solution at $\lambda = 490$ nm after digestion with sulfuric acid and phenol (see 5.1.3). Adsorption tests were conducted at room temperature and repeated three times, whereas all UV readings were repeated two times, with a total of six readings for each point. Error bars show the standard error.

5.1.2. Equilibrium adsorption measurements

0.3 g of hexagonal pyrrhotite or 1.0 g of pentlandite was placed into a 250 mL beaker containing 100 mL of DI water at pH 9.0-9.5. The beaker was sealed and kept under magnetic stir for 60 min. N_2 was purged throughout the process. These tests were performed with PP, LP, and LC at concentrations varying from 25 to 200 mg/L (Figure 32).

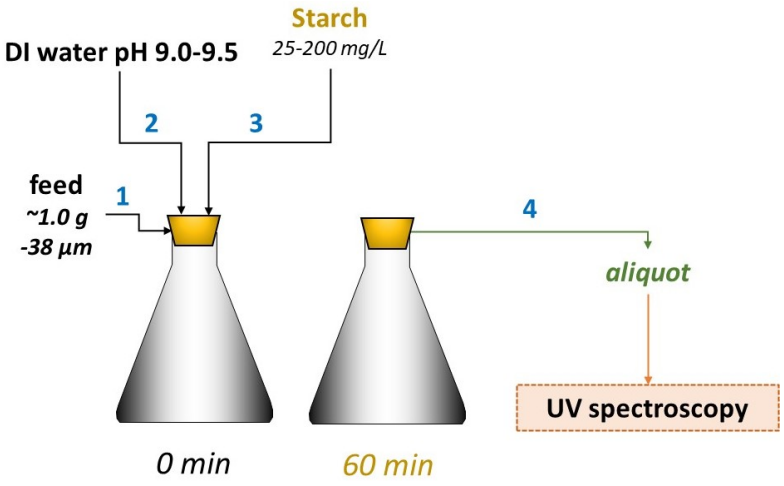

Figure 32: Procedure for the equilibrium adsorption tests performed for single minerals (-38 µm) at pH 9.0-9.5. A starch depressant with concentration ranging from 25 mg/L to 200 mg/L was added at 0 min, and a single aliquot was taken after 60 minutes for total carbohydrates analysis.

Co-adsorption experiments with PIBX were also performed (Figure 33). For those, PIBX was pre-adsorbed (step 3) for 30 minutes, followed by starch depressants at different concentrations. The starch was kept under agitation for an additional 60 minutes. The aim for the co-adsorption tests was to understand the impact on starch adsorption depending on the pre-adsorbed amount of collector.

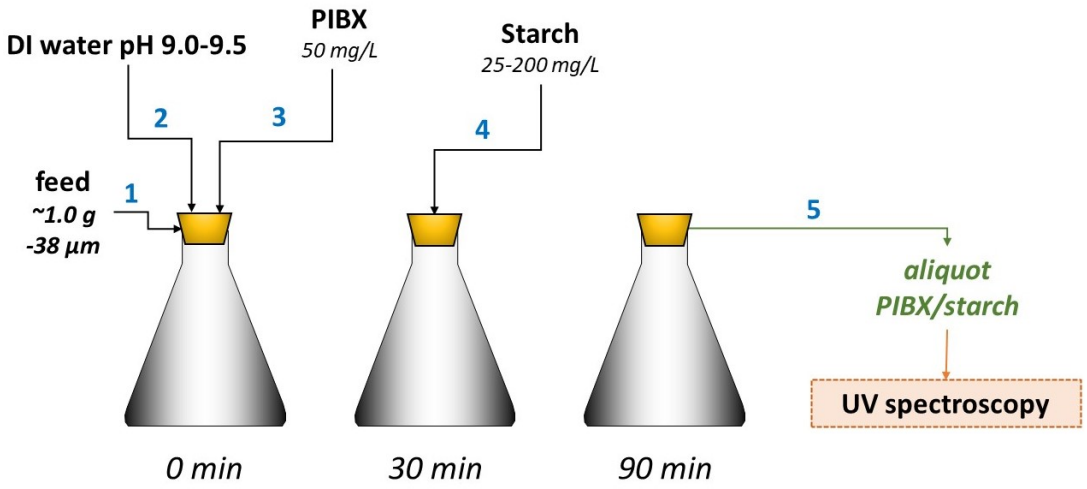

Figure 33: Procedure of the equilibrium co-adsorption tests performed for single minerals (-38 µm) at pH 9.0-9.5. Collector was added (50 mg/L) at 0 min, and conditioned for 30 min. A starch depressant with concentration ranging from 25 mg/L to 200 mg/L was added at 30 min. Two aliquots were taken after 90 minutes for total carbohydrates and remaining collector analysis.

The amount of depressant depleted from the solution at equilibrium is given by

$$q_e = \left(\frac{C_0 - C_e}{A}\right) V \tag{21}$$

where C_e is the D-glucose concentration at equilibrium (mg/L). The same reading procedure as explained in 5.1.1 applies.

Even though the Langmuir model may not be adequate to study the aforementioned systems, especially due to the fact that LC seems to slightly interact with pre-adsorbed xanthate (Figure 28), this model was used to calculate the maximum adsorbed amount (q_{max}), the equilibrium constant (K_{eq}) as well as the free energy of adsorption (ΔG^o), as follows

$$K_{eq} = \exp\left(-\frac{\Delta G^{\circ}}{RT}\right) \quad (22)$$

Beattie et. al (104) stated that polymer adsorption does not fit all the Langmuir model assumptions. It is important to note that the three main assumptions of this model are: each available site can take one molecule; there is no interaction between adsorbed molecules; and the solid surface contains a constant number of adsorption sites.

The following demonstration of the Langmuir equation is based on several works (105–107). Considering a hypothetical species Z being adsorbed on the surface of a solid particle. C_z is the concentration of Z in solution while C_{zo} is the initial concentration of it, and V the volume of the solution. It can be assumed that

$$VC_{zo} = VC_z + Wq_z \quad (23)$$

where W is the mass of the adsorbent (solid particle) and q_z is the amount of Z absorbed on the surface. The process of Z being adsorbed/desorbed from the surface can be characterized by the equilibrium reaction

$$C_z + \text{open sites on the surface} \underset{K_f}{\overset{K_z}{\leftrightarrows}} q_z$$

in which K_f is the adsorption constant, and K_z the desorption constant. The equilibrium constant (K_{eq}) of Equation 22 is also given by

$$K_{eq} = \frac{q_z}{C_z(\text{open sites})} \quad (24)$$

However, mineral surfaces cannot be considered as possessing a large number of open sites. Therefore, the linear adsorption case cannot be applied. As the total number of available sites on the mineral surface can be described by S_T, the open sites in Equation 24 correspond to the difference between S_T and q_z. Replacing S_T in Equation 24, the Langmuir equation can be written as

$$q_z = \frac{K_{eq} C_z S_T}{1 + K_{eq} C_z} \tag{25}$$

Equation 25 is valid at equilibrium. In order to determine the maximum amount adsorbed by the surface (q_{max}) and K_{eq}, a linearization of Equation 25 is necessary, resulting in

$$\frac{C_e}{q_e} = \frac{C_e}{q_{max}} + \frac{1}{K_{eq} q_{max}} \tag{26}$$

Based on the q_{max} value calculated using Equation 26, the percentage of the mineral surface covered by the adsorbate at equilibrium (θ_e) can be calculated by

$$\theta_e = \frac{q_e}{q_{max}} \tag{27}$$

The presence of a pre-adsorbed layer of collector may not be adequately described by the Langmuir model. When necessary, the Brunauer–Emmett–Teller (BET) model was chosen. The BET model is given by

$$q_e = \frac{Q_M B C_e}{(C_s - C_e)\left[1 + (B-1)\left(\frac{C_e}{C_s}\right)\right]} \tag{28}$$

where Q_M is the amount adsorbed in a complete monolayer (mg/m^2), B the equilibrium constant (L/mg), and C_s the saturation concentration (mg/L). This model can be considered as an extension of the Langmuir model (Equation 25) in which multilayers are formed. Its linearization results in

$$\frac{C_e}{q_e(C_s - C_e)} = \frac{1}{(Q_M B)} + \left[\frac{(B-1)}{Q_M B}\right]\frac{C_e}{C_s} \tag{29}$$

5.1.3. Phenol-sulfuric acid method for carbohydrates determination

After the adsorption tests, the carbohydrate concentrations in the remaining solutions were assessed by the phenol-sulfuric acid method for total carbohydrates as described in Nielsen (89) based on Dubois (108). 2 ml of the solution was pipetted in a clean glass tube. 50 µl of an 80% phenol solution was added to the tube and mixed with a vortex mixer. Then, 5 ml of concentrated sulfuric acid was quickly pipetted into the tube. It is important to make sure that sulfuric acid is added on the surface of the solution. The tube was mixed again using a vortex mixer, and left standing at room temperature (~20 ºC) for 10 minutes. The process of cooling down was finished with the tubes being immersed in a water bath (25-30 ºC) for an additional 10 minutes. Before the UV reading, the tubes were mixed again with the vortex mixer. After the molecule was dehydrated and reacted with phenol, an orange solution was obtained (109) (Equation 30). The orange solution was read at λ = 490 nm using a UV spectrometer. Its absorbance (A) was converted to µg of glucose using the calibration curve (Figure 34) built for D-glucose (Table 8).

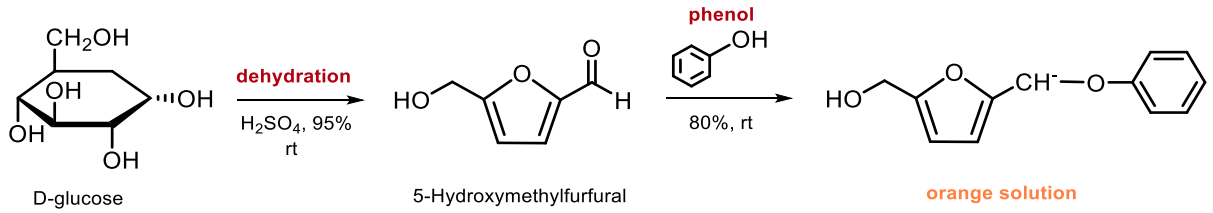

(30)

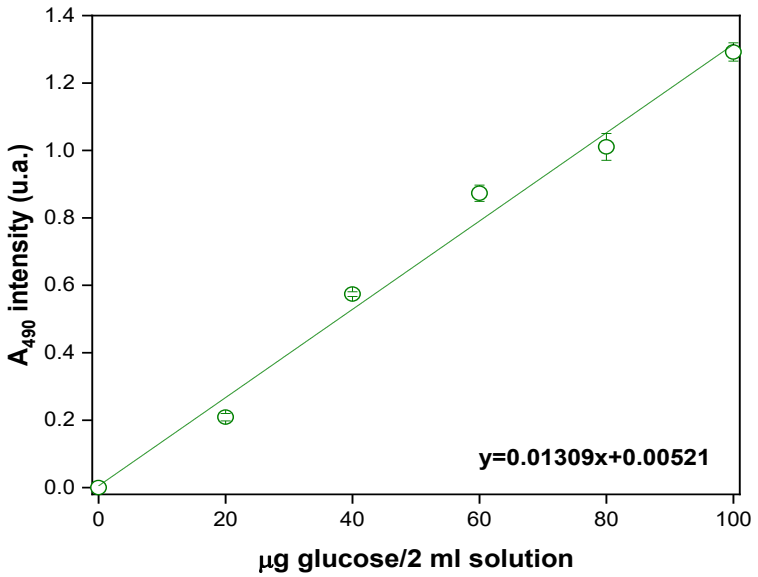

Figure 34: Glucose calibration curve obtained using a commercial D-glucose powder.

5.1.4. Brunauer–Emmett–Teller (BET) analysis for surface area measurement

The Brunauer–Emmett–Teller (BET) theory is used to measure the specific surface area of porous/powdered materials. In this theory, gas molecules are physically adsorbed on the solid surface forming a monomolecular layer (110). When nitrogen is used as the inert gas, the test is usually carried out at the temperature of liquid nitrogen (77 K). The duration of the surface area determination is dependent on the particle size distribution of the sample. The surface area of pentlandite and hexagonal pyrrhotite samples (-38 μm) was determined using an Autosorb-iQ-XR at nanoFAB. The first step consisted of outgassing the dry powder samples in a 6 mm glass cell. While degassing, the cell was heated up in three stages at 40, 100, and 200 ºC to remove remaining water molecules. After 60 min at 200 ºC, the cell was filled with nitrogen gas in order to be transferred to the analysis station. The method chosen was physisorption and the adsorbate gas, nitrogen. At this point, the cell was placed in a liquid nitrogen bath to enable the adsorption of the gas. For surface area measurement, only seven points of adsorption were set up.

5.1.5. Contact angle measurements

To measure the hydrophobicity of both minerals (33), a sequence of contact angle tests were performed. The contact angle (θ) (Figure 35) can be used to evaluate the wettability (induced or not) of a solid surface, and it is measured considering the liquid phase as the reference (Figure 35a).

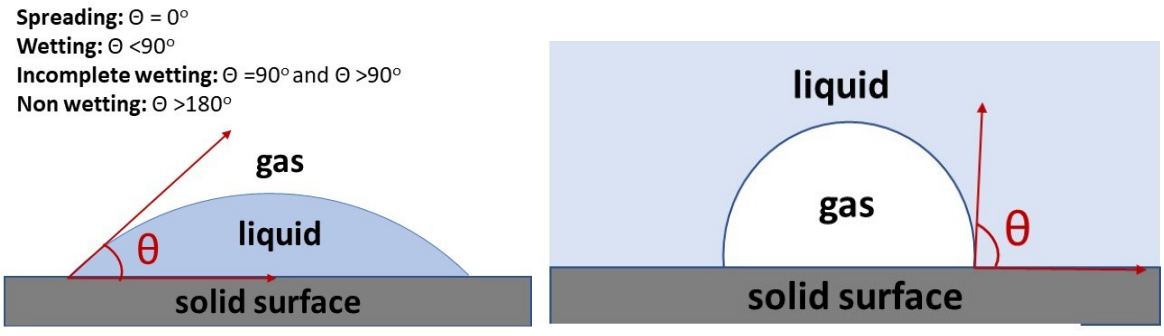

Figure 35: Schematic view of the contact angle on a smooth, flat, homogeneous, and inert solid surface.

In froth flotation (Figure 35b), the hydrophobic/hydrophilic aspect of the mineral surface dictates the mineral-air bubble attachment, and consequently, its floatability behavior. Usually, collectors such as xanthate are responsible to form hydrophobic species while depressants may act as a remover for those species or they can form hydrophilic layers, impairing the mineral particle interaction with the gas phase.

The Washburn method was carried out to quantify the contact angle of loose mineral powders (111) and determine the individual wettability of both minerals after conditioning with PIBX and starch depressants (PP, LP, and LC). It is the most reliable experiment to determine the contact angle of mineral particles (33). It is intended to directly evaluate the hydrophobic/hydrophilic balance on pentlandite and hexagonal pyrrhotite surfaces to justify the micro-flotation results (Chapter 4). It is based on the principle that the powder material can be defined as a collection of small capillaries, and the wetting liquid is able to penetrate into them due to capillary forces (111). The mass of liquid (w) penetrated in the powder material over time is provided by

$$\frac{w^2}{t} = C_w \frac{\rho^2 \gamma_{LV} \cos\theta}{\eta} \quad (31)$$

where η is the liquid viscosity in mPa.s, θ is the contact angle, and ρ is the liquid density in kg/m^3. Although it is recognized that the mineral particles studied have dissimilar surface roughness and chemistry, no further discussion and correlations with the Wenzel and Cassie-Baxter models are made in this study.

Before the experiments of wettability using water, the first set of tests (Figure 36) aimed to determine the capillary constant (C_w) which is characteristic of each powdered material. For that, a completely wetting liquid ($\theta = 0^o$), namely n-heptane ($\rho = 0.684$ g/m^3; $\eta = 0.409$ mPa.s; reference temperature 20 ^{o}C), was used. Tests specifications were: detection speed (6 mm/min); detection sensitivity (0.005 g); maximum measurement time (10 s); values (1000); acquisition (logarithmic); and fastest acquisition (300 s). For the measurements, a filter paper Kruss SH0621 was placed on the bottom of an aluminum cylinder and the powdered samples on top. The cylinder and a SV20 glass vessel 121.5 ml (70 mm) containing the wetting liquid were fixed in a Kruss 100 tensiometer (Figure 36). This allows the liquid to rise inside the cylinder when the contact with the wetting liquid surface happens. The capillary constants (Equation 31) obtained were 2.30×10^{-5} cm^5 and

$2.28x10^{-5}$ cm^5 for pentlandite and hexagonal pyrrhotite, respectively. The values were calculated considering the regression line obtained using the Kruss Laboratory Desktop software, in which several points were included for the average. The final average of three replicates was considered as the final value.

Figure 36: Set up for the Washburn experiment.

The contact angle θ was determined via the same specifications and calculations used for the C_w tests. For those, DI was used as the wetting liquid (ρ=0.998 g/m^3; η = 1.002 mPa.s; reference temperature 20 ºC), and single mineral measurements using 2.3-2.4 g of pentlandite or hexagonal pyrrhotite (-75+38 μm) were performed. Those samples are the same as the ones used for the micro-flotation tests (see 4.1.1). Before the Washburn tests, 2.50 g of the powdered mineral was conditioned in 50 ml of PIBX (50 mg/L) at pH 9.0-9.5 for 2 min. The starch depressants were added at a concentration of 75 mg/L and stirred for 5 min. This concentration was chosen based on the surface coverage values obtained during the equilibrium adsorption measurements. After conditioning, part of the water was discharged, and the remaining material (solids+water) was placed into a freezer for 24 hours. Those fractions were dried using a freeze-dryer for additional 48 hours. The dry powder was placed in aluminum cell as described above.

The last contact angle test was performed to assess the wettability of the Fe-S sensors after the QCM-D experiments (see 5.1.6). It was measured in air phase by the sessile drop method using the Instrument Attension|Theta by Biolin Scientific. A drop of MilliQ water (pH 7.03) was

deposited on the surface before and after the adsorption tests. Tests specifications were: Young-Laplace analysis mode; manually adjusted baseline; image recording 10 s at 1% (3.3 FPS). Tests were run at room temperature (19.8 ºC), and the OneAttension software used for data treatment.

5.1.6. Quartz Crystal Microbalance with Dissipation (QCM-D)

The QCM-D technique allows the measurement of the mass uptake of an absorbate per unit area of the sensor. This is based on alterations in frequency (Δf), and losses of energy (usually given in terms of dissipation - ΔD) of a quartz crystal balance once the system voltage has been turned-off. The ΔD behavior allows to also infer the nature of the absorbate, i.e., rigid or viscoelastic.

The adsorption of PP and LP on a hexagonal pyrrhotite-like surface (i.e., Fe-S sensor) was investigated by QCM-D (Q-Sense QE401). The hexagonal pyrrhotite-like sensor was purchase from Nanoscience, and made using a hexagonal pyrrhotite sample composed of 2.18% Mg, 0.39% Al, 2.83% Si, 32.63% S, 4.01% Ca, 0.39% Mn, 55.03% Fe, 1.02% Cu, 1.47% Zn, and 0.05% As. The purpose of this test is to explore the difference on adsorption of the different MW distribution paste starches. The Fe-S sensors were purchased from Nanoscience Instruments. To avoid oxidation of the iron sulfide coated sensors, they were only cleaned with ultrapure nitrogen gas before mounting them in the module. After mounting, milli-Q water at pH 9.2 was pumped into the instrument using an ISMATEC pump at a flow rate of 0.150 ml/min. This process was extended until a stable baseline was acquired (usually between 5-10 minutes). To better mimic the flotation conditions, a 50 mg/L solution of PIBX at pH 9.2 was pumped in for 20 minutes, followed by milliQ water at pH 9.2 for 2-3 minutes (rinsing step), then 100 mg/L of the paste starch solution at pH 9.2 for 1 hour and 30 min. All injections had the same flow rate and controlled temperature (22 ºC). To LP, 40 more minutes was added to the adsorption time in order to verify if desorption could happen with low MW depressants. Finally, the sensor was rinsed with pH 9.2 milli-Q water until new frequency stabilization. After the experiment, the sensor was dried with ultrapure nitrogen gas and contact angle measurements were taken (see 5.1.5). The obtained data were analyzed using the QSorft 401 software, and only the frequencies 3, 5, and 7 are shown.

5.1.7. Atomic Force Microscopy (AFM)

Hexagonal pyrrhotite (87% purity) and pentlandite (92% purity) samples from the Copper Cliff South mine in Sudbury, ON, Canada, purchased from Kaygeedee Minerals, were used for the AFM tests. They were cut and mounted in an epoxy base (2.5 cm diameter x 0.5 cm height). Prior to each imaging test, the epoxy mounted mineral sample was wet sanded using silicone carbide grinding papers (Buehler) of 600, 800, and 1200 grid for 1, 2, and 3 min each, respectively. The polishing steps (5 min each) consisted of using a MicroCloth Polishing Cloth (Buehler) with a 9 μm followed by a 3 μm polycrystalline diamond suspension (MeaDi Supreme – Buehler). Finally, a 0.05 μm MicroPolish Alumina (Buehler) was used as the last polishing step. The sample was then sonicated in 100 ml of nitrogen purged milliQ water (pH 7.86) for 5 min, and dried using nitrogen gas. The samples not subjected to conditioning were considered fresh surfaces. Additionally, as a baseline, both samples were conditioned in milliQ water at pH 9.0-9.5. PP, LP, and LC solutions at 200 mg/L were separately utilised for conditioning the mineral samples. All conditioning processes were run for 20 minutes.

AFM imaging was obtained via AFM tapping mode in nitrogen purged milliQ water (pH = 7.86) using an MFP-3D AFM system coupled with a Carl Zeiss Axiovert 200 inverted microscope. A triangular Scanasyst Fluid+ tip (Bruker) with a spring constant 0.7 N/m, and a triangular cantilever of silicone nitride (Bruker) were used for the measurements. Mineral samples were scanned over a 2 x 2 μm^2 area. Images were analyzed by the Asylum Research software. The root-mean-squared roughness (RMS) and the peak-to valley distance (PTV) for both minerals were determined using the processed images. The apparent layer thickness (ΔPTV) was calculated subtracting the PTV value for the mineral surface conditioned at pH 9.0-9.5. It was not calculated with the PTV value of fresh surface because sulfide minerals are very reactive and the layer thickness can have a contribution of metal hydroxides precipitation and/or surface dissolution (Figure 2). The starch surface coverage was calculated using ImageJ.

5.1.8. X-ray photoelectron spectroscopy (XPS)

In order to identify which mineral surface species reacted with paste starches (PP) and crosslinked starch (PC), 1.25 g of hexagonal pyrrhotite or pentlandite (-75+38 μm) was mixed in a

beaker with 50 ml of DI water at pH 9.2 for 1 min and then, a depressant was added at a concentration of 60 mg/L and mixed for 5 min. No xanthate was added. The pulp was frozen for 24 hours and dried using a freeze dryer under vacuum for an additional 72 hours. After that, they were immediately submitted to XPS analysis. The same specifications given in the section 3.1.2 apply for these XPS measurements.

5.1.9. Electrokinetics measurements

Zeta potential distributions were measured using a Brookhaven ZetaPALS at room temperature (20.0 ºC). 0.05 g of hexagonal pyrrhotite (-38 μm) from Virginia, United States, were freshly ground in a mortar for 40 s with a small amount of a 0.001 M NaCl nitrogen purged electrolyte solution (around 1 ml) with adjusted pH (from 2 to 12). The ground mineral was then mixed with 200 ml of the same NaCl solution, sonicated for 20 s, and then measurements were taken. Additionally to the baseline, other tests included reagents such as $CuSO_4$ salt (0.0001 mol/L) and the starch depressants (LP and LC) at 20 mg/L. Those additional reagents were conditioned for 2 minutes before the zeta potential measurements. All data were performed in triplicates and analyzed using the BIC Pals Zeta potential software.

5.2. Results

5.2.1. Surface area measurement

Since the results of adsorption of starch on the mineral surfaces are given in mg of glucose per m^2 of mineral surface, the surface area was determined. For pentlandite, the surface area is 4.257 m^2/g, while for hexagonal pyrrhotite is 14.240 m^2/g.

5.2.2. Kinetics adsorption measurements

The adsorption amounts of D-glucose per square meter of mineral surface (q_t) in the absence and presence of collector are given in Figure 37. The concentration used was 25 mg/L of starch depressant (PP, LP, and LC). At this concentration, almost no difference between pentlandite

and hexagonal pyrrhotite was verified, except for a slightly lower adsorption of LC on pentlandite (Figure 37a). Additionally, the stabilization of the adsorption amount of all depressants was fast and occurred in the first 30 minutes. This shows the great affinity of both mineral surfaces by starch. This affinity was independent of the MW distribution and crosslinking agents at 25 m g/L dosage.

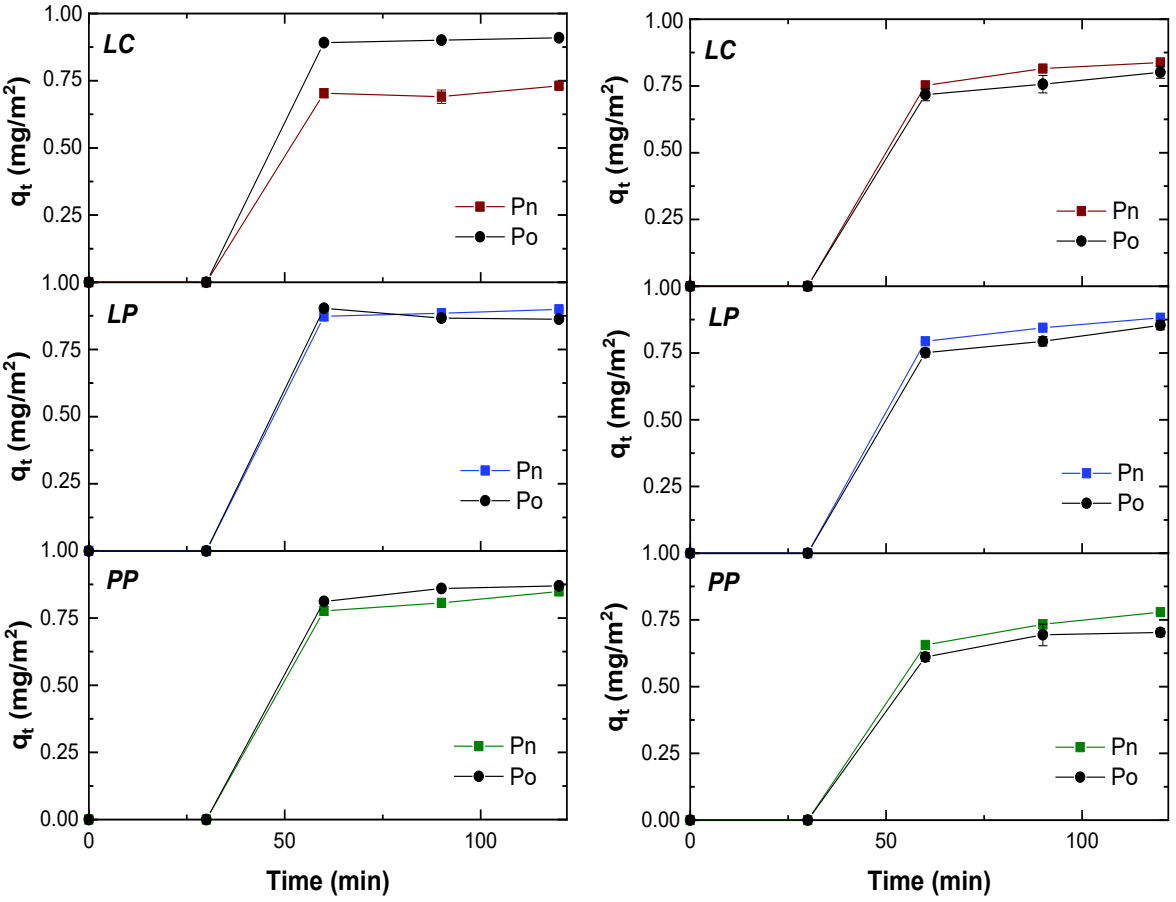

Figure 37: Adsorption amounts of D-glucose per square meter of mineral surface without the pre-adsorbed layer of PIBX (a) and the with pre-adsorbed layer of PIBX (b). Note: the size of the scatter points hindered the visualization of the error bars.

Although high collector dosages were used (50 mg/L), only a small influence on PP adsorption was observed (Figure 37b). The stabilization of the adsorbed amount occurred later than in the absence of collector at 60 minutes after the starch depressant addition. The collectors can,

therefore, interfere in the adsorption rate of polysaccharides depressants. Conversely, the addition of depressants did not have any major effect on the PIBX adsorption, as can be seen in Figure 38. This shows that, at low concentrations (25 mg/L), the depressants molecules might not replace the collector and/or the number of available adsorption sites is enough for both reagents. Pentlandite, however, adsorbs four times more PIBX than hexagonal pyrrhotite, reinforcing the high mass recoveries accomplished in the micro-flotation tests (Chapter 4).

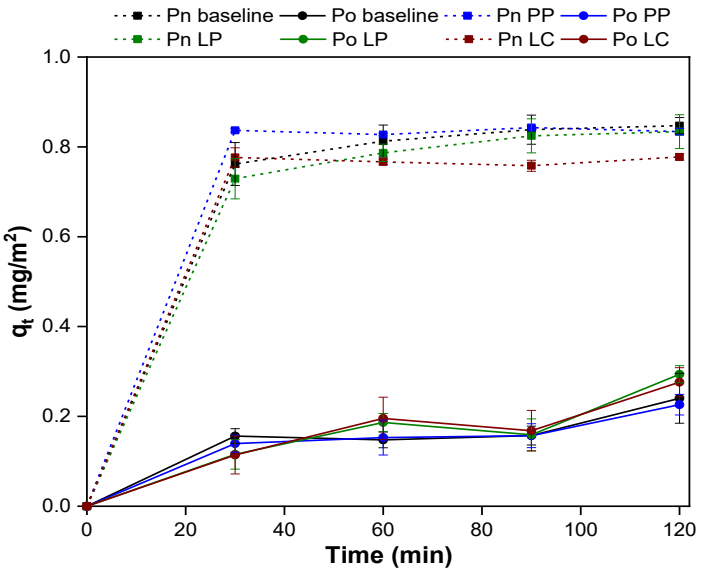

Figure 38: Adsorbed amount of PIBX on hexagonal pyrrhotite (Po) and pentlandite (Pn) as a function of time in the presence of starch depressants. Initial PIBX concentration was 50 mg/L while for all depressants their initial concentrations were 25 mg/L. Note that the PIBX baselines (only collector) for both minerals are included for comparison. The dash lines correspond to PIBX adsorption on pentlandite.

5.2.3. Equilibrium adsorption measurements

Further investigations regarding the adsorption behavior of PP, LP, and LC on hexagonal pyrrhotite and pentlandite were carried out at different concentrations, since the adsorption of polymers such as starch on solid surfaces is a complex phenomenon. Conversely to other reagents such as collector or metal ions, their adsorption is dependent not only on the affinity between the polymer and the surface but also on other factors such as polymer charge density, the molecular weight distribution (103), and the influence of lateral adsorbed molecules (112).

5.2.3.1. Comparison of the adsorption of paste starches on hexagonal pyrrhotite and pentlandite

The adsorption isotherms of PP and LP are given in Figures 39 and 40, respectively. The values of the adsorbed amount of D-glucose (q_e) are plotted against its concentration at equilibrium (C_e). With the exception of PP adsorption data with a pre-adsorbed PIBX layer, all data were fitted using the type I Langmuir adsorption model given by Equation 26 (Table 9). The linearization of all models can be consulted in Appendix 3.

Even though the Langmuir model may not be accurate to describe polymer interactions with solid surfaces (104,112), the purpose of this fitting is to provide a relative comparison between the three depressants used. As explained by Piccin et al. (113), the Langmuir model can give information about the maximum amount of D-glucose adsorbed (q_{max}), the affinity between the adsorbent and the adsorbate, thermodynamic parameters such as the Gibbs free energy (ΔG_{ads}) (Equation 22), as well as the interaction mechanism. Note that ΔG_{ads} is given in terms of kcal/mol of monomer and calculations are done considering the molecular weight of one α-D-glucose monomer, i.e., 180.16 g/mol, and R=8.314 J/mol.K. In this study, ΔG_{ads} was not used to determine the nature of the interaction, i.e. physisorption or chemisorption (114).

Table 9: Parameters calculated using the Langmuir model to fit the adsorption of paste starches on pentlandite and hexagonal pyrrhotite.

Pentlandite	**q_{max} (mg/m^2)**	**K_{eq} (L/mol)**	**R^2**	**ΔG_{ads}^***
LP	2.972	3.02E+05	0.99970	-7.32437
PP	2.985	2.03E+04	0.99662	-5.75878
PIBX-LP	4.642	1.24E+04	0.99156	-5.47266
Hex. Pyrrhotite	**q_{max} (mg/m^2)**	**K_{eq} (L/mol)**	**R^2**	**ΔG_{ads}^***
LP	3.108	1.18E+05	0.99951	-6.78177
PP	4.153	4.64E+04	0.99942	-6.23724
PIBX-LP	3.770	1.42E+04	0.98762	-5.55112

At all concentrations in a collectorless scenario, LP is similarly adsorbed by both minerals, (Figure 39). These results show great affinity of LP by pentlandite and hexagonal pyrrhotite

surfaces and confirms the kinetics adsorption data (Figure 37a). In fact, the q_{max} and ΔG_{ads} are very close (Table 9). The higher adsorbed amount of LP by pentlandite in a collector scenario seems to be controversial to the micro-flotation results (Chapter 4). However, this may indicate that either the collector molecules interact with paste starch macromolecules or the mineral wettability is not a direct function of adsorbed amount of depressant. Both assumptions are further discussed in the following sections.

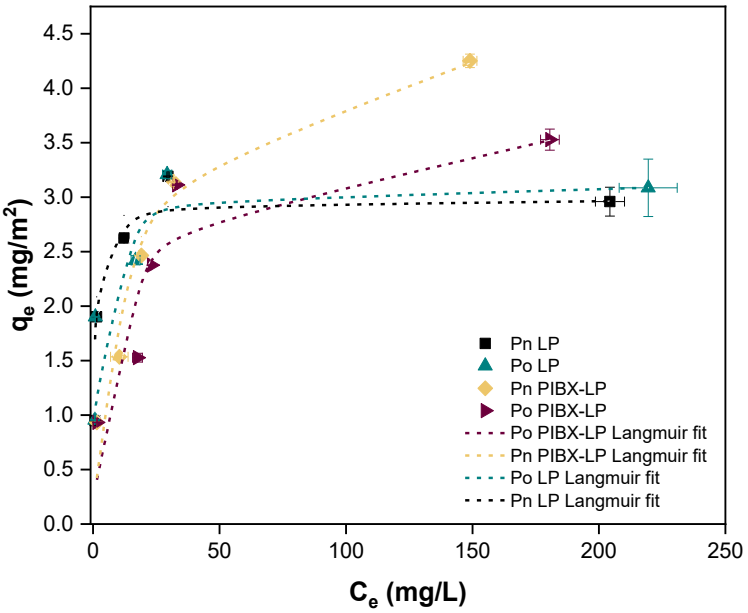

Figure 39: Adsorption amount of LP on hexagonal pyrrhotite (Po) and pentlandite (Pn) in the presence and absence of PIBX.

Significant differences in the affinity of PP on pentlandite and hexagonal pyrrhotite were only seen in the absence of the pre-adsorbed collector layer (Figure 40). Upon addition of PIBX, the amount of PP adsorbed was considerably lower and very similar for both minerals. In this case, the BET model given by Equation 29 for multilayers appeared to be more adequate (Table 10). In addition, B shows the affinity between adsorbent and adsorbate and usually ranges from 100 to 200. Values above 200 suggest that the solid surface can present a certain porosity, which may be consistent with real surfaces after the grinding process. The fitting with the BET model does not reveal that PP chains are in totality superimposed. However, the presence of PIBX might shape the conformation of PP in an arrangement similar to “tails-up” (Figure 42a).

Table 10: Parameters calculated using the BET model to fit the adsorption of PP on pentlandite and hexagonal pyrrhotite with the pre-adsorbed layer of PIBX.

mineral	Q_M (mg/m^2)	C_s (mg/L)	B (L/mg)	R^2
Hexagonal pyrrhotite	1.10	354	269.82	0.99936
Pentlandite	0.77	253	109.98	0.99938

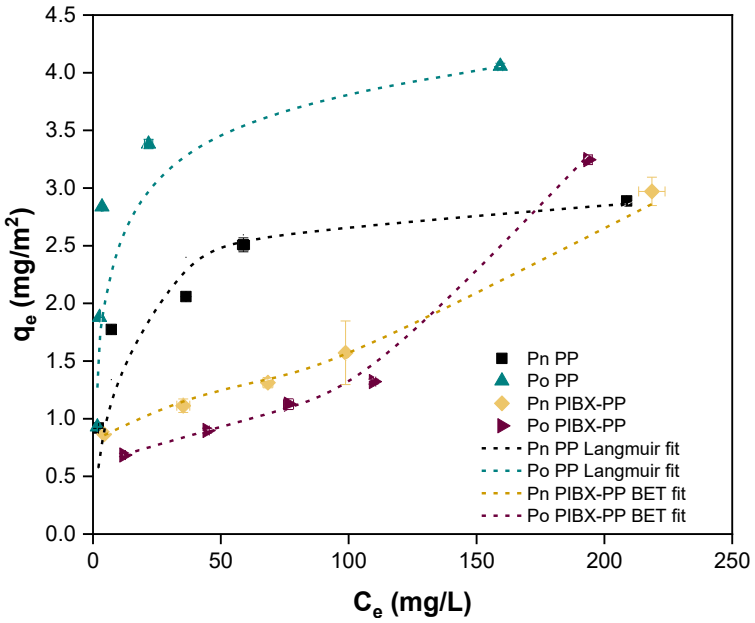

Figure 40: Adsorption amount of PP on hexagonal pyrrhotite (Po) and pentlandite (Pn) in the presence and absence of PIBX.

Furthermore, at equilibrium and in a collectorless scenario, the adsorption of both paste starches on pentlandite is independent of the molecular weight (Figures 39 and 40). Hexagonal pyrrhotite, however, adsorbs more of PP (Figure 40), showing a higher affinity by the higher MW paste starch. The lower stability in solution of polymers with high molecular weights explains this affinity (24). Therefore, the loss in conformational entropy of PP chains is compensated by a favorable interaction (24) between starch groups and hexagonal pyrrhotite surface.

The difference comparing the adsorption amount of PP and LP in the presence of PIBX (Figures 39 and 40) on both minerals is also associated with the molecular weight distribution. The adsorption fitting might be an indirect response of the conformation assumed by the paste starch depressants once adsorbed. The small chains may assume a denser packing on the mineral surface

and can still be adsorbed even in the presence of collector, simulating a monolayer (Langmuir model fitting). On the other hand, PP is likely under a certain steric hindrance with the lateral collector molecules. Therefore, the nature and size of collector molecules can be used to modulate the density of hydrophilic species on a mineral surface.

5.2.3.2. Adsorption of the low molecular weight crosslinked starch on hexagonal pyrrhotite and pentlandite

The addition of metal ions seems to increase the interaction between depressant-mineral surface, especially for hexagonal pyrrhotite (Figure 41). The greater depressing effect of LC observed in Chapter 4 is likely due to its conformation (i.e., distribution on the surface). The presence of copper ions in the starch structure may not only promote a change in the size but also the shape of the polymer chains, stretching the structure in a similar manner to that of sodium ions during the gelatinization process (85), i.e. by repulsion. Therefore, this depressant might cover a larger surface area (Figure 42b), promoting a higher mineral hydrophilicity. The coverage of this large area is possible since the polysaccharide may assume a "lay-flat" conformation (Figure 42b). Therefore, its mechanism of depression certainly differs from the one of paste starches.

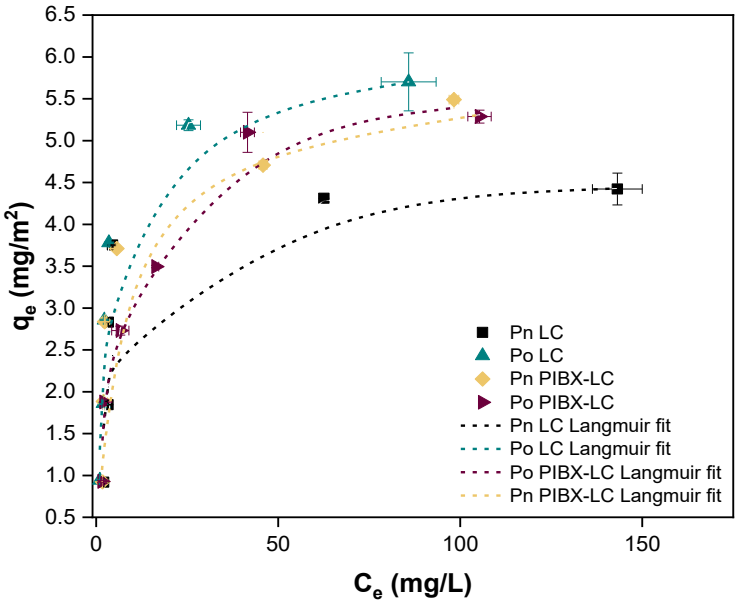

Figure 41: Adsorption amount of LC on hexagonal pyrrhotite and pentlandite in the presence and absence of PIBX.

Additionally, LC adsorption is more significant on hexagonal pyrrhotite, demonstrating the higher affinity of this surface for the new crosslinked starch as hypothesized (Figure 41 and Table 11). Nevertheless, in a collector scenario, pentlandite and hexagonal pyrrhotite adsorb the same amount of depressant, confirming that this parameter is not relevant to explain the differences in wettability of both minerals.

Table 11: Parameters calculated using the Langmuir model to fit the adsorption of the crosslinked starch on pentlandite and hexagonal pyrrhotite.

Pentlandite	**q_{max} (mg/m^2)**	**K_{eq} (L/mol)**	**R^2**	**ΔG_{ads}^***
LC	4.551	4.60E+04	0.99811	-6.23253
PIBX-LC	5.676	3.48E+04	0.99373	-6.07072
Hex. Pyrrhotite	**q_{max} (mg/m^2)**	**K_{eq} (L/mol)**	**R^2**	**ΔG_{ads}^***
LC	5.938	5.09E+04	0.99871	-6.29181
PIBX-LC	5.662	2.58E+04	0.99693	-5.89638

At this point, it might be possible to deduce that the starch chain size (molecular weight) is not the only factor affecting the aforementioned minerals' floatability but its surface arrangement given indirectly by the model fitting (Langmuir vs BET). Both factors will be further investigated.

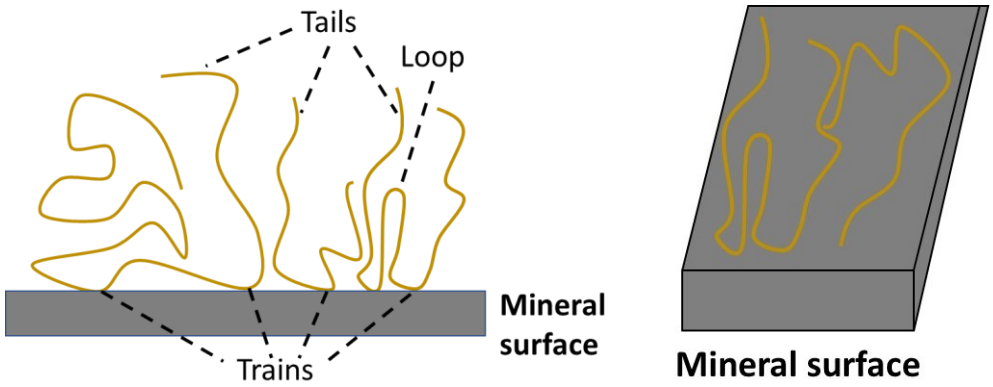

Figure 42: Schematic representation of a homopolymer conformation adsorbed on a mineral surface, showing the trains, tails, and loops ("tails up") (a), and laying flat on the solid surface (b). Modified from (117).

5.2.3.3. Adsorption of collector on hexagonal pyrrhotite and pentlandite in the presence of starch depressants

To investigate the interaction of starch depressants with collector molecules, the amounts of adsorbed PIBX according to the concentration of the starch depressant is also given (Figure 43). Although in general the amount of pre-adsorbed PIBX is kept at constant levels, particularly for pentlandite (Figure 43a), it is noticeable that some interaction with the depressants can happen (Figure 39, 40 and 41). The presence of considerable amounts of starch (i.e. 100-200 mg/L) seems to be a point of adsorption improvement of available PIBX in the pulp for hexagonal pyrrhotite (Figure 43b). It is known that polysaccharides can interact with hydrophobic substances such as oleates (115,116). This may not indicate that the increased amount of PIBX is necessary on the mineral surface. The PIBX molecules are trapped within the helical form of starch chains (especially amylose) via interaction with its hydrophobic groups, explaining its depletion from the solution (115,116).

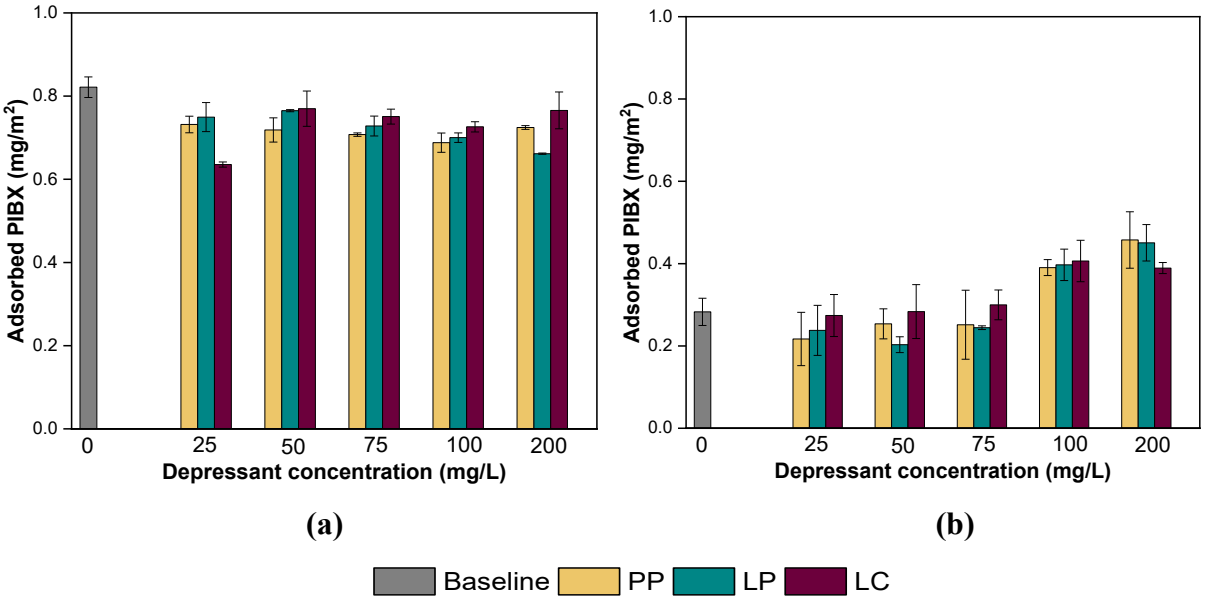

Figure 43: Comparison of PIBX amount adsorbed on (a) pentlandite and (b) hexagonal pyrrhotite followed by different concentrations of the starch depressants.

5.2.4. Wettability of single mineral systems with paste starches

To quantify the differences of hydrophobic/hydrophilic balance on mineral surfaces according to the molecular weight of the paste starch depressants, contact angles (θ) were obtained for powdered single mineral samples using the Washburn method (Figure 44).

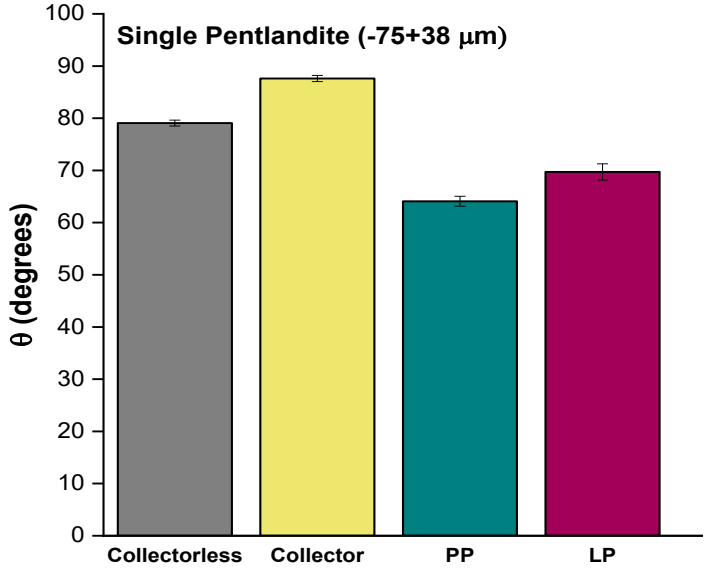

(a)

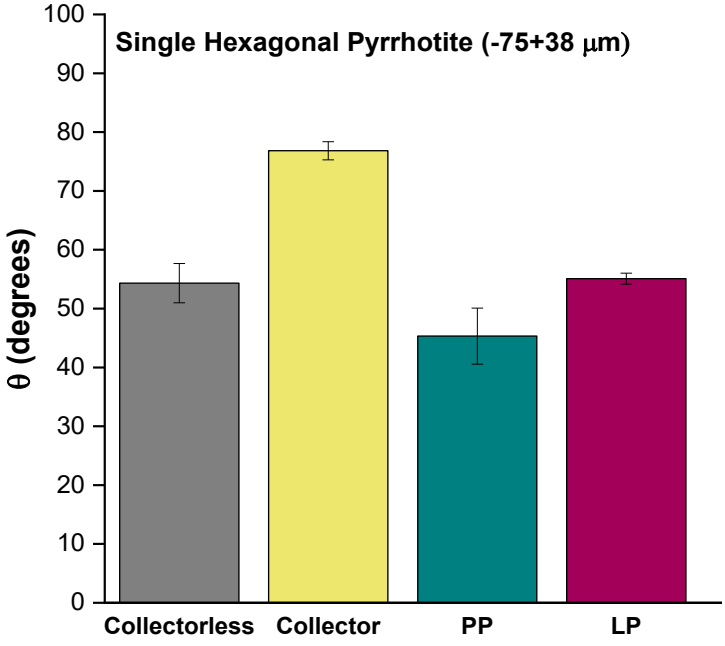

(b)

Figure 44: Contact angle values of pentlandite (a) and hexagonal pyrrhotite (b) obtained with the Washburn method for loose powdered materials.

Pentlandite contact angle close to 90º with no depressants confirms that this mineral in fact adsorb more PIBX than hexagonal pyrrhotite. In addition, the decrease in contact angle comparing the collector only and after depressants being used can be as significant as 20º for pentlandite, and 30º for hexagonal pyrrhotite. PP is responsible for the lower contact angle on both minerals. Specifically for hexagonal pyrrhotite, the contact angle generated by conditioning with PP is at around 50º (Figure 44b). Although this appears contrary to the equilibrium adsorption data in terms of adsorption amounts, these results firmly agree with the single micro-flotation recoveries (Figure 23). Therefore, these experiments have proven that the mechanism of depression is ruled by other factors than the adsorbed amount of paste starch. They may include additional factors such as the layer conformation and hydration levels of the paste starches (117,118).

Moreover, the θ values in Figure 44 are given by the speed that the wetting liquid rises into the cylinder, and cos θ can be calculated by the linear regression of the curve mass^2 vs time (Figure 45).

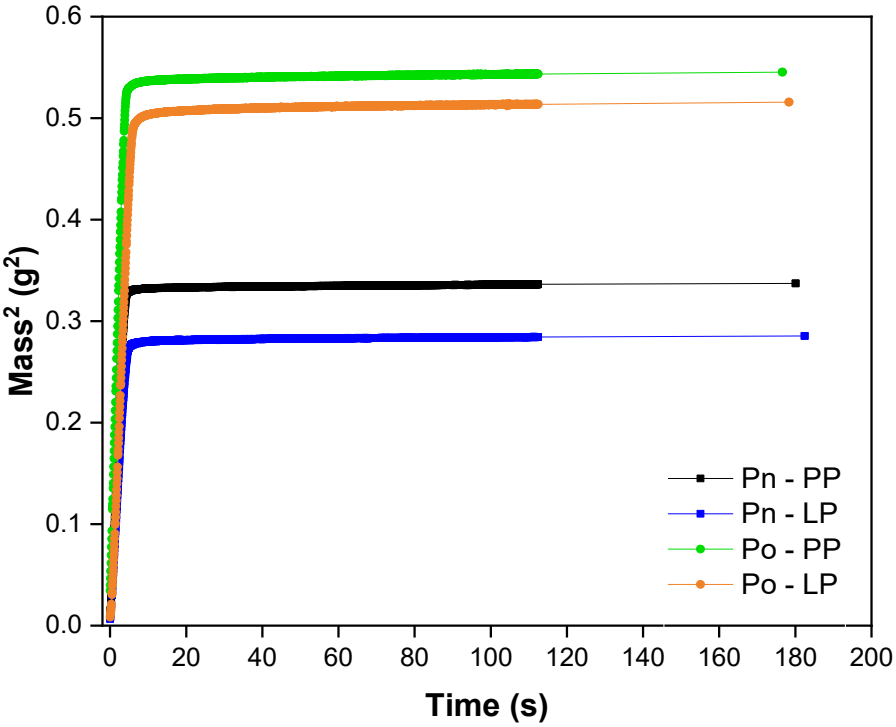

Figure 45: Mass^2 of water risen into the sample holder vs time for pentlandite (Pn) and hexagonal pyrrhotite (Po) after conditioning with paste starches.

The amount of water penetrated in the capillary cylinder (mass of the wetting liquid) also reinforces that hexagonal pyrrhotite is more hydrophilic than pentlandite after conditioning. Among all depressants used, PP is able to hold more water molecules. The difference in hydration of the different polysaccharides can determine which depressant is more detrimental to the flotation behavior of a certain mineral (118). A description of this phenomenon is detailed in the following sections. Only one replicate was used to show the difference of the amount of water that has risen into the tube after the conditioning of the mineral samples with paste starches. All mass^2 vs time graphics can be consulted in Appendix 4.

5.2.5 Adsorption of paste starches on a pyrrhotite-like sensor by QCM-D measurements

QCM-D measurements were performed to further observe the adsorption differences that can be generated due to the difference of MW distributions of paste starches (Figure 46). The mass uptake by the sensor after paste starch addition can be evaluated by the drop in frequency (Δf), while the dissipation (ΔD) gives the nature of the adsorbed material. The results showed that the addition of PIBX did not significantly modify Δf and ΔD, as expected, suggesting that these molecules behave similar to a rigid layer (119) (Figure 46).

After the rinse step and addition of a 100 mg/L of starch solution, Δf dramatically decreased whereas ΔD increased. The latter confirmed the softness of the layer that has been adsorbed. Both starch depressants did not fit the Sauerbrey model approach due to the great energy dissipation observed (Figure 47). The decrease in Δf was more pronounced for the lower MW paste starch (Δf~30 Hz), suggesting a more significant mass uptake of this depressant by the Fe-S sensor (Figure 46). This agrees with the adsorption data of powdered minerals (Figures 39 and 40 1) in a collector scenario. Similarly, ΔD of LP also experienced a more significant rise, which can also indicate an increase in viscoelasticity of the adsorbed layer. Nevertheless, although more of LP adsorbed on the sensor (Figure 4b), this depressant provides the higher final contact angle at 13.0º. This validates the contact angle measurements using the Washburn method (Figure 44), and reinforces that the depression mechanism cannot be explained by the amounts adsorbed.

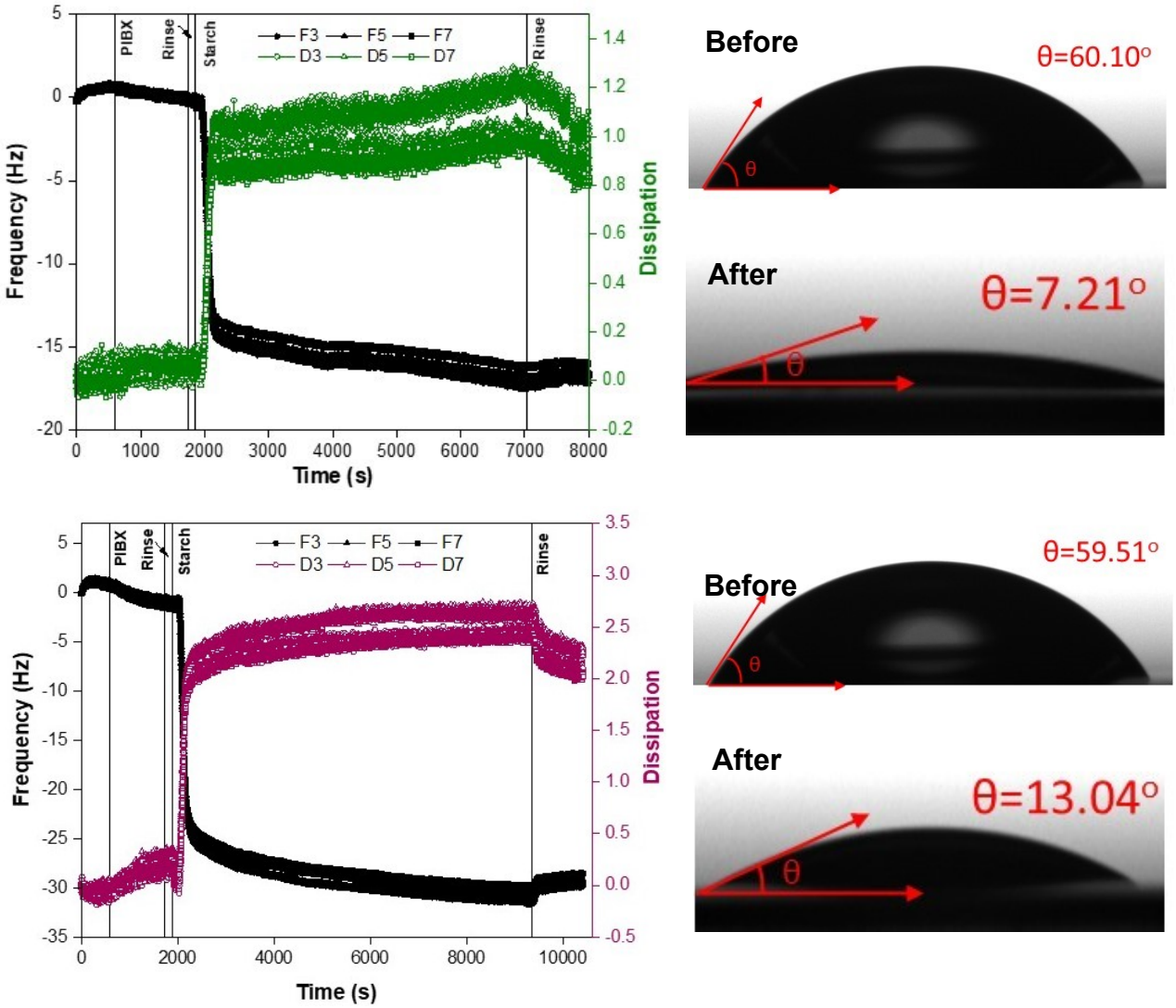

Figure 46: Changes in frequencies (Δf) and dissipations (ΔD) upon addition of collector and PP (a) or LP (b) on a Fe-S sensor, and their respective contact angles values before and after the QCM-D tests.

Since the QCM-D measurement provides a more controlled adsorption environment, the conformation of paste starches was modelled in terms of layer thickness (120). The measurement of the layer thickness was obtained by using the Kelvin-Voigt viscoelastic model available in the Q-Tools software. This approach considers that the adsorbed layer has a relative "rigidity", albeit it cannot be modeled by the Sauerbrey model. While fluid density (1,000 kg/m^3) and viscosity (0.001 kg/ms), and the adsorbed layer density (1,200 kg/m^3) were kept as fixed parameters, the adsorbed layer thickness, viscosity and shear modulus were attributed an interval and could be

modeled. Since the first layer corresponding to PIBX adsorption is a rigid layer, the starch layer was modeled as the only layer (layer 1). The harmonics 5 and 7 were used due to the smaller chi-square (χ^2) obtained. The x-limits used can be seen in Appendix 5. The layer thickness of both starches stays steady till the last rising step (Figure 47). For PP, the layer thickness ranged from 14 to 16 nm, and for LP, it varied from 16 to 18 nm. Therefore, considering the values of the mass uptake and dissipation of LP, since both depressants have a similar layer thickness, it is clear that LP assumes a denser (more viscoelastic) and compact packing conformation/arrangement.

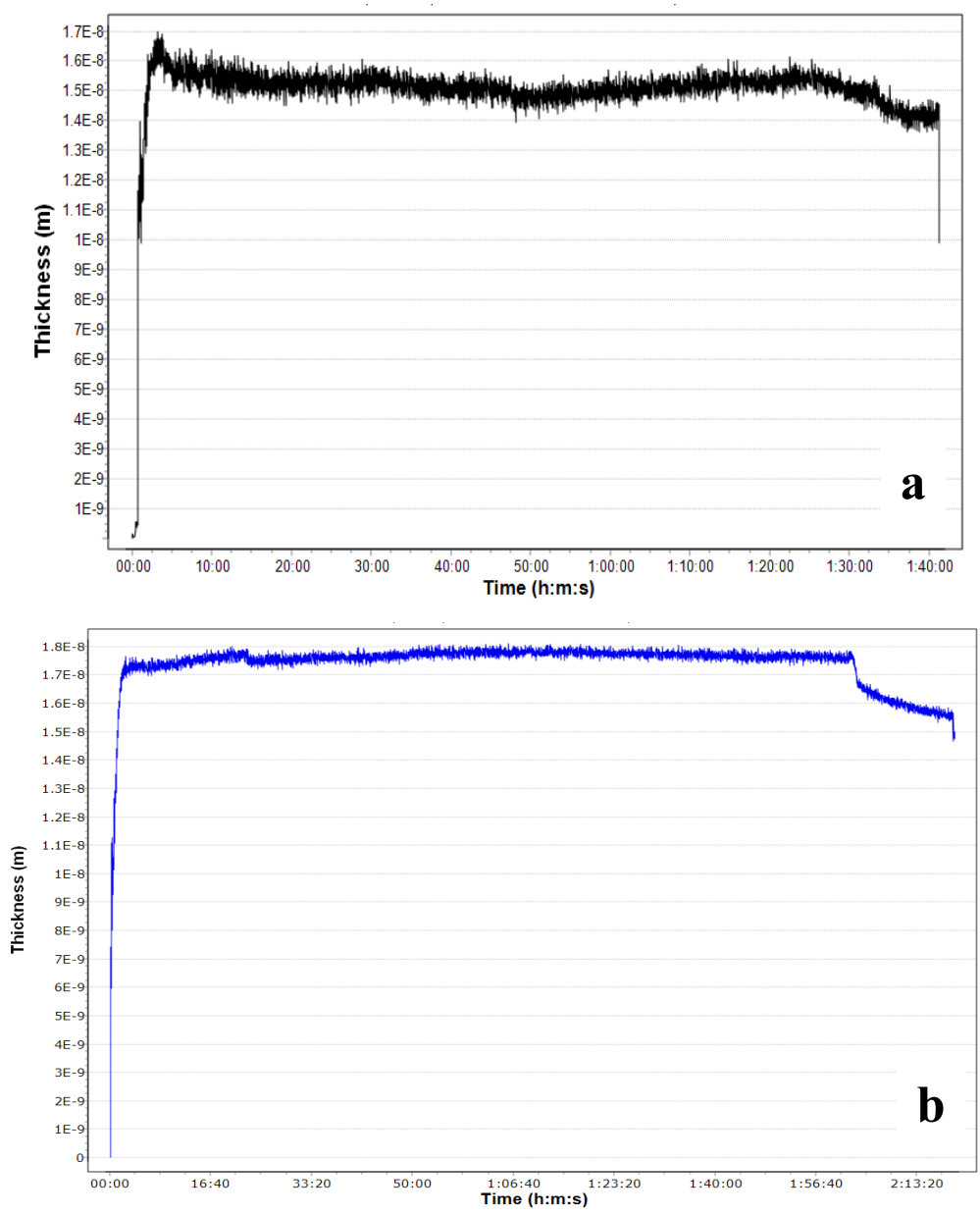

Figure 47: Layer thickness of the PP (a) and LP (b) on the Fe-S sensor.

5.2.6. Topography, morphology, and surface coverage of starch depressants by AFM imaging

Images acquired by the tapping mode AFM are given in Figures 48 and 49 for individual pentlandite and hexagonal pyrrhotite, respectively. Only the height images are provided for fresh and pH 9.0-9.5 conditioned surfaces. It can be noted that both mineral surface roughness increased after being conditioned with milliQ water at pH 9.0-9.5. For pentlandite (Figure 48b), it appears evident that some products might have been precipitated, for instance metal hydroxides. The same could be applied to hexagonal pyrrhotite (Figure 49b). However, this mineral surface seems to have been modified due to its surface dissolution (Figure 2) given by the small holes (Figure 49b) while a metal hydroxide layer has been deposited (see the difference in RMS with the bare mineral surface). The details of the surface topography can be consulted in Table 12.

Table 11: Topography and surface coverage details of starch depressants (200 mg/L) adsorbed on pentlandite and hexagonal pyrrhotite (pH 9.0-9.5)

		RMS (nm)	**PTV (nm)**	**ΔPTV (nm)**	**Coverage (%)**
Pentlandite	Fresh	1.06	10.28	-	-
	pH 9.0-9.5	1.64	18.80	8.52	-
	PP	5.10	24.03	13.75	18.40
	LP	4.73	43.53	33.25	3.36
	LC	6.56	43.44	33.17	22.59
Hexagonal Pyrrhotite	Fresh	0.83	8.93	-	-
	pH 9.0-9.5	1.40	12.42	3.49	-
	PP	5.18	49.36	40.43	27.48
	LP	2.34	21.11	12.18	25.66
	LC	1.77	12.80	3.87	44.96

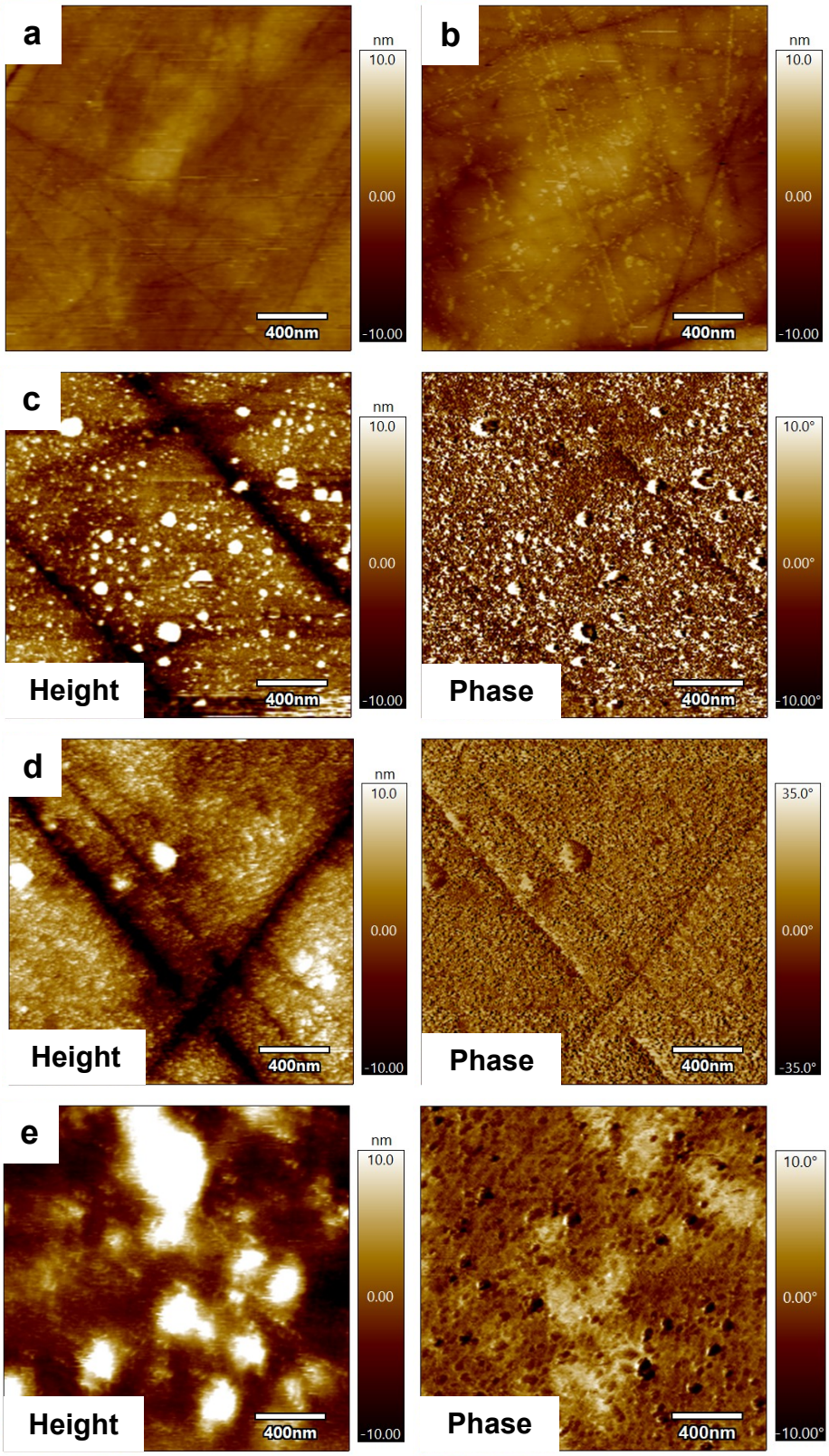

Figure 48: AFM images of pentlandite (a) fresh surface; (b) pH 9-9.5; (c) PP; (d) LP; and (e) LC.

A 2D analysis of the height indicates the topography and morphology of the adsorbed layer of starch depressants. The conformation/distribution and layer thickness are very distinct on both minerals, and no pattern was detected. To a certain extent, a patterned distribution may occur when the polysaccharide directly interacts with the atoms present on the mineral lattices of a specific cleavage plan. In the case of sulfide minerals, since it is understood that polysaccharides interact with the metal hydroxylated species (24), their distribution can be random. These images also confirm that all depressants adsorb on both minerals as demonstrated by the adsorption tests. In general, their disposition on the mineral surface is not homogenous but rather characterized by the formation of structures with a hemispherical-like feature.

More specifically, in the case of pentlandite, PP forms medium to small structures (Figure 48c) whereas LP generates more isolated but medium to big structures (Figure 48d). In addition, LC forms the biggest structures on pentlandite (Figure 48e) which agrees with the highest roughness values (Table 12). Although rougher, LC has the same apparent layer thickness (ΔPTV) as LP.

For hexagonal pyrrhotite, the greatest RMS value was observed for PP (5.18 nm) (Figure 49c). LP generates disseminated small structures (Figure 49d). Similarly, even though LC has a more detrimental effect on hexagonal pyrrhotite's floatability, this depressant has a topographically low distribution (Figure 49e), indicating that its mechanism of depression is not associated with the depressant roughness. Furthermore, the difference of the depression mechanisms of paste starch and crosslinked starch is likely related to the surface coverage of LC on both mineral surfaces (Table 12). While LP can cover only 3.4% of pentlandite surface, LC covers 22.6%. Similarly, LC covers 45.0% of hexagonal pyrrhotite surface while LP is only distributed on 25.7% of this mineral surface. These results agree with the equilibrium adsorption data. They also show that the presence of crosslinking agents such as copper ions can modify the conformation of the depressant on the mineral surface more than the molecular size.

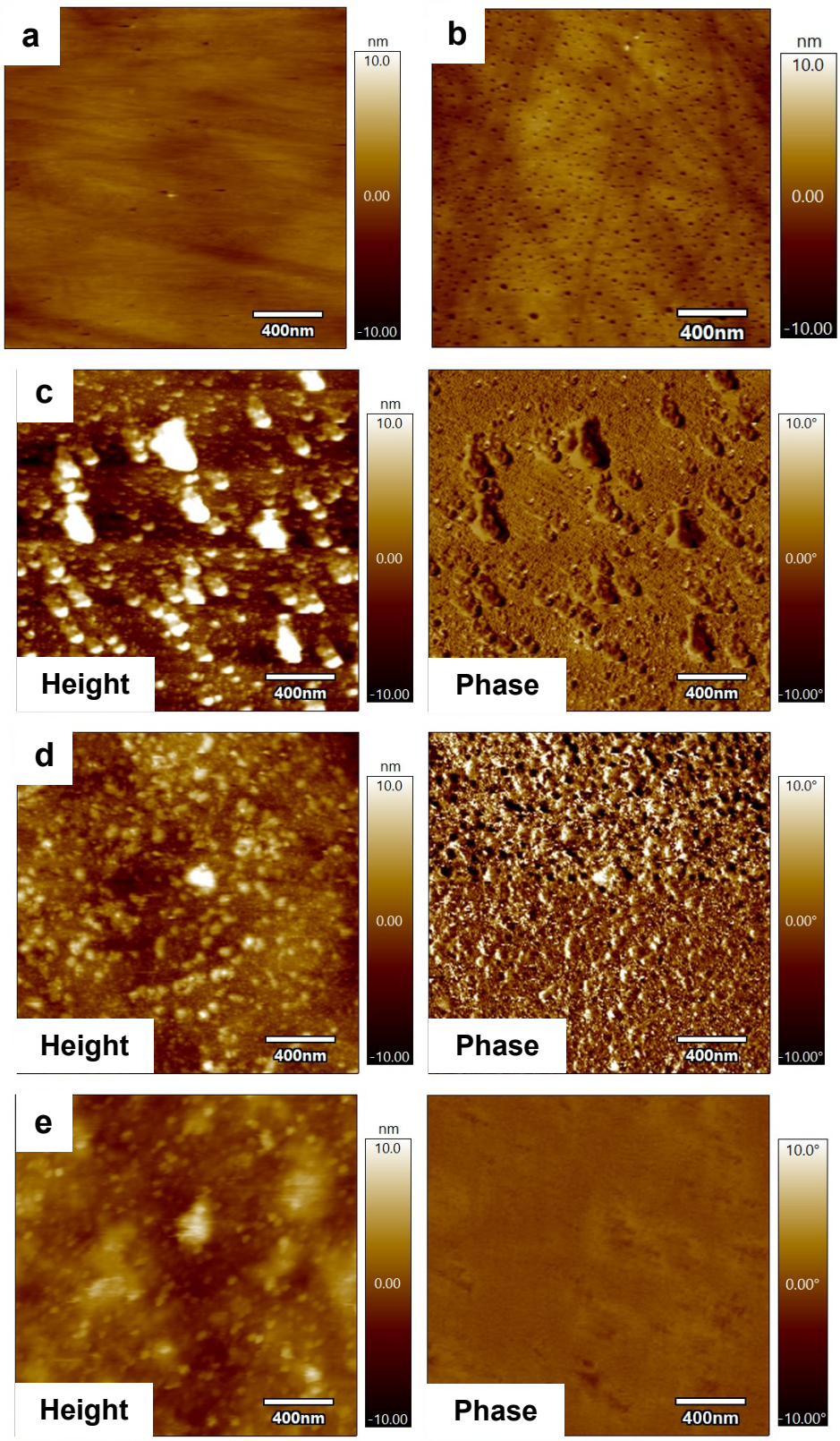

Figure 49: AFM images of hexagonal pyrrhotite (a) fresh surface; (b) pH 9; (c) PP; (d) LP; and (e) LC.

Moreover, the size and shape of these patches do not have any correlation with the molecular weight of the starch depressant. For instance, PP and LP can form starch assemblages of similar size and shape on pentlandite surface (Figures 48c and 48d). The size appears to be a function of the concentration used (Figure 50). At 50 mg/L and 100 mg/L, adsorbed PP on hexagonal pyrrhotite surface (Figure 50) forms small starch agglomerates. For 200 mg/L the size is dramatically increased (Figure 49c). Their assemblage (and shape) might be driven by the strong interaction of the hydrophobic parts on the starch, exposing the hydroxyl groups similar to an amphiphile assembly.

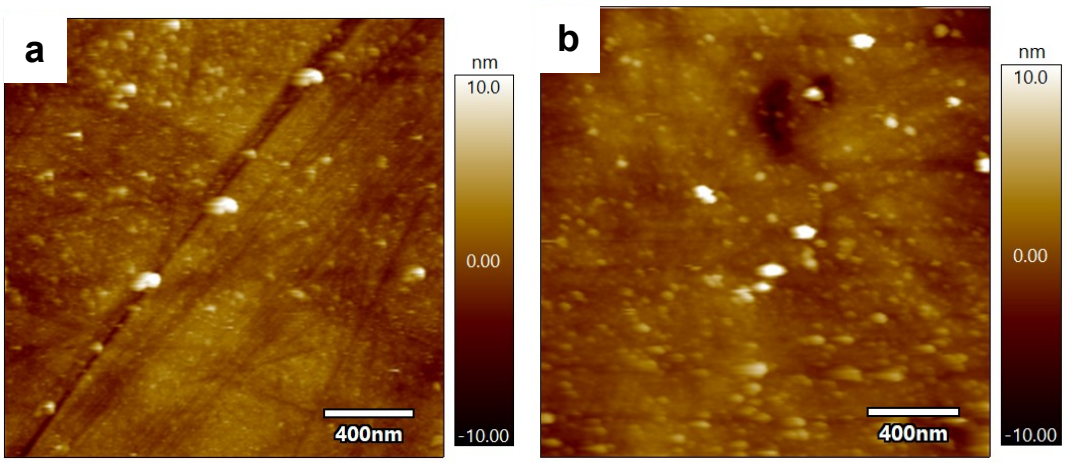

Figure 50: AFM images of PP adsorbed on hexagonal pyrrhotite surface. (a) 50 mg/L and (b) 100 mg/L.

The qualification of mechanical aspects (i.e. softness and stiffness) of the adsorbed starch layers using the phase images of pentlandite (Figure 48) and hexagonal pyrrhotite (Figure 49) was proven to be challenging, especially for the topographically low distributed depressants (Figure 49e). The 3D topography painted with the phase colours in Appendix 6 enables a better correlation between phase and topography.

Additionally, as suggested by (117,118), AFM data and the q_{max} values of the Langmuir model fitting can be used to calculate the volume of hydrated water (V_{HYD}) within the adsorbed layer of the paste starch depressants (V_{AFM}). A similar calculation was performed considering starch density (ρ_{starch}) 1200 kg/m^3 (Table 13). However, it is only an indication of the starch depressant's hydration level since their adsorption distribution on the mineral surface is very

heterogenous, and this calculation provides the averaged layer thickness (ΔPTV). The volume of adsorbed starch on the mounted mineral surface was calculated by

$$V_{AFM} = \Delta PTV * \text{surface coverage} \quad (32)$$

while the volume of adsorbed starch on mineral particles during the adsorption tests (V_{ads}) is given by

$$V_{ads} = \frac{q_{max}}{\rho_{starch}} \quad (33)$$

The final volume of hydration water (V_{hyd}) was obtained with

$$V_{HYD} = V_{AFM} - V_{ads} \quad (34)$$

As expected, the volume of hydration water is dramatically more substantial for PP than LP, supporting all interpretations obtained with previous experiments such as the Washburn test (Figure 45). On the other hand, the application of V_{HYD} values of LC to explain its mechanism of depression is not satisfactory. Again, the mechanism of depression of LC differs from the one of paste starches.

Table 12: Volume of adsorbed hydration water of PP, LP, and LC on pentlandite and hexagonal pyrrhotite surfaces.

		V_{AFM} (10^{-9} m^3)	**V_{ads} (10^{-9} m^3)**	**V_{HYD} (10^{-9} m^3)**
Pentlandite	PP	96.36	2.49	93.87
	LP	83.04	2.48	80.57
	LC	556.77	3.79	552.98
		V_{AFM} (10^{-9} m^3)	**V_{ads} (10^{-9} m^3)**	**V_{HYD} (10^{-9} m^3)**
Hex. Pyrrhotite	PP	1015.02	3.46	1011.56
	LP	222.97	2.59	220.38
	LC	17.00	4.95	12.05

5.2.7. Interactions of paste starch and crosslinked starch with pentlandite and hexagonal pyrrhotite by XPS

XPS was used to investigate the interaction mechanism between starch depressants and the mineral surfaces, in other words, the adsorption bonds (Figures 51 and 52). Due to the presence of similar groups of paste starches after gelatinization, the XPS experiments were performed using (LP) and crosslinked starch (LC) only. All peaks were assigned based on previous works (23,46,121,122).

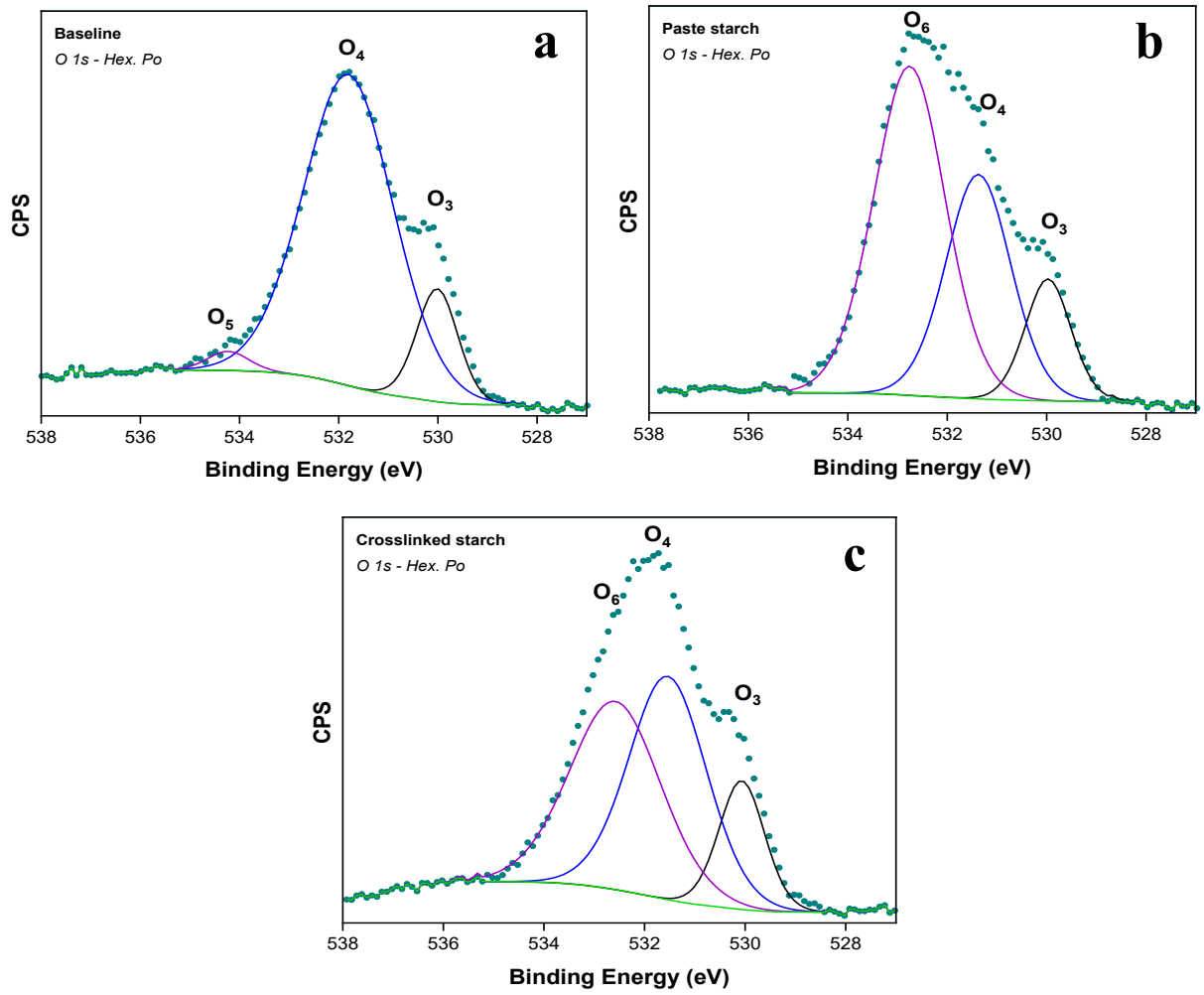

Figure 51: O 1s spectra comparison between baseline (a), paste starch (b), and crosslinked starch (c) interactions with hexagonal pyrrhotite surface.

From the O 1s high resolution spectrums, a clear information of the interactions between the starch groups and metal species on the mineral surfaces was obtained. In the O 1s spectrum of hexagonal pyrrhotite baseline (Figure 51), three peaks at 530.02, 531.79, and 534.13 eV were assigned to metal oxides such as CuO and/or Fe(III)-O (O_3); metal hydroxides such as Fe(III)-OH (O_4), and water (O_5), respectively (Figure 51 and Table 14). The baseline refers to the mineral conditioned at pH 9.2 without any reagents. With paste starch and crosslinked starch additions, the water peak (O_5) disappeared, and although O_3 and O_4 still remained, the Fe(III)-OH area dramatically decreased. The new peak at 532.5-532.8 eV corresponds to the organic bonds of oxygen to metal atoms (Fe(III)-$OH_{organic}$ - O_6) (122), forming species such as FeOOH (23,122).

Table 13: XPS results of hexagonal pyrrhotite in the presence and absence of starch depressants.

	Baseline			Paste starch			Crosslinked starch		
Specie	**BE (eV)**	**FWHM**	**Area**	**BE (eV)**	**FWHM**	**Area**	**BE (eV)**	**FWHM**	**Area**
C-C/C-H	284.80	1.45	78.64	284.80	1.26	38.84	284.80	1.30	50.96
C-O	286.40	1.45	13.38	286.40	1.26	41.76	286.30	1.96	37.81
O-C-O	-	-	-	287.60	1.26	10.62	-	-	-
O-C=O	288.80	1.45	7.97	289.00	1.89	8.78	288.50	1.95	11.23
Cu-O/Fe-O (O_3)	530.02	0.98	14.45	529.97	1.08	12.78	530.07	1.07	14.56
Fe(III)-OH (O_4)	531.79	2.11	83.59	531.37	1.54	33.37	531.54	1.82	42.92
Fe(III)-$OH_{organic}$ (O_6)	-	-	-	532.76	1.69	53.84	532.58	2.14	42.52
Water (O_5)	534.13	0.98	1.96	-	-	-	-	-	-
$Fe_{1-x}S$	707.23	1.11	25.10	707.16	1.18	35.20	707.23	1.04	43.39
Fe(III)-S	708.63	2.23	11.77	708.56	1.88	19.84	708.63	1.56	16.69
Fe(III)-O	710.64	1.89	31.86	710.57	1.65	21.42	710.62	1.77	21.43
Fe(III)-O_{mult1}	711.73	1.34	13.28	711.56	1.18	8.64	711.73	1.04	7.15
Fe(III)-O_{mult2}	712.63	1.00	7.71	712.56	1.18	6.60	712.63	0.93	5.65
Fe(III)-O_{mult3}	713.63	1.11	6.95	713.56	1.18	5.07	713.63	1.04	3.88
Fe(III)-O_{mult4}	714.63	1.11	3.35	714.56	1.18	3.25	714.63	1.04	1.71
$Fe_{1-x}S$	161.40	0.98	20.04	161.16	0.63	2.79	161.45	0.93	20.68
S_2^{2-}	162.43	0.98	43.52	162.46	1.57	27.25	162.46	0.93	43.85
S_n^{2-}	163.61	1.27	29.88	163.76	2.71	47.56	163.61	1.22	30.04
SO_4^{2-}	168.62	1.46	6.56	167.54	4.20	22.40	168.53	1.50	5.42
Cu-S	932.25	1.15	95.52	932.12	1.31	95.82	932.26	1.15	92.17
Cu-O	933.74	1.72	4.48	933.74	1.70	4.18	933.31	2.88	7.83

Other spectrums such as Fe 2p can be more adversely affected by factors that may mask (or improve) the mineral interaction with starch such as oxidation species. The reason for not using the Fe $2p_{3/2}$ spectrum is that starch can form a passivation layer on the mineral surface, impairing usual electrochemical reactions (11), i.e. the correspondence with the baseline may not be consistent. The passivation is confirmed by the rise in the Fe_{1-xS} species area when starch depressants were added (Table 14). While the baseline shows a 25.10% Fe_{1-xS} species, with paste starch, this value is 35.20%. Additionally, the Fe 2p spectrum can also receive contributions from the Cu LMM peak which may promote shifting and/or changes in areas which are not related to the mineral interaction with the depressant. The oxidation number of iron species was determined from the distance and shape of the Fe $2p_{3/2}$ satellite (23). Four multiplets were assigned to the Fe $2p_{3/2}$ (Table 14) and are related to the Fe(III)-O species (121). Multiplets are observed for high spin compounds such as Fe (III). Additional spectrums (C 1s, Fe $2p_{3/2}$, Cu $2p_{3/2}$, and S 2p) can be seen in Appendix 7.

Similar results could be observed for pentlandite regarding the disappearance of the water peak (O_5), and the increase of metal ions interactions with organic oxygen (O_9) (Table 15 and Figure 52). Since it was not possible to differentiate the type of metal oxides and hydroxides (nickel or iron) present on this mineral, generic metallic species were named (Me). Conversely to hexagonal pyrrhotite, pentlandite did not show surface passivation after starch depressant addition. This is given by the close values of $(Ni,Fe)_9S_8$ for the baseline (10.56%), paste starch (10.22%), and crosslinked starch (12.12%), respectively.

It can be verified that the increased percentage of Ni-OH after the addition of starch depressants indicates that the nickel sites are a potential adsorption site for starch molecules. The distinction between inorganic Ni-O and organic Ni-O bonds could not be evaluated using the Ni $2p_{3/2}$ spectrum. However, a 0.2 eV shift on the binding energy of Me-O bond (Table 15) compared with the $Fe\text{-}OH_{organic}$ in Table 14 suggests that the organic oxygen bond on pentlandite surface is not purely between the iron atoms and oxygen.

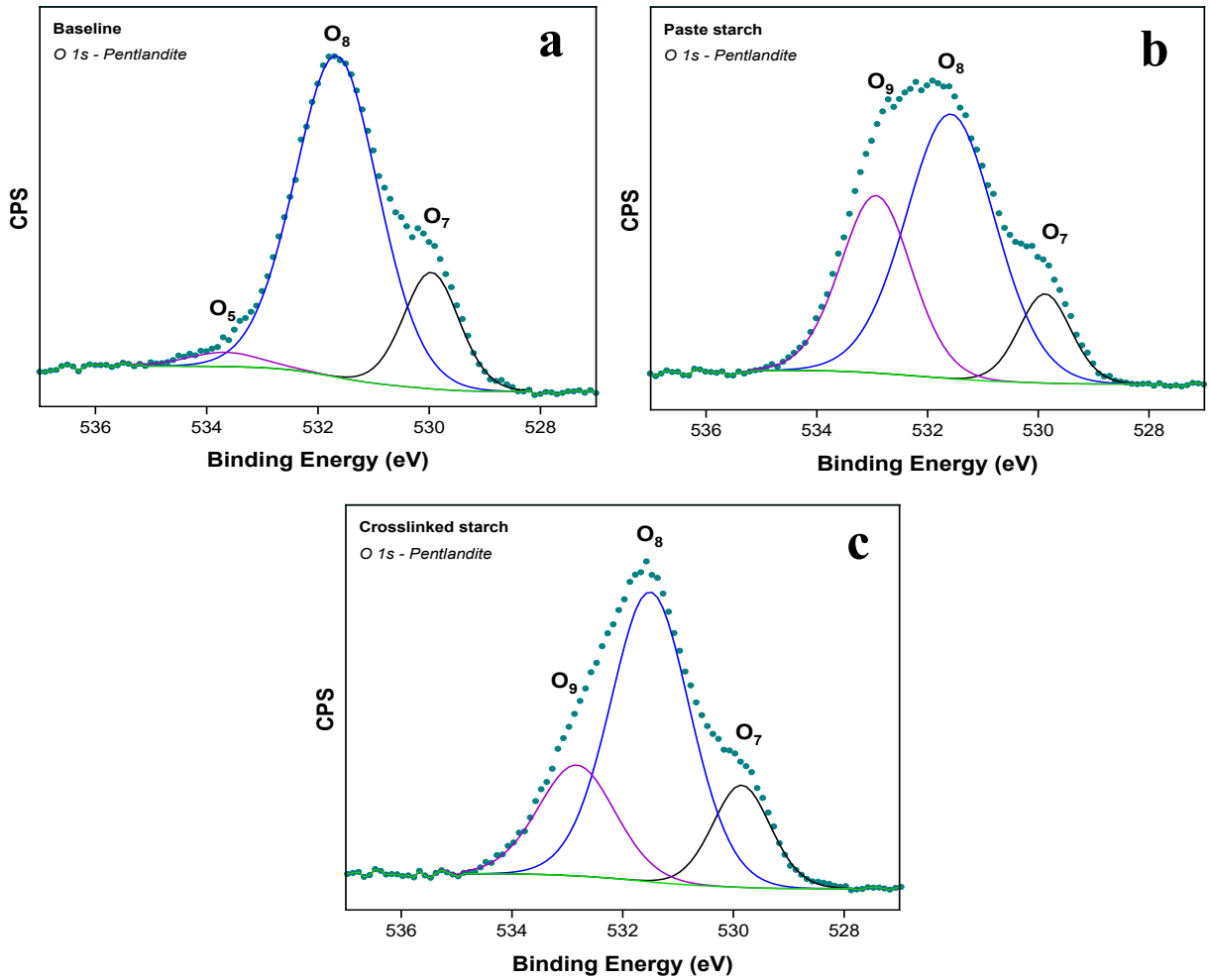

Figure 52: O 1s survey spectra comparison between baseline (a), paste starch (b), and crosslinked starch (c) interactions with pentlandite surface.

Additionally, the Ni(II)-OH binding energy has a ~0.2 eV shift which may indicate that this bonding is not totally between the Ni (II) and an inorganic oxygen after starch depressant addition. However, in a collector scenario, these Ni sites are likely to be occupied by collector molecules (36,39), reducing the density coverage of the starch depressants on pentlandite. Although small, these binding energy shifts can be considered since they are greater than the detection limit (0.1 eV). The crosslinked starch (22.6%) also had a lower percentage of the Me-$OH_{organic}$ species than paste starch (30.8%).

Table 14: XPS of pentlandite in the presence and absence of starch depressants (121,122).

	Baseline			Paste starch			Crosslinked starch		
Specie	**BE (eV)**	**FWHM**	**Area**	**BE (eV)**	**FWHM**	**Area**	**BE (eV)**	**FWHM**	**Area**
C-C/C-H	284.80	1.33	74.14	284.80	1.27	44.53	284.80	1.28	55.96
C-O	286.30	1.33	11.98	286.40	1.27	36.02	286.30	1.28	27.80
O-C-O	287.60	1.33	4.30	287.60	1.90	15.11	287.80	1.28	9.46
O-C=O	288.80	1.33	9.57	289.00	1.27	4.34	288.80	1.28	6.78
Me-O (O_{7})	529.96	1.18	18.88	529.88	1.10	11.35	529.85	1.23	15.83
Me-OH (O_{8})	531.66	1.77	78.08	531.58	1.90	57.85	531.50	1.69	61.55
Me-$OH_{organic}$ (O_{9})	-	-	-	532.93	1.51	30.79	532.83	1.63	22.61
Water (O_{5})	533.67	1.56	3.04	-	-	-	-	-	-
$(Ni,Fe)_9S_8$	707.18	1.93	9.34	707.19	2.00	7.81	707.31	1.73	7.04
Fe(III)-O	710.30	1.93	45.69	710.40	2.00	40.35	710.31	2.03	42.92
Fe(III)-O_{mult1}	711.48	1.93	31.98	711.39	2.00	18.49	711.31	1.73	19.84
Fe(III)-O_{mult2}	712.48	1.93	7.76	712.39	2.00	20.19	712.31	1.73	18.78
Fe(III)-O_{mult3}	713.48	1.93	2.30	713.39	2.00	7.50	713.31	1.73	7.45
Fe(III)-O_{mult4}	714.48	1.93	2.93	714.39	2.00	5.66	714.31	1.73	3.98
$(Ni,Fe)_9S_8$	853.23	1.43	10.56	853.02	1.24	10.22	853.20	2.21	12.12
Ni(II)-OH	856.04	2.01	47.38	856.16	2.25	68.36	856.20	2.21	58.59
$NiSO_4$	857.50	4.57	3.88	-	-	-	-	-	-
Ni(II)-$OH_{satellite}$	861.98	2.58	38.17	861.98	2.89	21.42	861.75	3.42	29.29
Cu-S	932.26	1.48	83.39	932.36	1.67	100	932.27	1.58	84.14
Cu-O	934.26	1.48	16.61	-	-	-	934.38	1.58	15.86

5.2.8. Starch-hexagonal pyrrhotite surface interactions by electrophoretic measurements

Figure 53 presents the zeta potential of hexagonal pyrrhotite as a function of pH. The isoelectric point (iep) of fresh hexagonal pyrrhotite is 3.7 which is close to values found in the literature (123). As discussed by Multani et. al (123), values above 3.5 indicate that the surface is partially or completely oxidized. Similarly, pentlandite is also negatively charged above pH 2 as discussed by Bremmel et al. (124). The addition of copper sulfate significantly increased the surface potential of hexagonal pyrrhotite which is characterized by positive values. Above pH 10, the surface became negatively charged again.

Moreover, the addition of paste starch slightly shifted the surface potential to more positive values. Interestingly, at acidic pH such as 2 and 3, the surface became negative, following the trend

for causticized starch (23,30,125). Starch molecules are considered a non-ionic depressant (63) which is consistent with values near 0 mV from pH 2 to 6. Upon crosslinking reaction with metal ions, starch presents a more positive zeta potential value, albeit this is dependent on the metal ions used (30). This corroborates the trend found for hexagonal pyrrhotite adsorbed with the synthesized crosslinked starch.

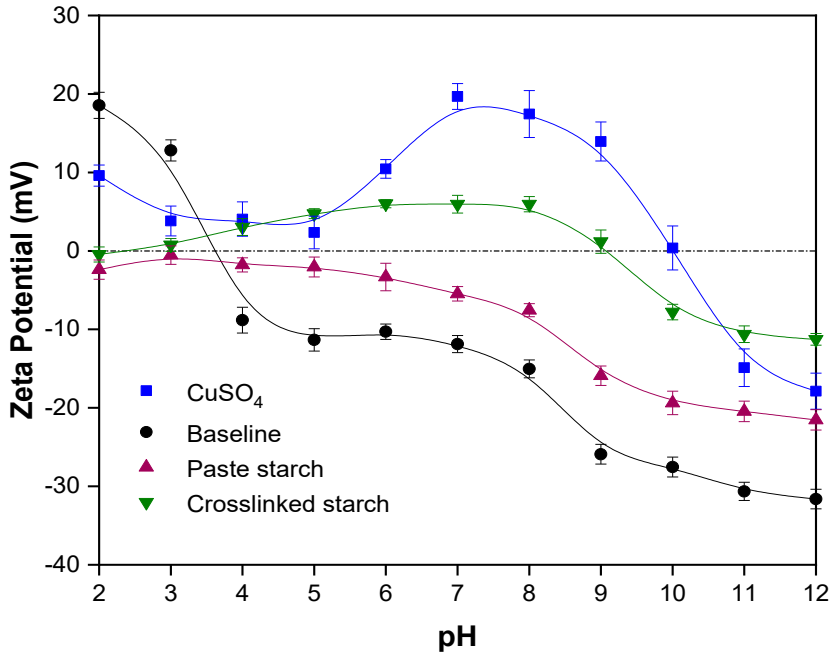

Figure 53: Zeta potential values of single hexagonal pyrrhotite using copper sulfate, paste starch, and crosslinked starch.

5.3. Discussion

5.3.1. Mechanism of depression of paste starches and crosslinked starch on hexagonal pyrrhotite and pentlandite

The previous results suggest that the mechanism of depression of the paste starches and the crosslinked starch are associated with a variety of factors other than adsorbed amount of depressant. Even though starch depressants showed a great affinity for hexagonal pyrrhotite and pentlandite surfaces, the assumption that the depressant affinity by the gangue mineral surface is one of the most important parameters could not be entirely true for polysaccharides. Flotation recovery

appears to be mostly ruled by the density of hydrophilic and/or hydrophobic species on the mineral surface, generating a balance. Although pentlandite adsorbs all the starch depressants, this mineral also adsorbs more PIBX (Figures 38 and 43), and consequently is more hydrophobic (Figure 44), justifying its higher recovery (Figure 23).

The apparent layer thickness (ΔPTV) values obtained with the AFM imaging have been used for different authors to differentiate the contact angle and/or hydration data of other adsorbed polysaccharides on naturally hydrophobic minerals (117,126) and molybdenite (118) in order to justify the flotation data. However, in this study, no correlation among RMS, ΔPTV, and wettability could be determined. The first reason is the absence of PIBX on the AFM experiments. The collector molecules were proven to highly influence the adsorption of starch depressants (Figures 39, 40 and 41). Secondly, as obtained by the previous experiments, the depressing effect of the starch depressants is connected with the hydrophobic/hydrophilic species balance on both mineral surfaces, and the thickness of the starch assembly plays no role on the surface wettability as confirmed by the QCM-D tests (Figure 46). It must be highlighted that the starch adsorption verified in the AFM tests considerably differs in terms of layer thickness and seems to be contrary to the values calculated using the Kelvin-Voigt viscoelastic model. This can be justified by the differences between a chemically heterogenous and fairly rough real mineral surface, and the smooth and chemically homogeneous surface of a Fe-S sensor surface. Another important parameter is that the QCM-D tests were performed in collector scenario. They are therefore complementary.

An assessment of the relative volume of hydration water given by the AFM imaging and the adsorption tests is more appropriate for the formulation of the mechanism of depression of the paste starches on hexagonal pyrrhotite and pentlandite. The concept of hydration for mineral depression has been proven by different authors regarding dextrin adsorption on naturally hydrophobic minerals (117,118). This concept was first proposed by Pugh (12) who named this phenomenon as structural hydration forces which arise when hydrophilic groups such as OH and COOH are present on the depressant macromolecules and strongly bound to water molecules via hydrogen bonding (66). These hydrophilic groups are characterized by an ion-dipole structure, modifying the orientation of water molecules near the adsorbed polysaccharide layer (Figure 54). The bubbles would be repelled when close to this “oriented” water zones, i.e. the hydration forces fundamentally promote repulsion between the mineral surface and the air-bubbles (12). The

strength of these repulsion forces is connected with the polysaccharide conformation (12). The paste starch conformation on a mineral surface (i.e. layered flat or "tails-up") is considered in this study dependent on the molecular weight, validating the importance of this parameter for an effective mineral depression. In this manner, PP is able to accommodate more water molecules within its chains than LP (Figure 54) due to a lower packing density, generating a stronger net hydration force. This corroborates the single micro-flotations (Chapter 4) and the contact angle results (Figure 44). These authors (118) also stated that at pH 9, the presence of deprotonate carboxyl groups (Chapter 3) would further improve the hydration of a polysaccharide layer. The greater water uptake given by the Washburn test (Figure 45) reinforces the conclusion that PP can be more hydrated than LP.

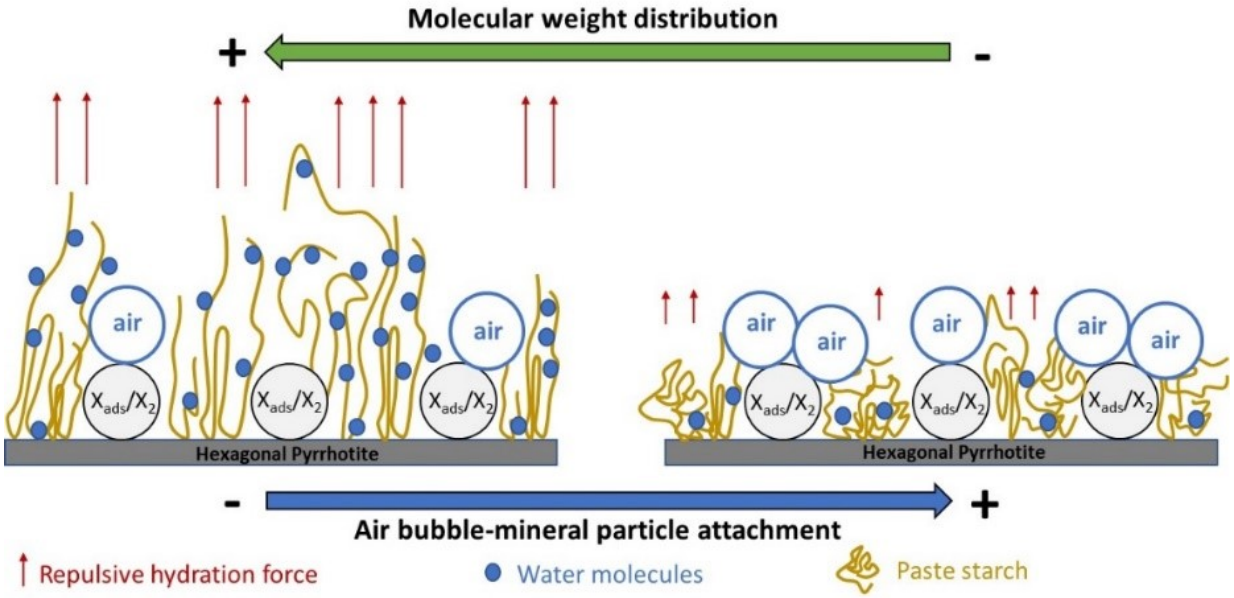

Figure 54: Proposed mechanism of depression on pentlandite and hexagonal pyrrhotite by paste starches with different MW distributions. Note: X_{ads}/X_2 represents hydrophobic surface species formed after PIBX addition such as metal-xanthate and/or dixanthogen.

The addition of a crosslinked agent, however, influenced on the mechanism of depression of LC on hexagonal pyrrhotite and pentlandite. In this case, a comparison between the surface coverage is more relevant (Table 12). The images processed via the ImageJ software used for this calculation are in Appendix 6. LC showed the higher surface coverage area when compared with PP and LP. The percentage of both minerals' covered area by LC is the most considerable and

likely to be responsible for increasing the wettability of both minerals. Nevertheless, LC coverage on hexagonal pyrrhotite (44.96%) is twice the one on pentlandite (22.59%). As a result, hexagonal pyrrhotite becomes more hydrophilic, explaining the more significant drop in floatability observed in micro-flotation results.

Therefore, factors that could be combined to influence the hydrophobic/hydrophilic balance of all starch depressants on hexagonal pyrrhotite and pentlandite surfaces are: the presence of collector, the surface coverage, and the hydration levels of the adsorbed layer. In the following section, an investigation on the interaction of the starch depressants on hexagonal pyrrhotite and pentlandite will provide a complementary outlook of the described situation.

5.3.2. Mechanism of adsorption of paste starch and crosslinked starch on hexagonal pyrrhotite and pentlandite

The mechanism of adsorption of the starch depressants was investigated by XPS and zeta potential measurements. The new Fe-$OH_{organic}$ and Me-$OH_{organic}$ peaks (23,122) on hexagonal pyrrhotite and pentlandite after paste starch and crosslinked additions proves that the polysaccharides depressants can be chemically adsorbed on both minerals through a mechanism similar to that proposed by (24,29). The interactions of sulfide minerals with the polysaccharides depressants seem to be associated with metal ions receiving electrons from the polysaccharide species (e.g. hydroxyl groups of a D-glucose unit), configuring an acid-base interaction (29). According to Liu (63) and Laskowski et al. (66), these metal ions form bridges between mineral surface and the polysaccharide hydroxyl-groups (Figure 55a). The aforementioned adsorption mechanism has been proven for a variety of polymetallic minerals (25–27,29). In addition, the fact that the crosslinked starch has a lower area percentage of the Fe-$OH_{organic}$ or Me-$OH_{organic}$ peaks than paste starch (~8-10% less) but still a more depressing effect suggests that the crosslinked starch also presents an additional mechanism of adsorption that might not be limited to chemisorption. Therefore, further investigation regarding the mechanism of interaction was carried out via electrokinetics measurements for the hexagonal pyrrhotite.

The mechanism of adsorption of the crosslinked starch is a consequence of the mineral surface becoming negative at very alkaline pH, namely pH 9 (Figure 53), and the crosslinked starch of being weakly electronegative. Therefore, this depressant would be attracted to the

hexagonal pyrrhotite surface through electrostatic attraction (Figure 55b). This explains the additional mechanism of adsorption for the crosslinked starch and a possible higher coverage density of this depressant on hexagonal pyrrhotite surface which promotes the higher hydrophilic aspect of this mineral surface. For pentlandite, the same mechanism is suggested, and it elucidates the lower mass recoveries obtained for the micro-flotation experiments.

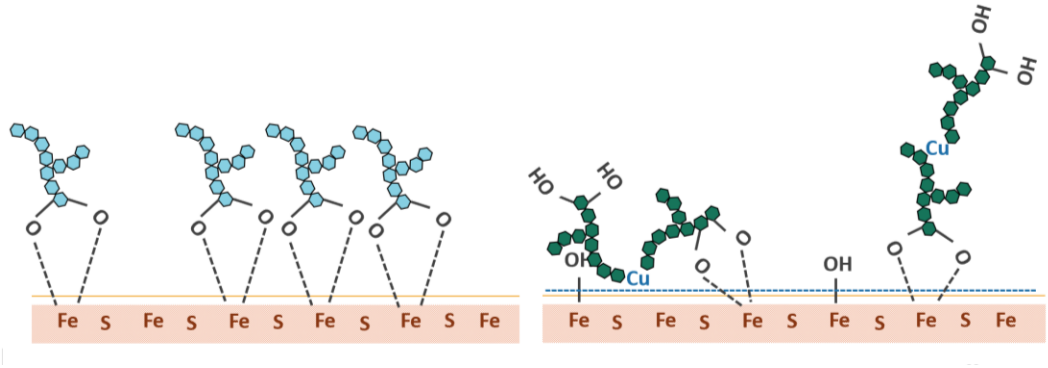

(a) **(b)**

Figure 55: Schematic representation of the mechanism of interaction of paste starch (a) and crosslinked starch (b) on the surface of hexagonal pyrrhotite.

5.4. Summary

It has been demonstrated that hexagonal pyrrhotite and pentlandite interact with the starch depressants, and this interaction is independent of the molecular weight distribution and the presence of crosslinked agents such as copper ions. The adsorption amounts of starch depressants on both minerals is mostly influenced by the presence of a pre-adsorbed layer of PIBX. It was also indirectly verified that the amount of depressant adsorbed is not necessarily responsible for the hydrophilic aspect of the mineral surface.

The conformation (i.e., arrangement on the surface) of the adsorbed layer of the starch depressants is the main factor dictating their depressing effect. In the case of paste starches, it is assumed to be related to their molecular weight distribution. The size of starch macromolecules can, therefore, influence the packing density of the layer. The packing density is connected to the hydration levels of the paste starch depressants. The Langmuir and BET models allowed a relative comparison between the depressants used, and indirectly gave the lower packing density of PP. This information was further confirmed by the QCM-D and AFM results. The lower packing

density of PP enables the accommodation of more water molecules within this depressant's chains. This hydration of PP is responsible for impairing mineral particle-air bubble attachment due to a stronger repulsive hydration force. In fact, in a collector scenario, PP adsorbs less on both mineral surfaces in comparison with LP but adversely affects pentlandite and hexagonal pyrrhotite floatabilities more. Therefore, the wettability generated by the adsorption of paste starches on hexagonal pyrrhotite and pentlandites surfaces are a function of the hydration and does not have any connection with the adsorbed amounts. It was also shown that the presence of copper ions complexed in the starch structure (crosslinked starch) can change the depressant conformation. A possible stretching of LC structure, due to the repulsion between the copper ions, promoted an easier spreading of this depressant. Therefore, contrarily to the paste starches, its mechanism of depression is related to the surface area coverage on both mineral surfaces.

The interaction/bonding between paste starches and crosslinked starches occurs through chemisorption. The hydroxyl groups present on the polysaccharide structures react with the metal hydroxylate species on both mineral surfaces. Although nickel sites of pentlandite also interact with starch, they are not considered as the principal adsorption point. Moreover, the crosslinked starch also interacts with the mineral surfaces by electrostatic attraction.

Chapter 6 Final conclusions and future recommendations

This thesis contributed to the advancement of topics related to the preparation of starch depressants, the understanding of the mechanism of depression on polysaccharides on hexagonal pyrrhotite and pentlandite, and the confirmation of their mechanism of interaction. In fact, the mechanism of depression is often omitted, and great efforts were directed to the understanding of the mechanism of adsorption. However, the use of three starch depressants to selectively separate mixtures with high ratios of hexagonal pyrrhotite from pentlandite did not achieve the level of desired nickel and iron recoveries (Ni 90% and Fe 20%).

The gelatinization process used to synthesize paste starches was shown to be highly influenced by the presence of sodium hydroxide. The sodium ions enhanced the disruption of starch granules due to repulsion, generating smaller starch chains. The gelatinization method also affected the crosslinking reactions with copper ions. Additionally, the amount of complexed copper on the starch structure was directly related to the metal ion source. Chlorine anions were very detrimental to copper complexation, and greater amounts were complexed using copper sulfate. The crosslinked starch produced is likely to have a copper center bound to two exposed oxygens of the α-D-glucose units (Cu-O specie), and coordinated with two unreacted alcohol groups. This structure may be subjected to changes since copper has a flexible coordination number. The use of a 3,000 g/mol membrane to narrow the molecular weight distribution of a depressant resulted in a paste starch depressant 2.20 times smaller (on average) in terms of weight.

The effect of depressants with different molecular weight distributions and crosslinking additives was observed for single and binary mineral systems. Overall, hexagonal pyrrhotite and pentlandite recoveries were lower for the higher MW paste and crosslinked starches. The addition of metal ions such as copper before paste starch during conditioning was further detrimental to hexagonal pyrrhotite and pentlandite recoveries and did not have the same effect as the crosslinked starches. Therefore, it is likely that the copper complexed in the starch structure provided a distinct mechanism of mineral depression as hypothesized. The best Ni recovery of mixed mineral systems was attained using low dosages of starch (5 mg/L), and a relatively high concentration of PIBX (9.66×10^{-6} M equivalent to 240 g/t). Although the increased collector dosage slightly raised Ni recovery, it was not beneficial to Ni grades.

The mechanism of depression for each starch depressants is different. This shows the complexity of the studied system and the interaction of polymers with sulfide mineral surfaces. An attempt to summarize the mechanism is given in Figure 56 since some similarities were found considering both minerals. The experiments described in Chapter 5 confirmed that the depressing effect of all used starches seems to be explained by a hydrophobic/hydrophilic balance on pentlandite and hexagonal pyrrhotite surfaces. This balance of hydrophobic/hydrophilic species was in great part governed by the amounts of collector that a specific mineral can adsorb, i.e., pentlandite or hexagonal pyrrhotite. As previously established, pentlandite can adsorb more collector, hence it was more hydrophobic than pyrrhotite, although pentlandite can still adsorb the starch depressants. This hypothesis was confirmed by the values of contact angles.

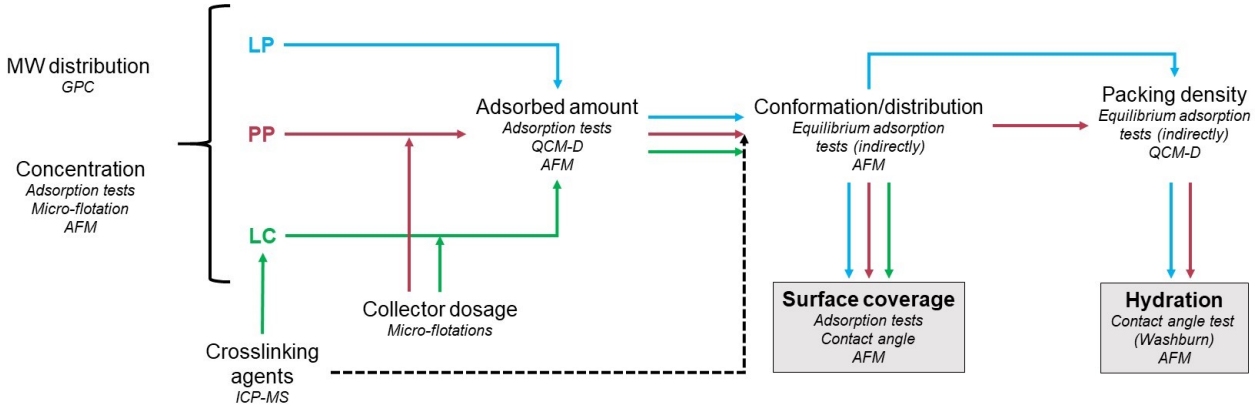

Figure 56: General mechanisms of depression of the starch depressants on pentlandite and hexagonal pyrrhotite at pH 9.0-9.5.

Other factors influencing the balance were the surface coverage of starch depressants that can differ according to the presence of crosslinked agents. The more covered a mineral surface, the more hydrophilic it became. However, this is only valid for the crosslinked starch. The layer thickness of the polysaccharide did not influence the degree of hydrophilicity. For instance, paste starches can form very thick isolated islands on the mineral surface and still be less detrimental than the crosslinked starch which was quite homogeneously spread across both mineral surfaces.

For paste starches, their conformation given in terms of packing density is the most important factor affecting the wettability of hexagonal pyrrhotite and pentlandite. The packing density has been proven to be related to only the molecular weight and influences the levels of

hydration provided by the starch depressants. Polar groups present in the structure of starch were responsible of changing the configuration of neighboring water molecules, generating a repulsion force called hydration force. This also hindered the mineral attachment to air bubbles.

Finally, the mechanism of interaction between the starch depressants and the mineral surfaces occurred mostly through chemisorption. The hydroxyl groups present on the polysaccharide structures reacted with the metal hydroxylate species, as previously stated. In the case of hexagonal pyrrhotite, this interaction occurred between iron hydroxide species while for pentlandite it happened with the nickel and iron hydroxides precipitated species. Nickel sites on pentlandite surface were not considered as the major adsorption point for starch since they can be mostly occupied by collector molecules in a collector scenario. Moreover, the crosslinked starch also interacted with the mineral surfaces by electrostatic attraction due to the presence of complexed copper. Therefore, the copper could be considered as a "driver" by providing regions with a weak electronegativity within the starch chains.

Improvements in this area can culminate in the use of greener reagents during froth flotation. Benefits for the industry would include the mitigation of safety (handling and storage) and environmental problems (disposal). Nevertheless, the complexity of interactions of the studied systems for different starch depressants demonstrated the necessity of further developments and understanding. Some suggestions of future research are given as follows.

6.1. Future recommendations

1) In order to improve the selectivity, it is recommended the use of collectors with molecular sizes other than PIBX. This is because the collector presence (and dosages) influences the adsorbed amounts of depressants. Collector molecules seem to interact with the polysaccharide chains (and replace them). Longer chain xanthates might provide a certain steric hindrance on the mineral surfaces.

2) Work should be done to evaluate the interactions of the starch depressants on hexagonal pyrrhotite and pentlandite at different pH conditions and temperatures. The latter is related to the fact that, in Canada, the mineral processing activities are subjected to seasonal changes.

3) Considering that the Eh influences the type of surface species on sulfide minerals, additional experiments to find a point where hexagonal pyrrhotite has more oxidation species than pentlandite would increase starch adsorption on the gangue mineral, improving selectivity.

4) Lastly, although the majority of the experiments were performed in a collectorless scenario to avoid any influence of the collector molecules, an assessment in a collector scenario should be conducted.

Bibliography

1. U.S. Geological Survey. Mineral Commodity Summaries: Nickel [Internet]. 2019 Feb. Available from: https://minerals.usgs.gov/minerals/pubs/commodity/nickel/
2. Haldar SK. Introduction. In: Platinum-Nickel-Chromium Deposits. Elsevier Inc.; 2017. p. 11–3.
3. Kelebek S. Effect of polyamines on mineral separation of nickel-copper ores: chelation equilibria in collectorless flotation with DETA. Trans Inst Min Metall. 1996;105:75–88.
4. Kelebek S, Wells PF, Fekete SO. Differential flotation of chalcopyrite, pentlandite and pyrrhotite in Ni-Cu sulphide ores. Can Metall Q. 1996;35(4):329–36.
5. Yoon R, Basilio C, Marticorenat M, Kerr1 A, Stratton-Crawley R. A study of the pyrrhotite depression mechanism by diethylenetriamine. Miner Eng. 1995;8(7):807–16.
6. Multani RS, Waters KE. Pyrrhotite Depression Studies with DETA and SMBS on a Ni-Cu Sulphide Ore. Can J Chem Eng. 2019;97(7):2121–30.
7. Marticorena MA, Hill G, Kerr AN, Liechti D, Pelland DA. INCO develops new pyrrhotite depressant. In: Innovations in Mineral Processing. Sudbury; 1994. p. 15–33.
8. Mendiratta NK, Yoon RH, Wilson S. Effects of diethylenetriamine and sulfur dioxide on pyrrhotite depression. In: R. Woods, F. M. Doyle, editors. Electrochemistry Society Proceedings. Electrochemistry Society Proceedings; 2000. p. 60–71.
9. Qi C, Liu J, Malainey J, Kormos LJ, Coffin J, Deredin C, et al. The role of Cu ion activation and surface oxidation for polymorphic pyrrhotite flotation performance in Strathcona Mill. Miner Eng. 2019 Jan;134:87–96.
10. Wiese JG. Investigating depressant behavior in the flotation of selected Merensky ores. University of Cape Town; 2009.
11. Chimonyo W, Fletcher B, Peng Y. Starch chemical modification for selective flotation of copper sulphide minerals from carbonaceous material: A critical review. Miner Eng. 2020;156:1–15.
12. Pugh RJ. Macromolecular organic depressants in sulphide flotation-A Review, 2. Theoretical Analysis of Forces Involved in the Depressant Action. Int J Miner Process. 1989;25(1–2):131–46.
13. Bulatovic S, Jessup TM, Jackson JF, Leighton G. Depressant for flotation separation of

polymetallic sulphide ores. United States: United States Patent; 5,693,692, 1997.

14. Bulatovic SM. Handbook of Flotation Reagents Chemistry, Theory and Practice: Flotation of Sulfide Ores. Vol. 1. Elsevier Science & Technology Books; 2007.
15. Braga PFA, Chaves AP, Luz AB, França SCA. The use of dextrin in purification by flotation of molybdenite concentrates. Int J Miner Process. 2014 Mar 10;127:23–7.
16. Fletcher B, Chimonyo W, Peng Y. A comparison of native starch, oxidized starch and CMC as copper-activated pyrite depressants. Miner Eng. 2020;156:1–8.
17. de Aquino TVP, Leal Filho L de S, de Lima JRB. Propriedades reológicas de soluções de amido: influência do método de preparação e desempenho da flotação. In: XXII ENTMME. Ouro Preto; 2007. p. 415–22.
18. Souza AC de, Magalhães DG. Influência do grau de gelatinização do amido de milho no processo de flotação reversa de minério de ferro. Tecnol em Metal Mater e Mineração. 2016;13(2):1–7.
19. Tang M, Wen S, Liu D. Effects of Heating- or Caustic-Digested Starch on its Flocculation on Hematite. Miner Process Extr Metall Rev. 2016;37(1):49–57.
20. Laskowski JS, Liu Q, Bolin NJ. Polysaccharides in flotation of sulphides. Part I. Adsorption of polysaccharides onto mineral surfaces. Int J Miner Process. 1991;33:223–34.
21. Pinto CLL, de Araujo AC, Peres AEC. The effect of starch, amylose and amylopectin on the depression of oxi-minerals. Miner Eng. 1992;5(3):469–78.
22. Yang S, Wang L. Structural and functional insights into starches as depressant for hematite flotation. Miner Eng. 2018;124:149–57.
23. Moreira GF, Peçanha ER, Monte MBM, Leal Filho LS, Stavale F. XPS study on the mechanism of starch-hematite surface chemical complexation. Miner Eng. 2017 Aug 15;110:96–103.
24. Liu Q, Laskowski JS. Adsorption of polysaccharides onto sulfides and their use in sulfide flotation. In: Polymers in Mineral Processing. Québec; 1999. p. 71–90.
25. Liu QI, Laskowski JS. The Interactions between Dextrin and Metal Hydroxides in Aqueous Solutions. J Colloid Interface Sci. 1989;130(1):101–11.
26. Nyamekye GA, Laskowski JS. Adsorption and Electrokinetic Studies on the Dextrin-Sulfide Mineral Interactions. J Colloid Interface Sci. 1993;157:160–7.

27. Rath RK, Subramanian S. Adsorption, electrokinetic and differential flotation studies on sphalerite and galena using dextrin. Int J Miner Process. 1999;57:265–83.
28. Bulatovic SM. Use of organic polymers in the flotation of polymetallic ores: A review. Miner Eng. 1999;12(4):341–54.
29. Liu Q, Zhang Y, Laskowski JS. The adsorption of polysaccharides onto mineral surfaces: An acid/base interaction. Int J Miner Process. 2000;60(3–4):229–45.
30. Yue T, Wu X. Depressing Iron Mineral by Metallic-Starch Complex (MSC) in Reverse Flotation and Its Mechanism. Minerals. 2018;8(85):2–11.
31. Haq F, Yu H, Wang L, Teng L, Haroon M, Khan RU, et al. Advances in chemical modifications of starches and their applications. Carbohydr Res. 2019 Apr 1;476:12–35.
32. Ayoub AS, Rizvi SSH. An overview on the technology of cross-linking of starch for nonfood applications. J Plast Film Sheeting. 2009;25:25–45.
33. Chau TT, Bruckard WJ, Koh PTL, Nguyen A V. A review of factors that affect contact angle and implications for flotation practice. Adv Colloid Interface Sci. 2009;150(2):106–15.
34. Wills BA, Finch JA. Froth Flotation. In: Wills' Mineral Processing Technology. 8th ed. Oxford: Butterworth-Heinemann; 2016. p. 265–380.
35. Hu Y, Sun W, Wang D. General review of electrochemistry of flotation of sulphide minerals. In Tsinghua University Press; 2009. p. 19.
36. Bozkurt V, Xu Z, Finch JA. Pentlandite/pyrrhotite interaction and xanthate adsorption. Int J Miner Process. 1998 Jul 25;52(4):203–14.
37. Rao SR. Surface Chemistry of Froth Flotation. Surface Chemistry of Froth Flotation. Springer US; 2004.
38. Rao GV. Nickel and cobalt ores: Flotation. In: Encyclopedia of Separation Science. Academic Press; 2004. p. 3491–500.
39. Hodgson M, Agar GE. Electrochemical investigations into the flotation chemistry of pentlandite and pyrrhotite: process water and xanthate interactions. Can Metall Q. 1989;28(3):189–98.
40. Adam K, Iwasaki I. Pyrrhotite-grinding media interaction and its effect on floatability at different applied potentials. Miner Metall Process. 1984 May;81–7.
41. Iwasaki I, Reid KJ, Lex HA, Smith KA. Effect of autogenous and ball mill grinding on

sulfide flotation. Min Eng. 1983;

42. Cheng X, Iwasaki I. Pulp Potential and Its Implications to Sulfide Flotation. Miner Process Extr Metall Rev. 1992 Dec 1;11(4):187–210.
43. Belzile N, Chen YW, Cai MF, Li Y. A review on pyrrhotite oxidation. J Geochemical Explor. 2004;84(2):65–76.
44. Rao SR, Finch JA. Galvanic Interaction Studies on Sulphide Minerals. Can Metall Q. 1988;27(4):253–9.
45. Multani RS, Waters KE. A review of the physicochemical properties and flotation of pyrrhotite superstructures (4C – Fe7S8/ 5C – Fe9S10) in Ni-Cu sulphide mineral processing. Vol. 96, Canadian Journal of Chemical Engineering. 2018. p. 1185–206.
46. Qi C, Khalkhali M, Grundy JS, Liu J, Malainey J, Liu Q. Unraveling Polymorphic Pyrrhotite Electrochemical Oxidation by Underlying Electronic Structures. J Phys Chem C. 2019 Oct 31;123(43):26442–9.
47. Mycrof JR, Nesbit HW, Pray AR. X-ray photoelectron and Auger electron spectroscopy of air-oxidized pyrrhotite: Distribution of oxidized species with depth. Geochim Cosmochim Acta. 1995;59(4):721–33.
48. Buckley AN, Woods R. Surface composition of pentlandite under flotation-related conditions. Surf Interface Anal. 1991;17:675–80.
49. Thornber MR. Mineralogical and electrochemical stability of the nickel-iron sulphides-pentlandite and violarite. J Appl Electrochem. 1983 Apr 6;13:253–67.
50. Monte MB de M, Peres AEC. Química de Superfície na Flotação. In: da Luz AB, Sampaio JA, Franca SCA, editors. Tratamento de Minerios. 5th ed. Rio de Janeiro: Cetem; 2010. p. 399–461.
51. Salopek B, Krasi D, Filipovi S. Measurement and Application of Zeta-Potential. Rud Zb. 1992;(4):147–51.
52. Sun Z, Forsling W, Snngren LR, Sjfberg S. Surface reactions in aqueous metal sulfide systems. 1. Fundamental surface reactions of hydrous PbS and ZnS. Int J Miner Process. 1991;33:83–93.
53. Tajadod J. Flotation Chemistry of Enargite and Chalcopyrite Using Potassium Amyl Xanthate and Depressants. Queen's University; 1997.
54. Otunniyi IO, Oabile M, Adeleke AA, Mendonidis P. Copper activation option for a

pentlandite–pyrrhotite–chalcopyrite ore flotation with nickel interest. Int J Ind Chem. 2016 May 30;7(3):241–8.

55. Senior GD, Shannon LK, Trahar WJ. The flotation of pentlandite from pyrrhotite with particular reference to the effects of particle size. Int J Miner Process. 1994;42:169–90.
56. Gerson AR, Jasieniak M. The effect of surface oxidation on the Cu activation of pentlandite and pyrrhotite. In: XXIV International Minerals Processing Congress IMPC. Beijing: Beijing Science Press; 2008. p. 1054–63.
57. Bulatovic S, Wyslouzil D. Selection and evaluation of different depressants systems for flotation of complex sulphide ores. Miner Eng. 1995;8(2):63–76.
58. Kelebek S, Fekete SO, Wells PF. Selective depression of pyrrhotite using sulphur dioxide-diethylenetriamine reagent combination. In: Proceedings XIX Int Mineral Processing Congress. San Francisco, CA: SME; 1995. p. 181–7.
59. Xu Z, Rao SR, Finch JA, Kelebek S, Wells P. Role of diethylene triamine (DETA) in pentlandite-pyrrhotite separation - Part 1: complexation of metals with DETA. Trans Inst Min Metall. 1997;106:15–20.
60. Bozkurt V, Xu Z, Finch JA. Effect of depressants on xanthate adsorption on pentlandite and pyrrhotite: Single vs mixed minerals. Can Metall Q. 1999;38(2):105–12.
61. Vreugdenhil A, Markwell R, Finch JA. Formation and characterization of nickel-DETA complexes related to flotation systems. In: Finch JA, Rao SR, Holubec I, editors. Processing of complex ores: mineral processing and the environment. 1997. p. 283–9.
62. John A. Dean. Lange's Handbook of Chemistry. 15th ed. McGraw-Hill Companies, editor. 1998.
63. Liu Q. The role of mineral surface composition and hydrophobicity in polysaccharide/mineral interactions. [Vancouver]: University of British Columbia; 1988.
64. Pugh RJ. Macromolecular Organic Depressants in Sulphide Flotation-A Review, 1. Principles, Types and Applications. Int J Miner Process. 1989;25:101–30.
65. Bogusz E, Brienne SR, Butler I, Rao SR, Finch JA. Technical note: Metal ions and dextrin adsorption on pyrite. Miner Eng. 1997;10(4):441–5.
66. Laskowski JS, Liu Q, O'Connor CT. Current understanding of the mechanism of polysaccharide adsorption at the mineral/aqueous solution interface. Int J Miner Process. 2007 Oct 19;84(1–4):59–68.

67. Peres AEC, Correa MI. Depression of iron oxides with corn starches. Miner Eng. 1996;9(12):1227–34.
68. BeMiller JN, Huber KC. Carbohydrates. In: Damodaran S, Parkin KL, Fennema OR, editors. Fennema's food chemistry [Internet]. Fourth. Boca Raton: CRC Press/Taylor & Francis; 2008. Available from: http://ebookcentral.proquest.com/lib/ualberta/detail.action?docID=4744279.
69. Schirmer M, Jekle M, Becker T. Starch gelatinization and its complexity for analysis. Starch/Staerke. 2015;67:30–41.
70. Wang S, Li C, Copeland L, Niu Q, Wang S. Starch Retrogradation: A Comprehensive Review. Compr Rev Food Sci Food Saf. 2015;14(5):568–85.
71. Ai Y, Jane JL. Understanding Starch Structure and Functionality. In: Sjöö M, Nilsson L, editors. Starch in Food: Structure, Function and Applications. Second. Woodhead Publishing; 2017.
72. Colonna P, Buleon A. Thermal transitions of starches. In: Starches. 2010.
73. Tomasik P. Specific Physical and Chemical Properties of Potato Starch. Food. 2009;3:45–56.
74. Ciesielski W, Lii C yi, Yen MT, Tomasik P. Interactions of starch with salts of metals from the transition groups. Carbohydr Polym. 2003;51(1):47–56.
75. Ciesielski W, Krystyjan M. Starch-metal complexes and their rheology. E-Polymers. 2009;9(1):1–13.
76. Ciesielski W, Tomasik P. Complexes of amylose and amylopectins with multivalent metal salts. J Inorg Biochem. 2004;98(12):2039–51.
77. Staroszczyk H, Ciesielski W, Tomasik P. Starch–metal complexes and metal compounds. J Sci Food Agric. 2018 Jun 1;98(8):2845–56.
78. Peres GL, Leite DC, da Silveira NP. Study of complexes formation between transition metal ions and amylopectin in DMSO/H2O solution. Starch/Staerke. 2016 Nov 1;68(11–12):1129–38.
79. Williams PC, Kuzina FD, Hlynka I. A rapid colorimetric procedure for estimating amylose content of starches and flours. Cereal Chem. 1970;(47):411–20.
80. Hostettler C, Kölling K, Santelia D, Streb S, Kötting O, Zeeman SC. Analysis of Starch Metabolism in Chloroplasts. In: John M. Walker, editor. Chloroplast Research in

Arabidopsis: Methods and Protocols, Volume II [Internet]. 2011. p. 387–410. Available from: http://www.springer.com/series/7651

81. Landers PS, Gbur EE, Sharp RN. Comparison of Two Models to Predict Amylose Concentration in Rice Flours as Determined by Spectrophotometric Assay. Cereal Chem [Internet]. 1991;68(5):545–8. Available from: http://www.aaccnet.org/publications/cc/backissues/1991/Documents/CC1991a132.html
82. Rudin A, Choi P. Basic Principles of Polymer Molecular Weights. In: The elements of polymer science and engineering. 2013. p. 63–87.
83. Cares J. Gel Permeation Chromatography-Part Two. J Chem Educ [Internet]. 1966;43(8). Available from: https://pubs.acs.org/sharingguidelines
84. Rudin A, Choi P. Practical Aspects of Molecular Weight Measurements. In: The elements of polymer science and engineering. 2013. p. 89–148.
85. Roberts SA, Cameron RE. The effects of concentration and sodium hydroxide on the rheological properties of potato starch gelatinisation. Carbohydrate. 2002;50:133–43.
86. Noda T, Tsuda S, Mori M, Takigawa S, Matsuura-Endo C, Kim SJ, et al. Determination of the phosphorus content in potato starch using an energy-dispersive X-ray fluorescence method. Food Chem. 2006;95(4):632–7.
87. Kizil R, Irudayaraj J, Seetharaman K. Characterization of irradiated starches by using FT-Raman and FTIR spectroscopy. J Agric Food Chem. 2002 Jul 3;50(14):3912–8.
88. Dankar I, Haddarah A, Omar FEL, Pujolà M, Sepulcre F. Characterization of food additive-potato starch complexes by FTIR and X-ray diffraction. Food Chem. 2018 Sep 15;260:7–12.
89. Nielsen SS. Food Analysis Laboratory Manual [Internet]. 3rd ed. Springer; 2010. Available from: www.springer.com/series/5999
90. Pavlovic S, Brandao PRG. Adsorption of starch, amylose, amylopectin and glucose monomer and their effect on the flotation of hematite and quartz. Miner Eng. 2003;16(11):1117–22.
91. Li Y, Lin S, Hu J, Liu G, Zhang G, Tu Y, et al. Metal ion induced-assembly of amylose in aqueous solution. Carbohydr Polym. 2014;
92. Tomasik P, Jane J -L, Spence K, Andernegg JW. Starch Ferrates. Starch - Stärke. 1995;47(2):68–72.

93. Stevens JS, Schroeder SLM. Quantitative analysis of saccharides by X-ray photoelectron spectroscopy. Surf Interface Anal. 2009;41(6):453–62.
94. Biesinger MC, Lau LWM, Gerson AR, Smart RSC. Resolving surface chemical states in XPS analysis of first row transition metals, oxides and hydroxides: Sc, Ti, V, Cu and Zn. Appl Surf Sci. 2010;257(3):887–98.
95. Hussain Z, Salim MA, Khan MA, Khawaja EE. X-ray photoelectron and auger spectroscopy study of copper-sodium-germanate glasses. J Non Cryst Solids. 1989;110(1):44–52.
96. Luo Z, Cheng W, Chen H, Fu X, Peng X, Luo F, et al. Preparation and properties of enzyme-modified cassava starch-zinc complexes. J Agric Food Chem. 2013;61(19):4631–8.
97. Pirsiavash F, Amani V, Abedi A. Coordination number in copper(II) complexes with bipyridine-dicarboxylate anion and diamine derivatives. Res Chem Intermed [Internet]. 2018;44(12):7411–26. Available from: https://doi.org/10.1007/s11164-018-3563-1
98. Dewitt C, Roper E. The surface relations of potassium ethyl xanthate and pine oil. Chem Dep Michigan Coll Min Technol. 1932;54:444–55.
99. Kosmulski M. Compilation of PZC and IEP of sparingly soluble metal oxides and hydroxides from literature. Adv Colloid Interface Sci. 2009 Nov 30;152:14–25.
100. Kosmulski M. Isoelectric points and points of zero charge of metal (hydr)oxides: 50 years after Parks' review. Vol. 238, Advances in Colloid and Interface Science. Elsevier B.V.; 2016. p. 1–61.
101. Kelebek S. The Effect of Oxidation on the Flotation Behaviour of Nickel-Copper Ores. In: XVlll lntemational Mineral Processing Congress. Sidney; 1993. p. 999–1005.
102. Hu Y, Sun W, Wang D. Natural Floatability and Collectorless Flotation of Sulphide Minerals. In: Electrochemistry of Flotation of Sulphide Minerals. Beijing: Tsinghua University Press; 209AD. p. 20–52.
103. Kronberg B, Holmberg K, Lindman B. Adsorption of Polymers at Solid Surfaces. In: Surface Chemistry of Surfactants and Polymers [Internet]. John Wiley & sons, ltd. Registered; 2014. p. 211–29. Available from: www.wiley.com.
104. Beattie DA, Huynh L, Kaggwa GBN, Ralston J. The effect of polysaccharides and polyacrylamides on the depression of talc and the flotation of sulphide minerals. In:

Minerals Engineering. 2006. p. 598–608.
105. Martins A, Nunes N. Adsorption of a textile dye on commercial activated carbon: A simple experiment to explore the role of surface chemistry and ionic strength. J Chem Educ. 2015 Jan 13;92(1):143–7.
106. Guirado G, Ayllón JA. A simple adsorption experiment. J Chem Educ. 2011 May 1;88(5):624–8.
107. Toth J. Adsorption Isotherms. In: Encyclopedia of Surface and Colloid Science. Taylor & Francis; 2015. p. 164–78.
108. Dubois M, Gilles KA, Hamilton JK, Rebers PA, Smith F. Colorimetric Method for Determination of Sugars and Related Substances. Anal Chem [Internet]. 1956;28(3):350–6. Available from: https://pubs.acs.org/sharingguidelines
109. Viel M, Collet F, Lanos C. Chemical and multi-physical characterization of agro-resources' by-product as a possible raw building material. Ind Crops Prod. 2018 Sep 15;120:214–37.
110. Pinto AMFR, Oliveira VB, Falcão DS. Experimental methods of characterization. Direct Alcohol Fuel Cells for Portable Applications. 2018. 113–155 p.
111. Susana L, Campaci F, Santomaso AC. Wettability of mineral and metallic powders: Applicability and limitations of sessile drop method and Washburn's technique. Powder Technol. 2012;226:68–77.
112. Yehia A, Miller JD, Ateya BG. Analysis of the adsorption behaviour of oleate on some synthetic apatites. Miner Eng. 1993;6(1):79–86.
113. Piccin JS, Cadaval TRSA, De Pinto LAA, Dotto GL. Adsorption isotherms in liquid phase: Experimental, modeling, and interpretations. Adsorption Processes for Water Treatment and Purification. 2017. 19–51 p.
114. Húmpola PD, Odetti HS, Fertitta AE, Vicente JL. Thermodynamic analysis of adsorption models of phenol in liquid phase on different activated carbons. J Chil Chem Soc. 2013;58(1):1541–4.
115. Liu Q, Laskowski JS, Li Y, Wang D. Synergistic effect of mineral surface constituents in dextrin adsorption. Int J Miner Process. 1994;42(3–4):251–66.
116. Somasundaran P. Adsorption of starch and oleate and interaction between them on calcite in aqueous solutions. J Colloid Interface Sci. 1969;31(4):557–65.

117. Mierczynska-Vasilev A, Ralston J, Beattie DA. Adsorption of modified dextrins on talc: Effect of surface coverage and hydration water on hydrophobicity reduction. Langmuir. 2008;24(12):6121–7.
118. Beaussart A, Parkinson L, Mierczynska-Vasilev A, Beattie DA. Adsorption of modified dextrins on molybdenite: AFM imaging, contact angle, and flotation studies. J Colloid Interface Sci [Internet]. 2012;368(1):608–15. Available from: http://dx.doi.org/10.1016/j.jcis.2011.10.075
119. Teng F, Liu Q, Zeng H. In situ kinetic study of zinc sulfide activation using a quartz crystal microbalance with dissipation (QCM-D). J Colloid Interface Sci [Internet]. 2012;368(1):512–20. Available from: http://dx.doi.org/10.1016/j.jcis.2011.10.048
120. Tadros T, Levecke B, Booten K. Polymeric Surfactants and Their Applications : Steric , Emulsion , and Suspension Stabilization. In: Zoller U, editor. Handbook of Detergents, Part E. 1st ed. Boca Raton; 2008. p. 504.
121. Legrand DL, Bancroft GM, Nesbitt HW. Oxidation/alteration of pentlandite and pyrrhotite surfaces at pH 9.3: Part 1. Assignment of XPS spectra and chemical trends. Am Mineral. 2005 Jul;90(7):1042–54.
122. Biesinger MC, Payne BP, Grosvenor AP, Lau LWM, Gerson AR, Smart RSC. Resolving surface chemical states in XPS analysis of first row transition metals, oxides and hydroxides: Cr, Mn, Fe, Co and Ni. Appl Surf Sci. 2011;257(7):2717–30.
123. Multani RS, Williams H, Johnson B, Li R, Waters K. The effect of superstructure on the zeta potential, xanthate adsorption, and flotation response of pyrrhotite. Colloids Surfaces A Physicochem Eng Asp. 2018 Aug 20;551:108–16.
124. Bremmell KE, Fornasiero D, Ralston J. Pentlandite-lizardite interactions and implications for their separation by flotation. Colloids Surfaces A Physicochem Eng Asp. 2005 Jan 20;252(2–3):207–12.
125. Rohem Peçanha E, da Fonseca de Albuquerque MD, Antoun Simão R, de Salles Leal Filho L, de Mello Monte MB. Interaction forces between colloidal starch and quartz and hematite particles in mineral flotation. Colloids Surfaces A Physicochem Eng Asp. 2019;562:79–85.
126. Jin S, Shi Q, Li Q, Ou L, Ouyang K. Effect of calcium ionic concentrations on the adsorption of carboxymethyl cellulose onto talc surface: Flotation, adsorption and AFM

imaging study. Powder Technol. 2018;331:155–61.

127. Ciesielski W, Tomasik P. Werner-type metal complexes of potato starch. Int J Food Sci Technol. 2004;39(6):691–8.

Appendix 1 Additional information about the synthesis of the starch depressants

The crosslinked starch synthesis was based on exploratory thermo and thermo-caustic gelatinization tests, and supported by methodologies described in (74–76,127) and (17). For both gelatinization processes, starch suspension became viscous at around 60 ºC, consistent with the values in the literature for potato starch gelatinization temperature (58.2-67.7 ºC) (71). This temperature is dependent on the botanic source of starch (73).

Preliminary tests with a 7% w/w aqueous starch suspension did not allow an adequate gelatinization resulting in a non-transparent gel (Figures 57a and 57d), most likely due to non disrupted granules. Although this milky condition, in a first moment, could be considered just as a loss of initial starch, this showed to be detrimental for the precipitation with ethanol (Figures 57b and 57e) and for the oven drying process (Figures 57c and 57f). Dried products could not be used for micro-flotations.

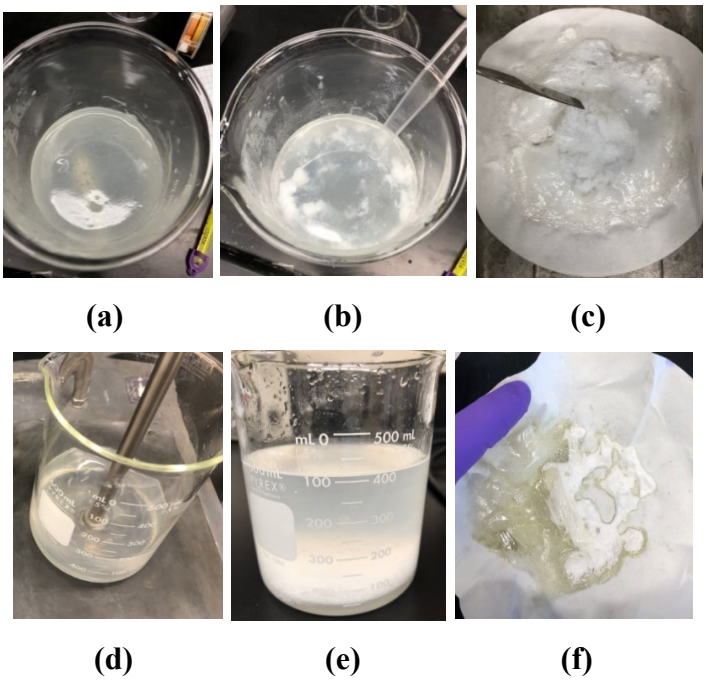

Figure 57: Main problems encountered in the gelatinization process (gel formation, precipitation with ethanol, and drying for 24 hours). Images (a), (b) and (c) are related to thermo gelatinization, while (d), (e) and (f) correspond to thermo-caustic gelatinization.

Solutions found to this incomplete gelatinization consisted of changing the heating set up to a water heating bath (for uniform heating transfer), the increase of the shear mixing power, the reduction of starch/water ratio, temperature, and time as described elsewhere (68,71). As a consequence, the produced gel had an aspect totally transparent (Figure 58a) as well as the solution after starch precipitation (Figure 58b), apparently lacking undisrupted starch granules. The dried paste starch (Figure 58c) is called PP. However, after drying in an oven, paste starch became extremely hard. Therefore, tests with a freeze-dryer were stablished as the new drying method, resulting in a softer final PP and LC.

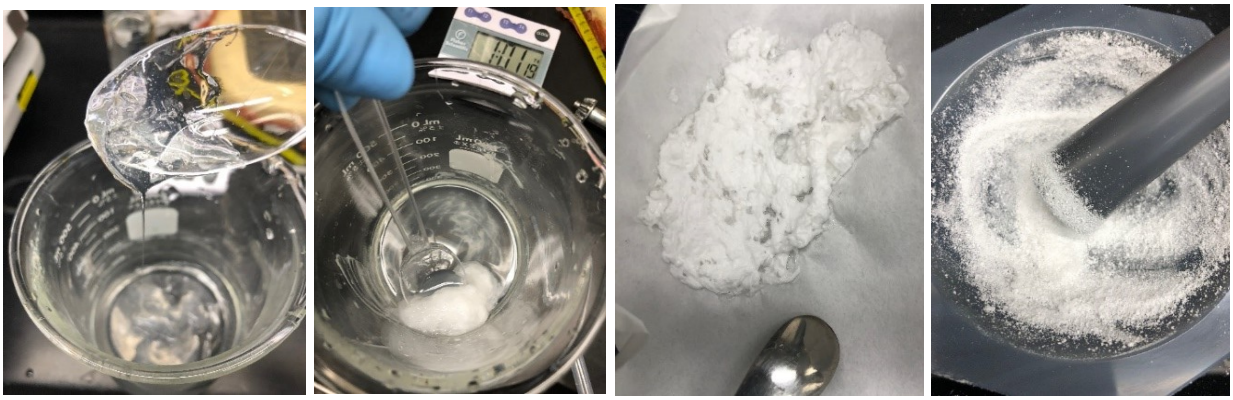

(a) **(b)** **(c)** **(d)**

Figure 58: Thermo gelatinization of potato starch under higher temperature and shear mixing power. Image (a) shows the final transparent gel, (b) the precipitation with ethanol, (c) dried PP after 24 hours, and (d) ground PP.

Ground PP (Figure 58d), with initial pH at 4, was mixed with 0.1 M $CuCl_2$ solution and kept under agitation for 24 hours at 500 RPM (room temperature). PP in water immediately formed gel aggregates. These aggregates did not dissolve even after 24 hours of mixing (Figure 59a). The dried final product could not be considered as a crosslinked starch because of its “green glass” aspect (Figure 59b). Due to this, a copper solution was added directly to the gel to enable the maximum coordination of metal ions (Chapter 3).

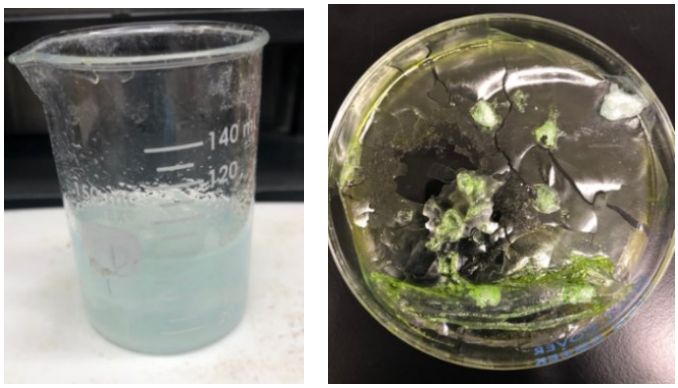

(a) **(b)**

Figure 59: Suspension with starch and $CuCl_2$ after 24 hours of mixing (a), and dried product of the crosslinked starch after a second precipitation process (b).

Appendix 2 Influence of Cu (II) and Ni (II) species in solution on pentlandite and hexagonal pyrrhotite floatabilities

Although metal ions are known as mineral activators (5,55), their presence in the pulp as an additive or due to the oxidation/dissolution of minerals can have depressing effects (54). In fact, a Positive Ions ToF-SIMS image of pyrrhotite in the primary rougher at Sudbury shows that nickel ions may be present in the tails as well (Figure 60).

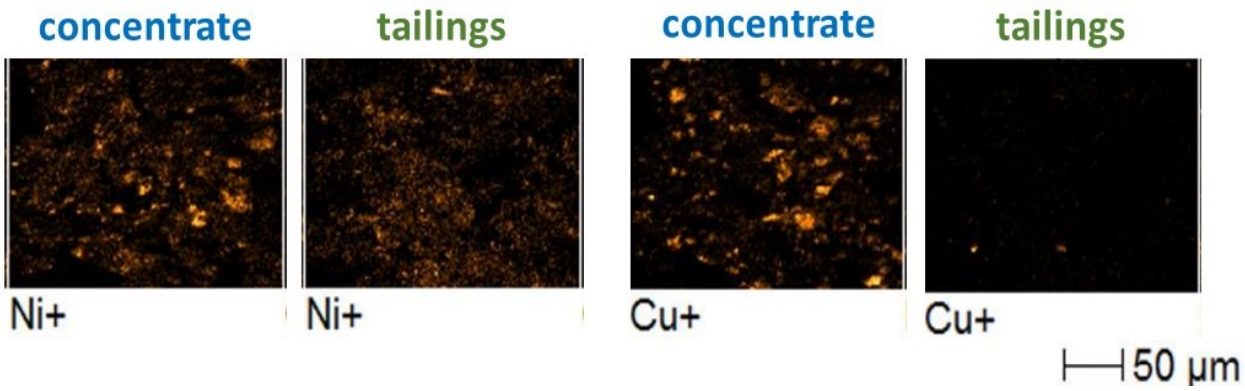

Figure 60: Positive Ion ToF-SIMS Image of hexagonal pyrrhotite in the primary rougher at the Sudbury plant in 2016. From: internal source.

Therefore, a short investigation about copper and nickel ions' impact on the floatabilities of hexagonal pyrrhotite and pentlandite was carried out. The micro-flotation procedure can be seen in Figure 61. Results with 9.66×10^{-6} M of PIBX (240 g/t) are not shown since the activation/depressing effects were masked by high dosages of collector. Tests were performed in triplicates.

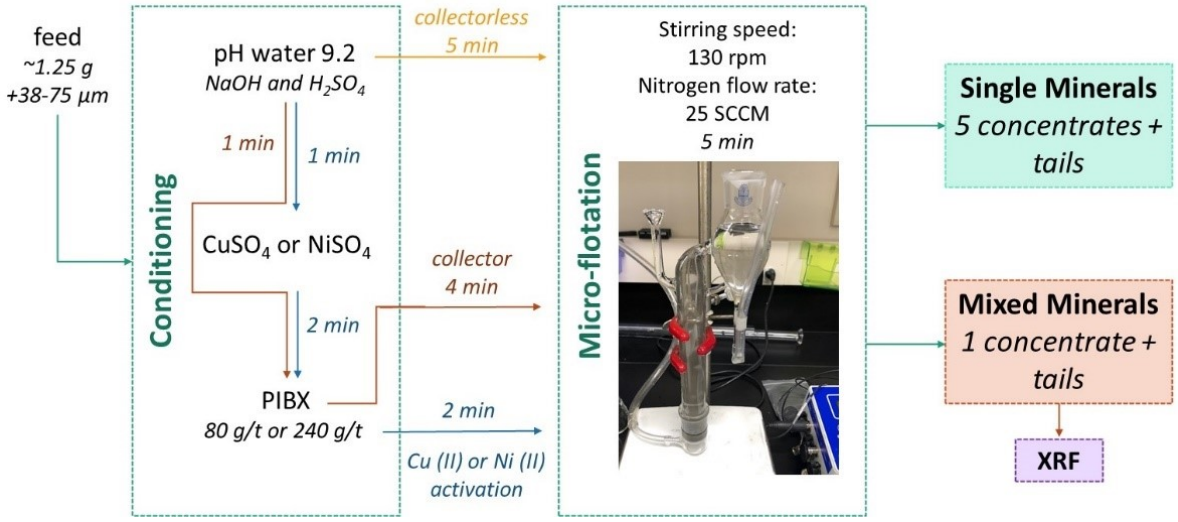

Figure 61: Procedure used for the micro-flotation tests using $CuSO_4$ and $NiSO_4$.

The results demonstrated that Ni (II) ions have a depressing effect on both minerals (Figure 62). Similarly, copper seems to contribute to pentlandite depression.

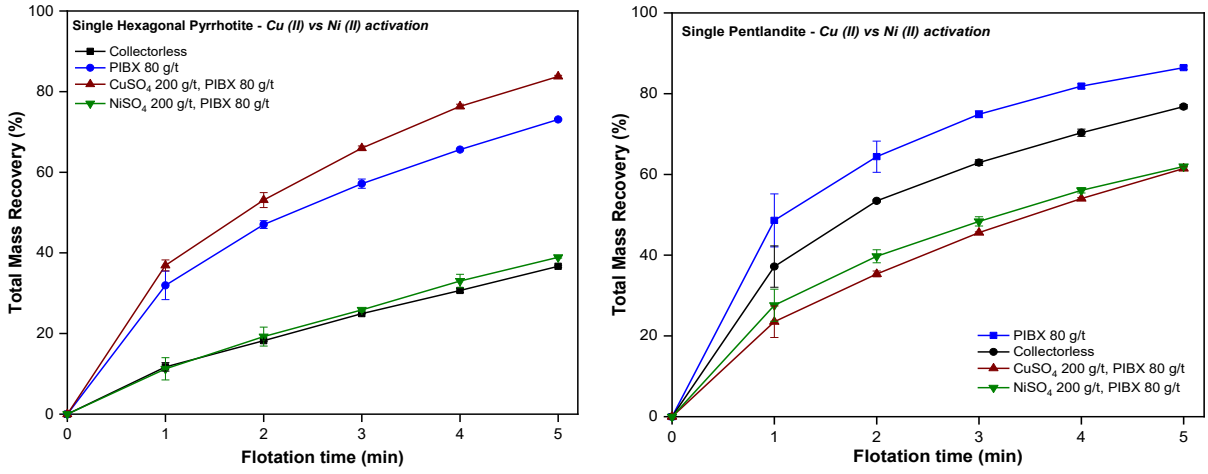

Figure 62: Kinetics micro-flotation results with copper and nickel ions of single pentlandite, and single hexagonal pyrrhotite. All flotations were performed with 3.22×10^{-6} M PIBX (equivalent to 80 g/t), and 9.49×10^{-6} M metal ion concentration (equivalent to 200 g/t of the corresponding sulfate salt).

The Cu(II) depressing effect on pentlandite is a consequence of $CuSO_4$ dosage (Figure 63). Above 20 g/t of $CuSO_4$, pentlandite is depressed while hexagonal pyrrhotite is activated and its recovery boosts.

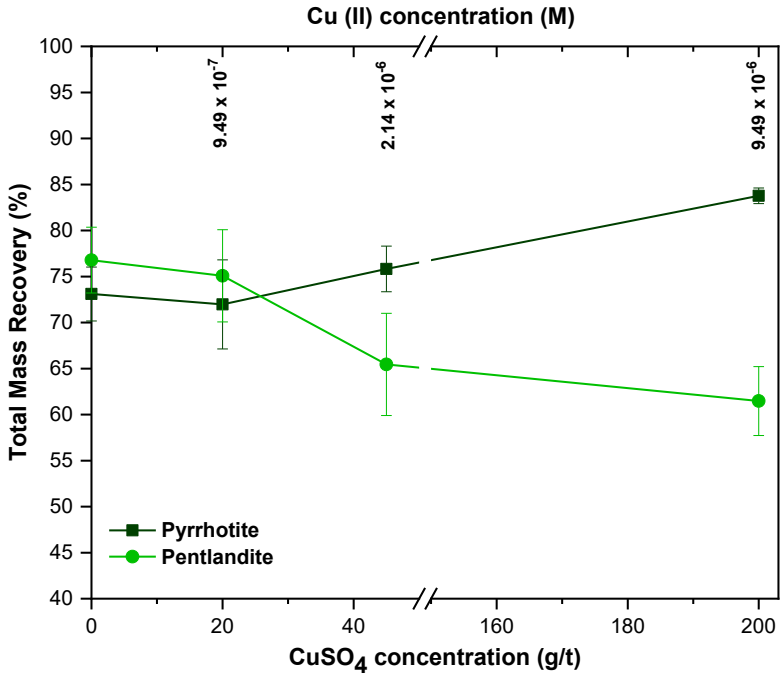

Figure 63: Single micro-flotation results using different concentrations of $CuSO_4$. All flotations were performed with $3.22x10^{-6}$ M PIBX (equivalent to 80 g/t).

A similar trend was verified for mixed minerals flotation (Figure 64). The addition of $NiSO_4$ still presents a depressing effect on both minerals. Conversely, the addition of $CuSO_4$ increased the recovery of hexagonal pyrrhotite (given by Fe associated with gangue minerals), and the final Ni grade was the lowest at 14.19% when compared with collector (15.12%) and the Ni activation test (16.42%).

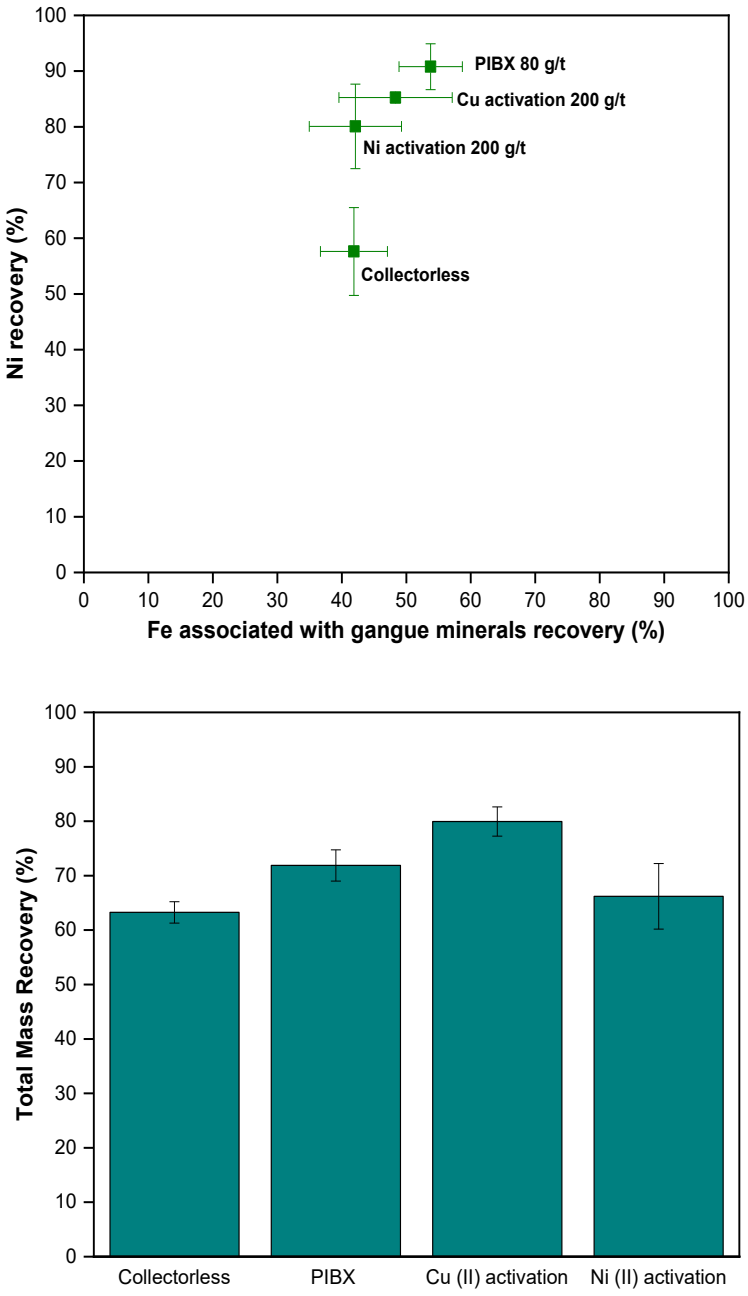

Figure 64: Metallurgical recovery and total mass recovery results of mixed micro-flotations with copper and nickel ions. All flotations were performed with 3.22×10^{-6} M PIBX (equivalent to 80 g/t) and 200 g/t of the metal sulfate salt.

Appendix 3 Linearization of the adsorption models

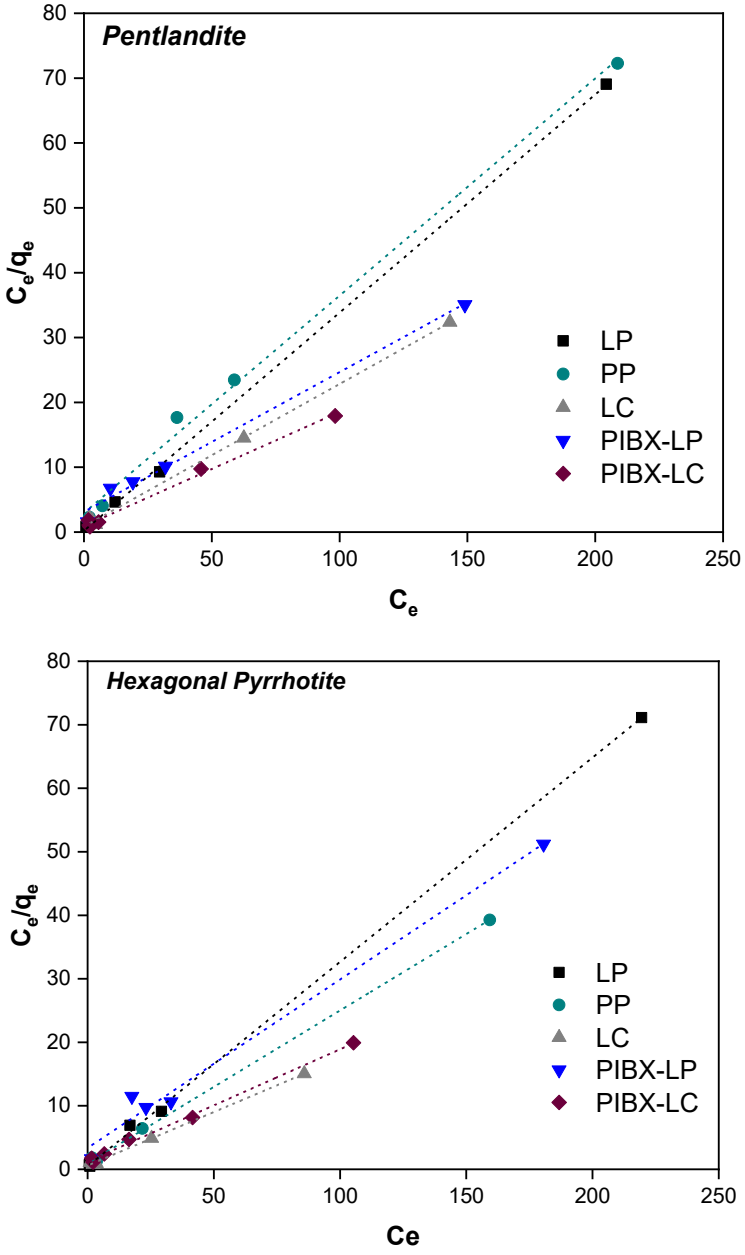

Figure 65: Linearization of the Langmuir model using Equation 26.

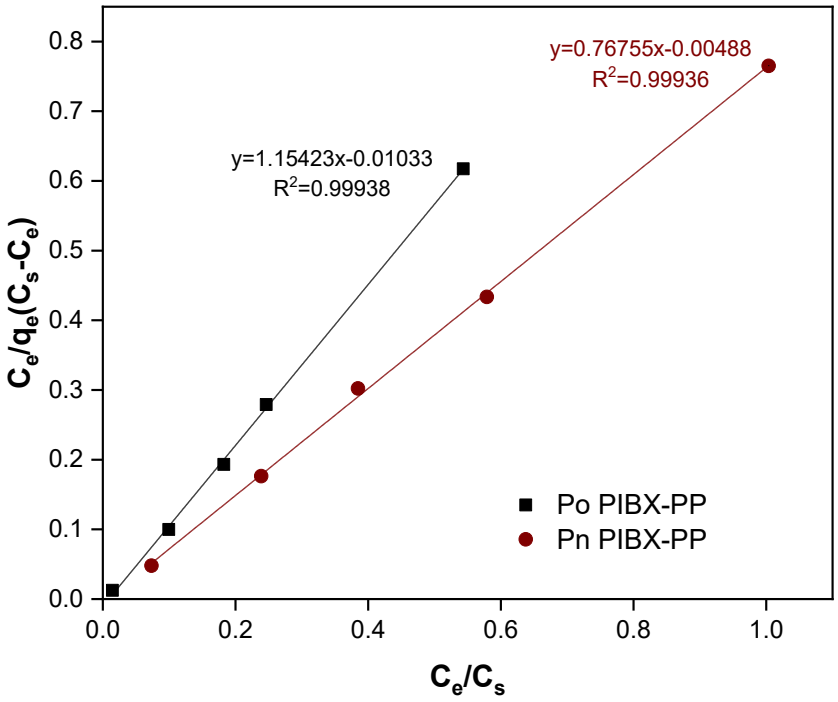

Figure 66: Linearization of the BET model of PP for co-adsorption measurement with PIBX using Equation 29.

Appendix 4 Graphics obtained with the Washburn method

- Capillary constant

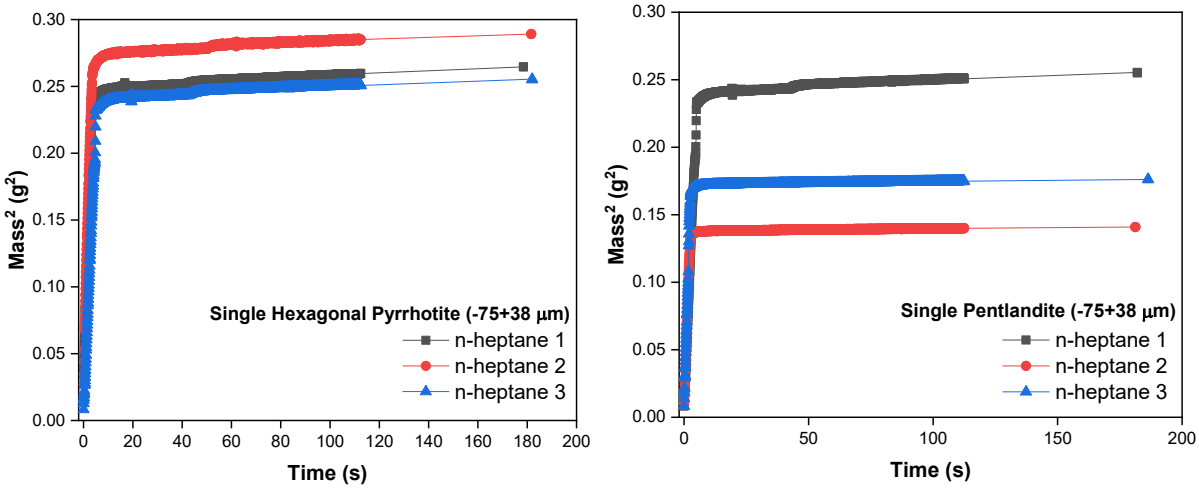

Figure 67: Mass^2 vs time graphics to determine the capillary constant (C_w).

- Single Hexagonal Pyrrhotite

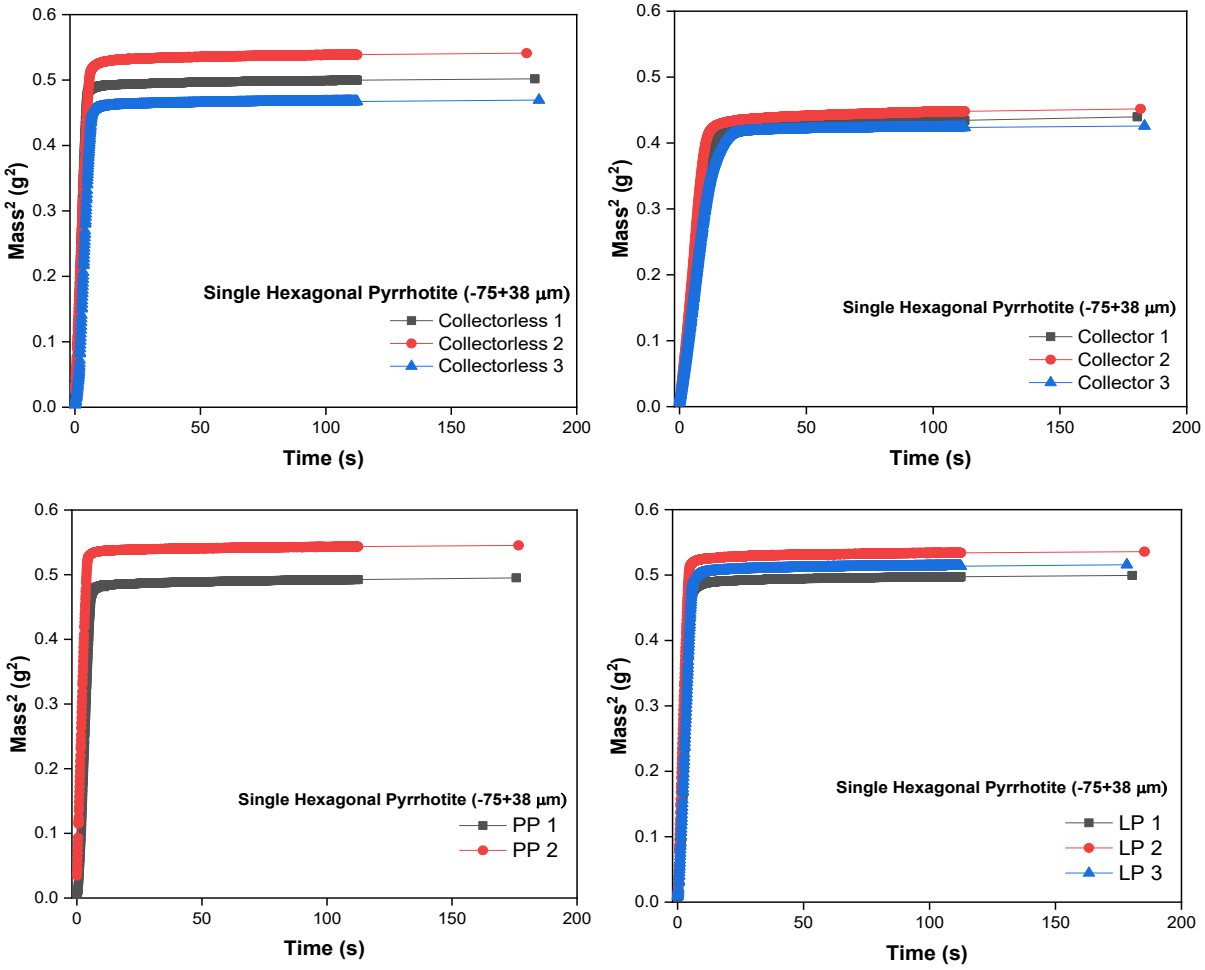

Figure 68: Mass^2 vs time graphics used to determine the contact angle of powdered hexagonal pyrrhotite.

- Single Pentlandite

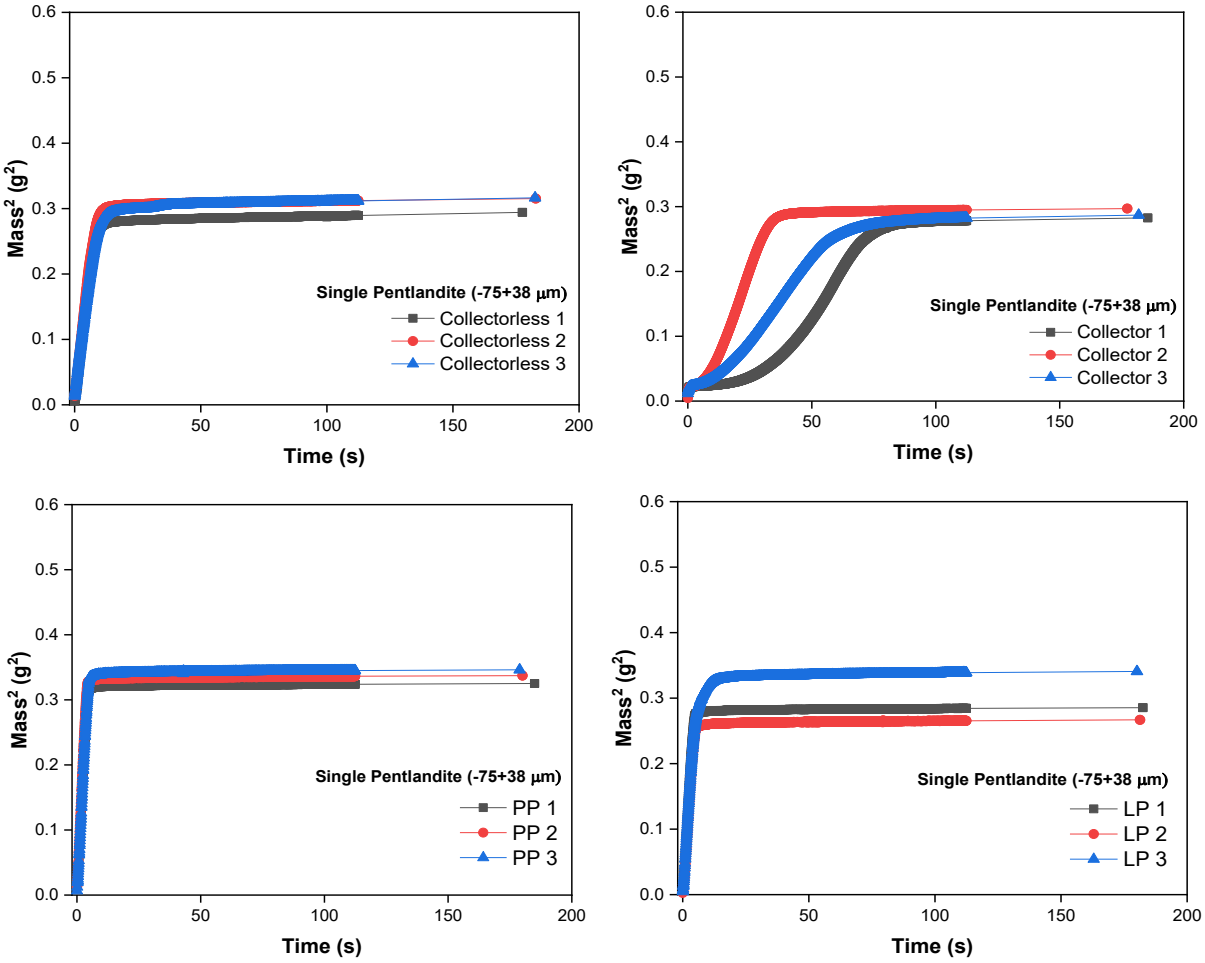

Figure 69: Mass^2 vs time graphics used to determine the contact angle values of powdered pentlandite.

Appendix 5 Additional information about the QCM-D tests

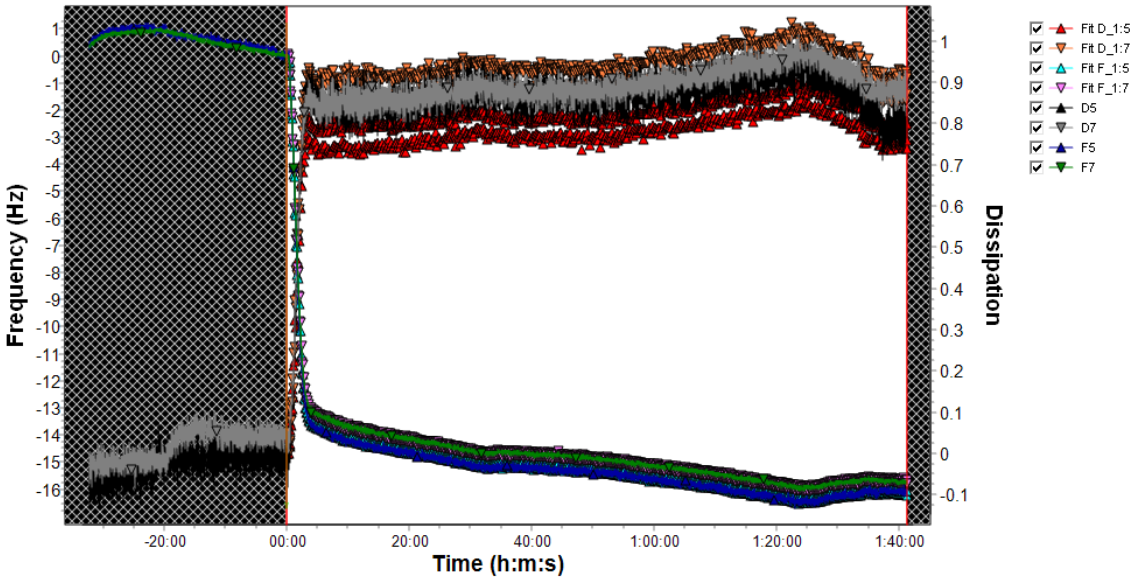

Figure 70: Limit x-values for modeling PP layer thickness.

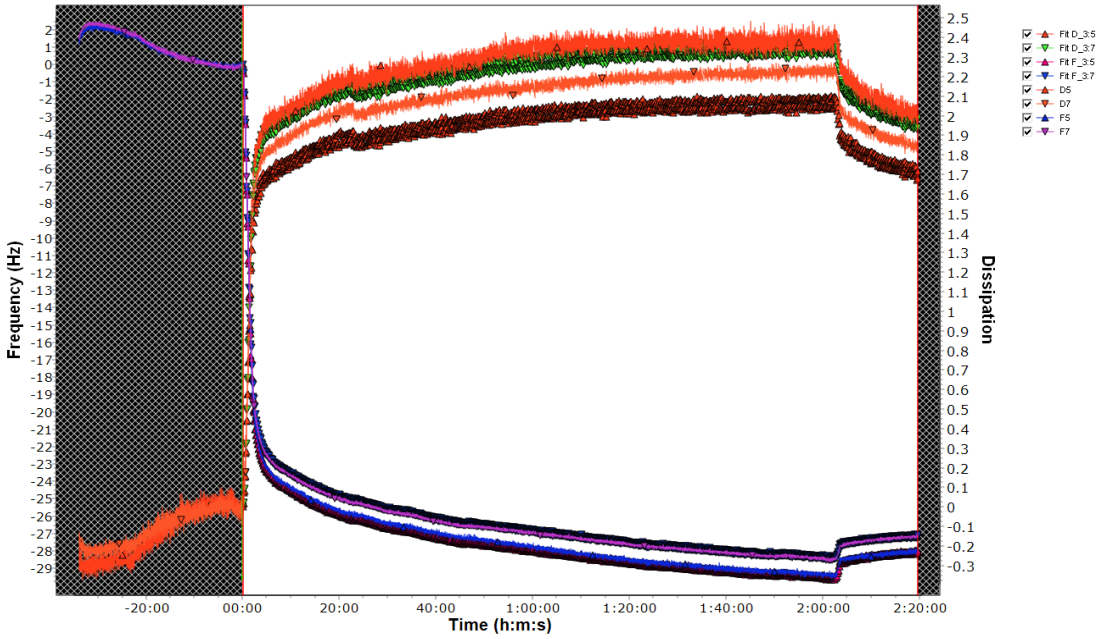

Figure 71: Limit x-values for modeling LP layer thickness.

Appendix 6 Additional AFM imaging

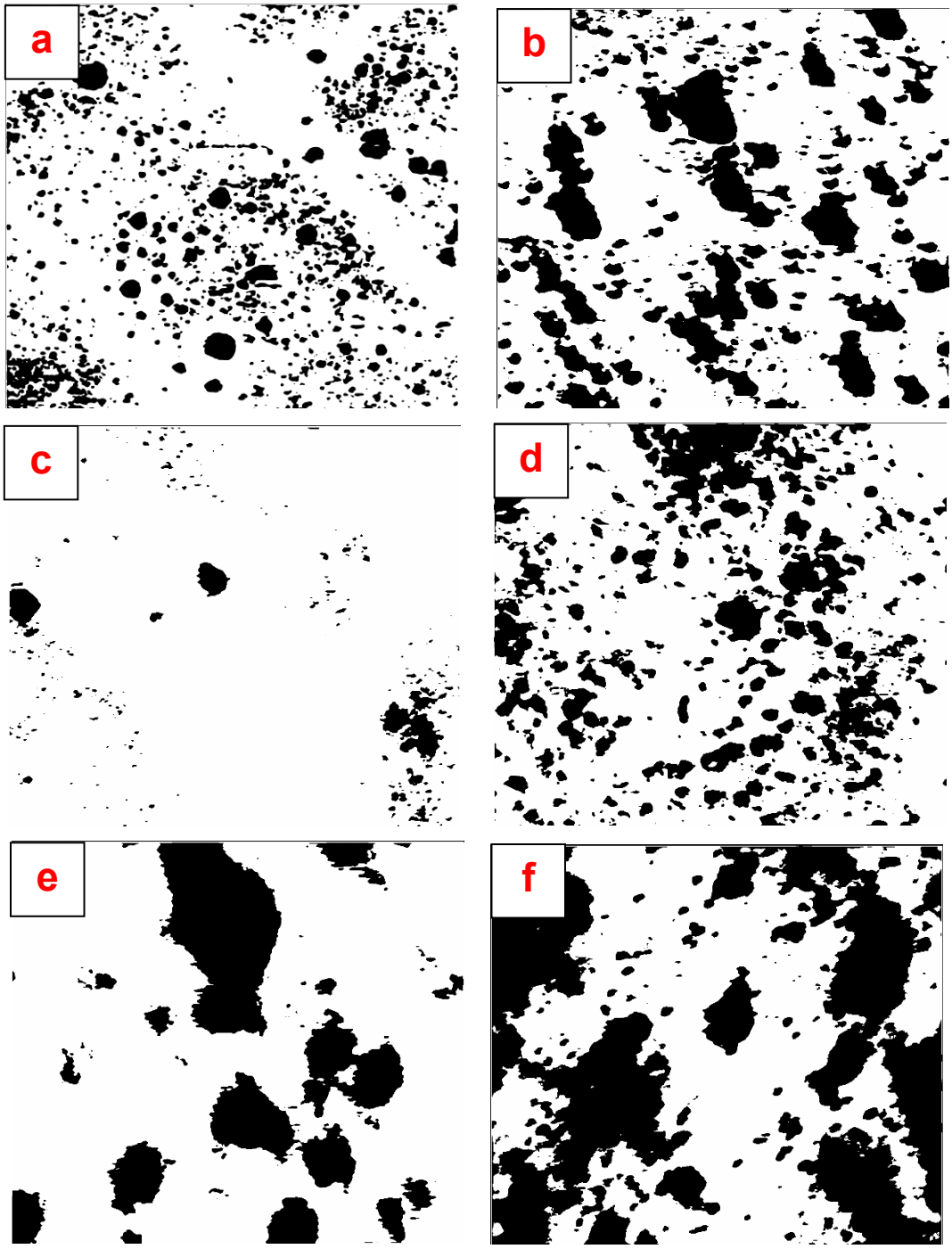

Figure 72: Processed images using ImageJ to calculate the surface covered areas by the starch depressants. (a) Pn-PP; (b) Po-PP; (c) Pn-LP; (d) Po-LP; (e) Pn-LC; (f) Po-LC.

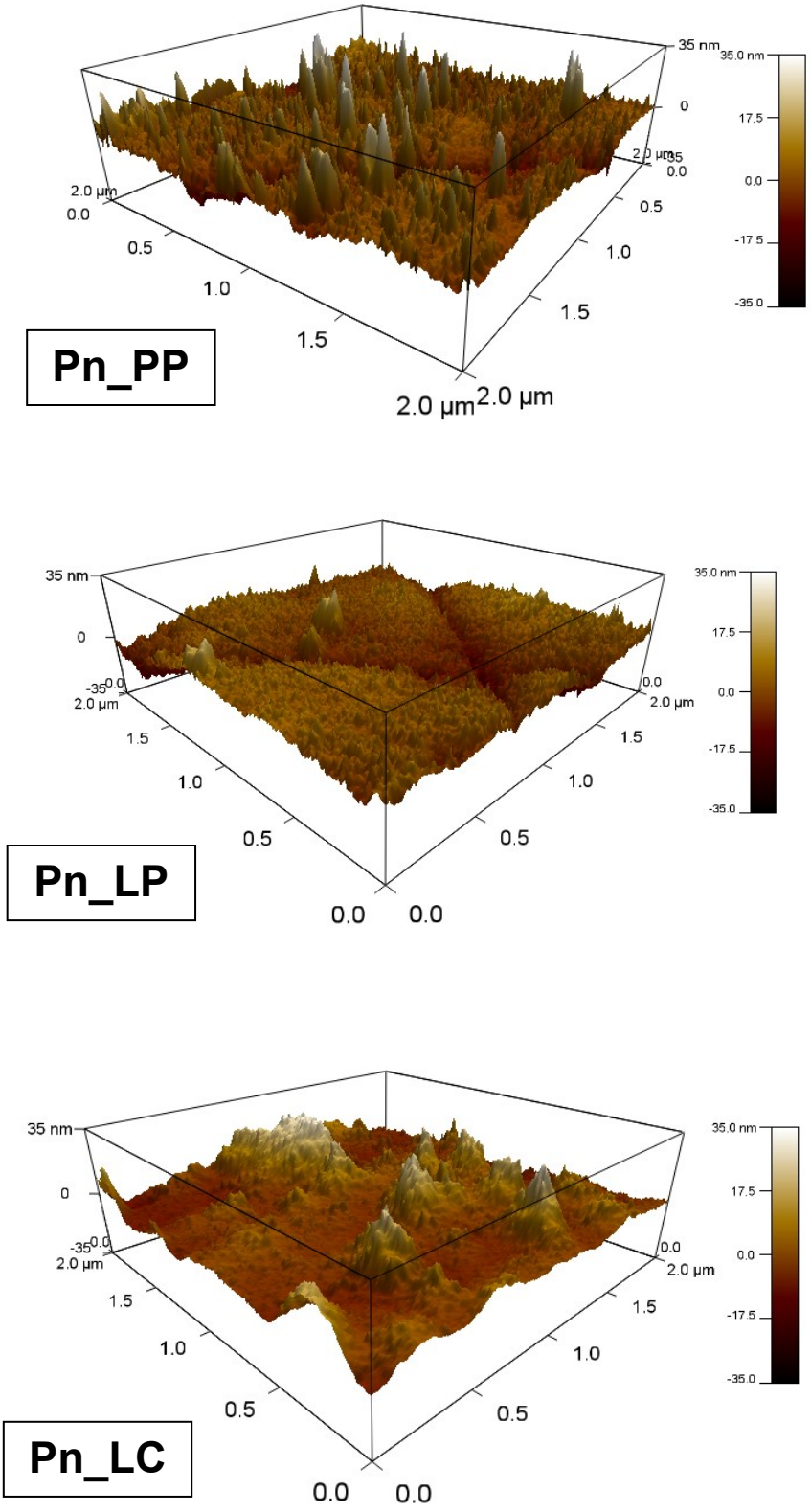

Figure 73: 3D view of the topography of the adsorbed layer of the starch depressants on pentlandite.

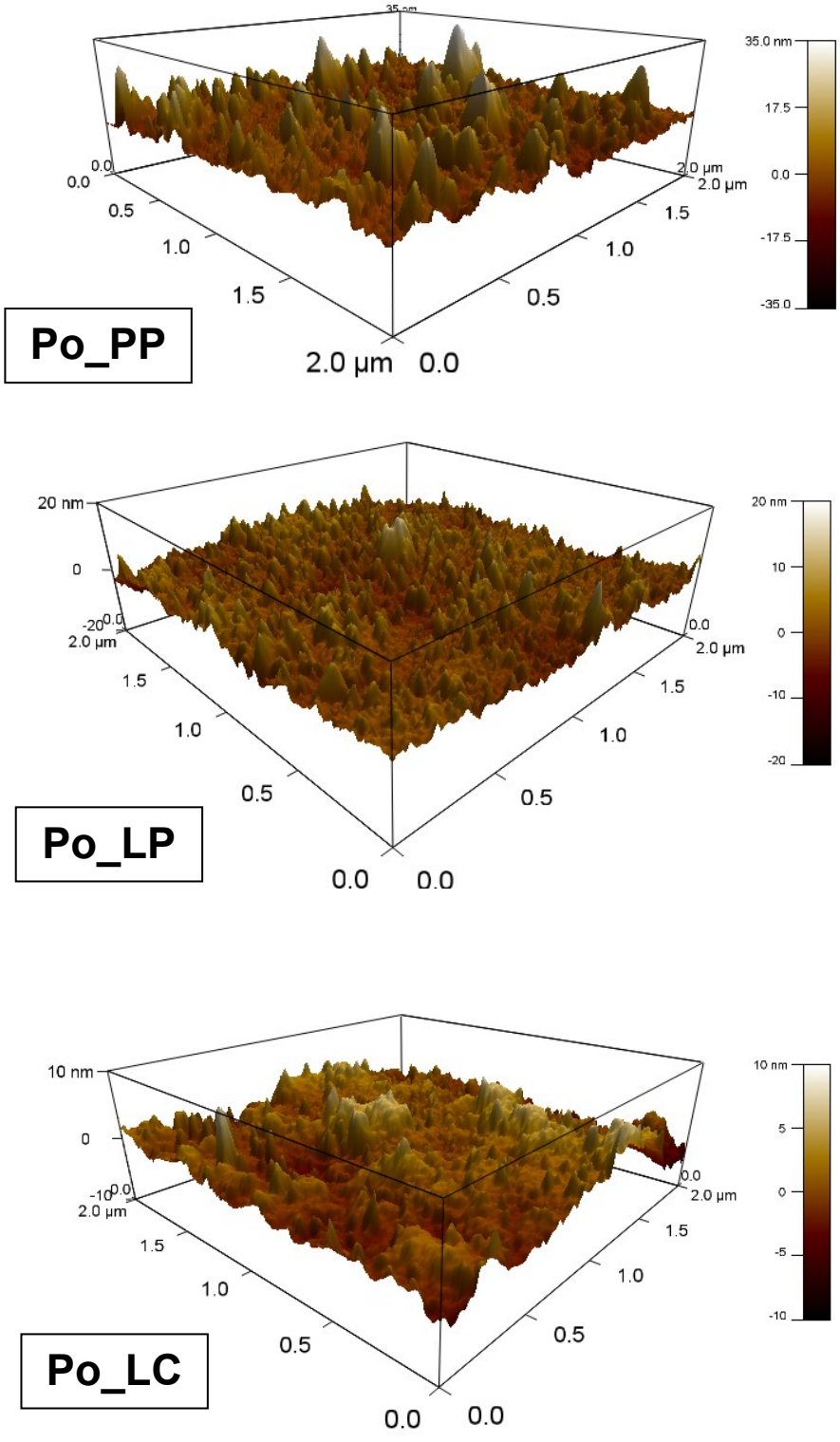

Figure 74: 3D view of the topography of the adsorbed layer of the starch depressants on hexagonal pyrrhotite.

Appendix 7 Additional XPS spectrums

- Hexagonal pyrrhotite

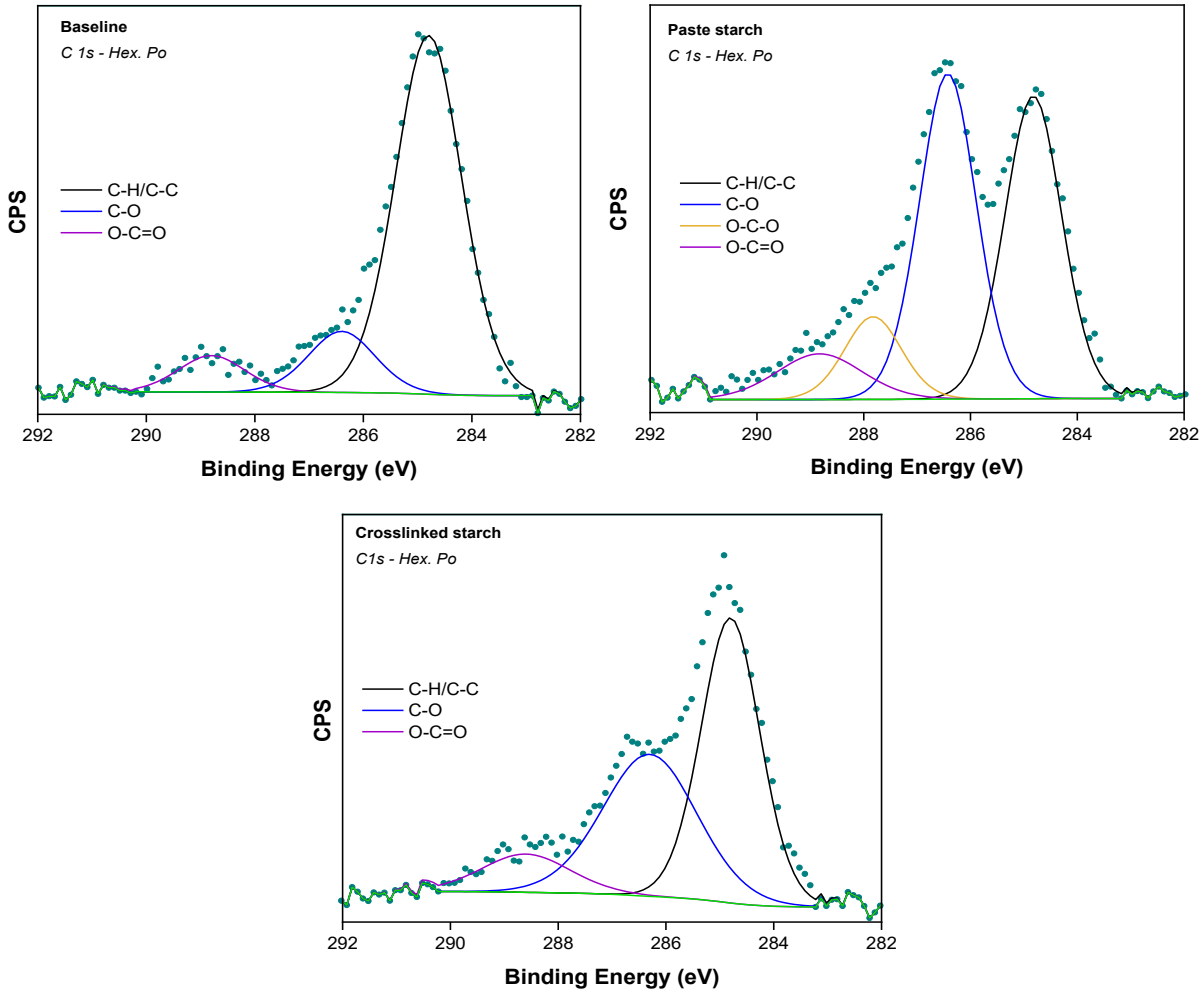

Figure 75: C 1s spectra comparison between baseline, paste starch, and crosslinked starch interactions with hexagonal pyrrhotite surface.

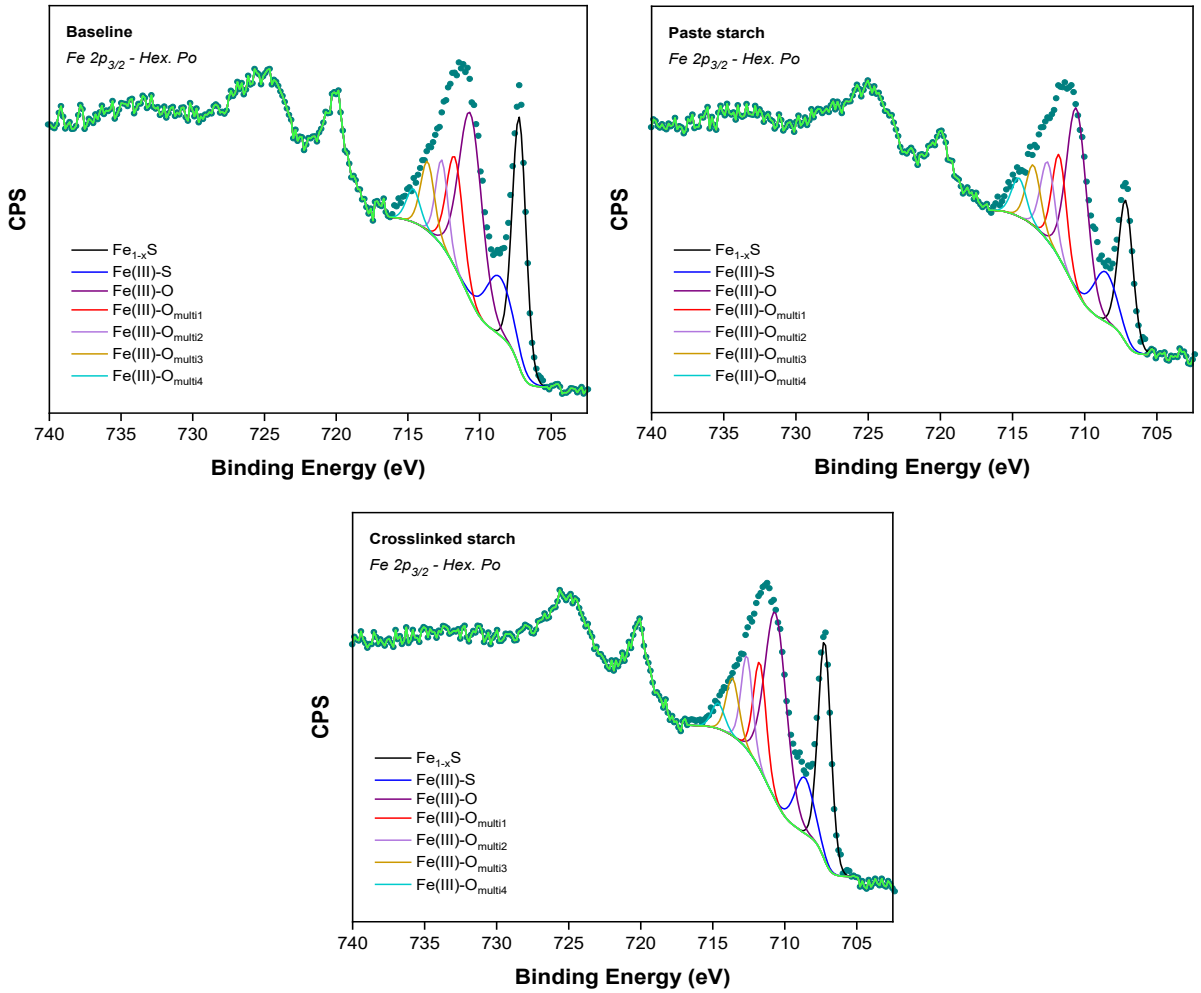

Figure 76: Fe $2p_{3/2}$ spectra comparison between baseline, paste starch, and crosslinked starch interactions with hexagonal pyrrhotite surface.

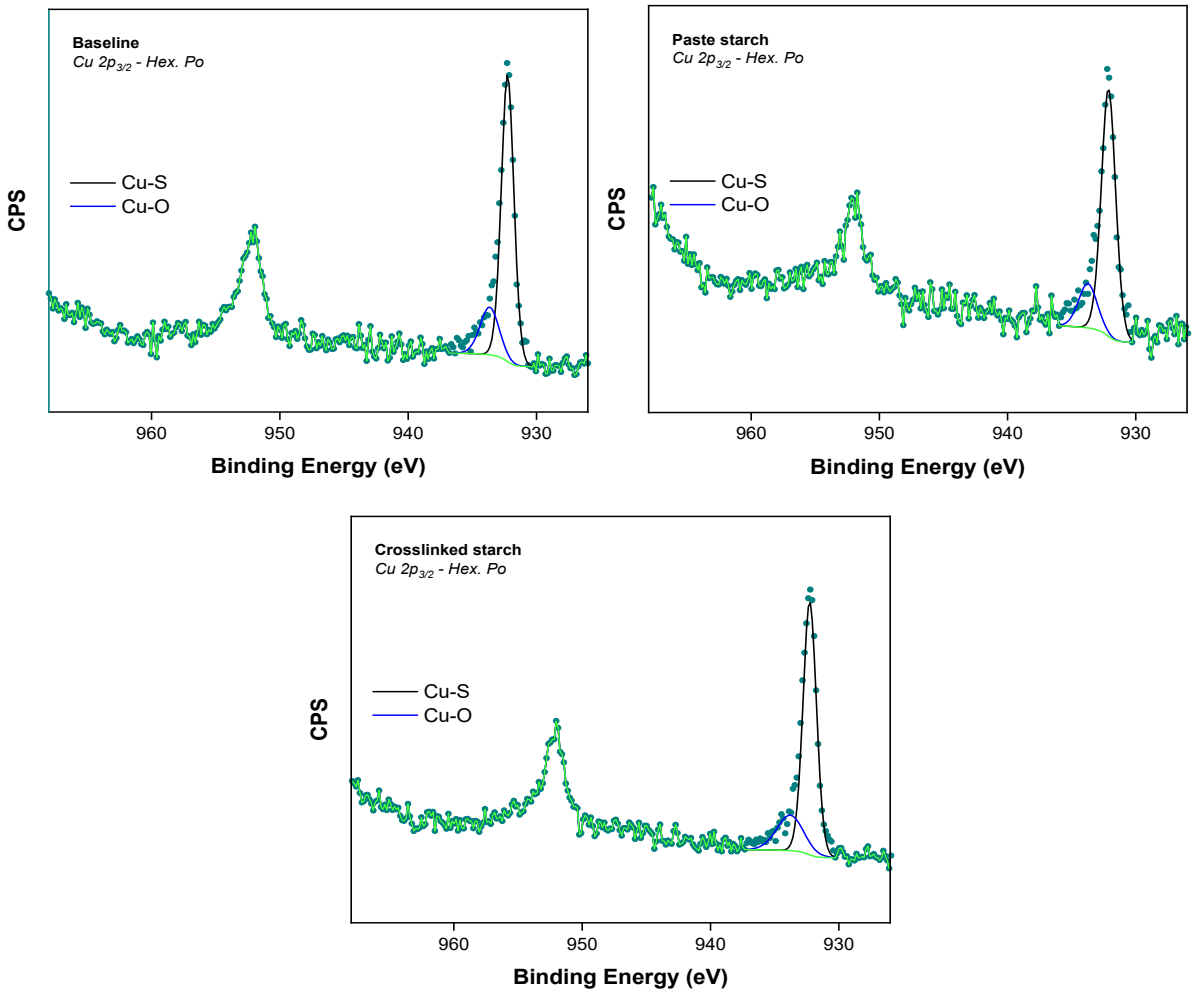

Figure 77: Cu $2p_{3/2}$ spectra comparison between baseline, paste starch, and crosslinked starch interactions with hexagonal pyrrhotite surface.

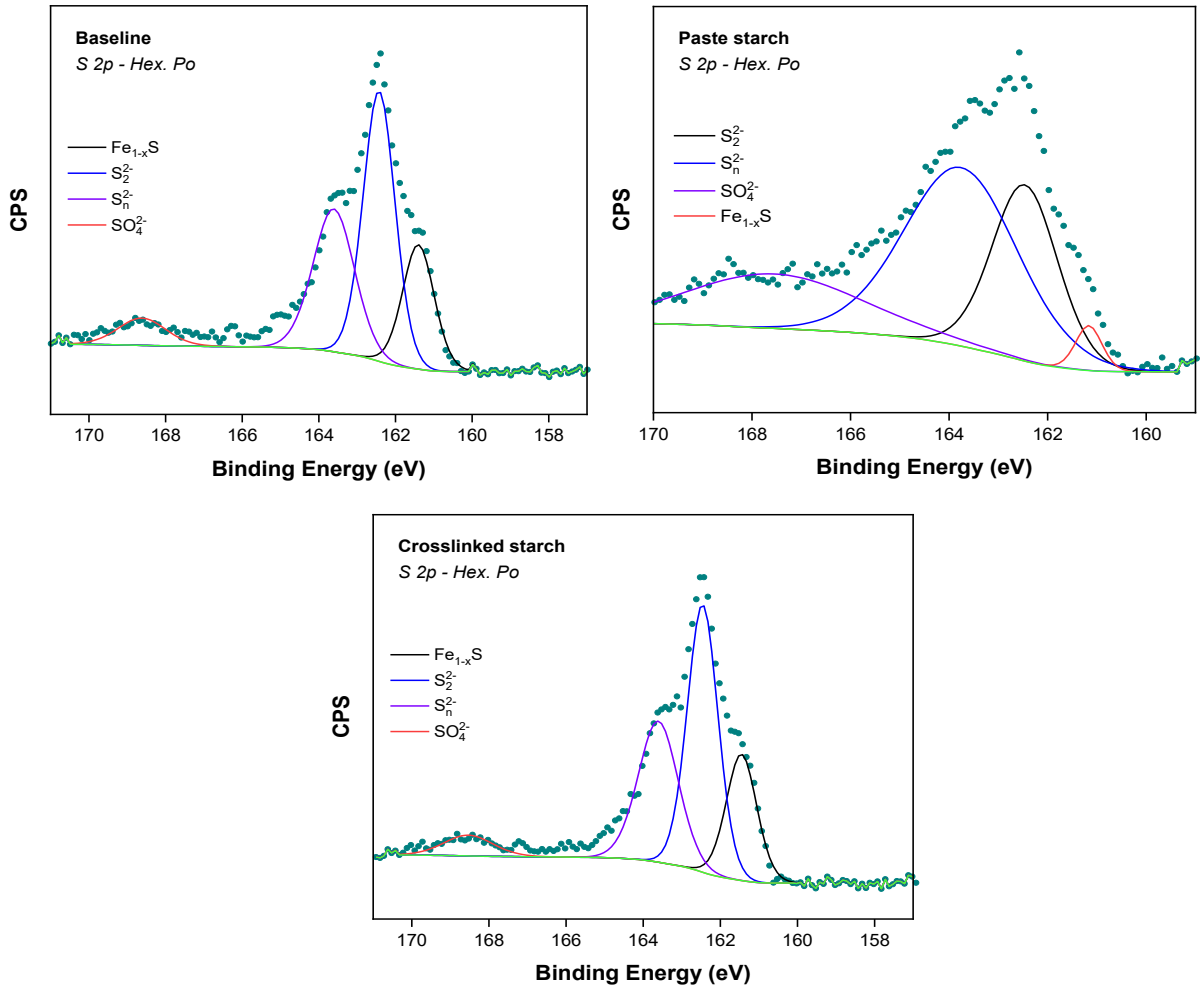

Figure 78: S 2p spectra comparison between baseline, paste starch, and crosslinked starch interactions with hexagonal pyrrhotite surface. Assigned values based on (46).

Table 15: Residual standard deviation (STD) obtained after fitting the hexagonal pyrrhotite data using a Shirley background.

Spectrum		STD		STD		STD
C 1s	Baseline	0.91	Paste starch	1.08	Crosslinked starch	1.08
O 1s		0.77		1.15		0.94
Fe $2p_{3/2}$		1.09		1.24		0.82
S 2p		2.31		1.12		1.76
Cu $2p_{3/2}$		0.94		1.05		0.94

- Pentlandite

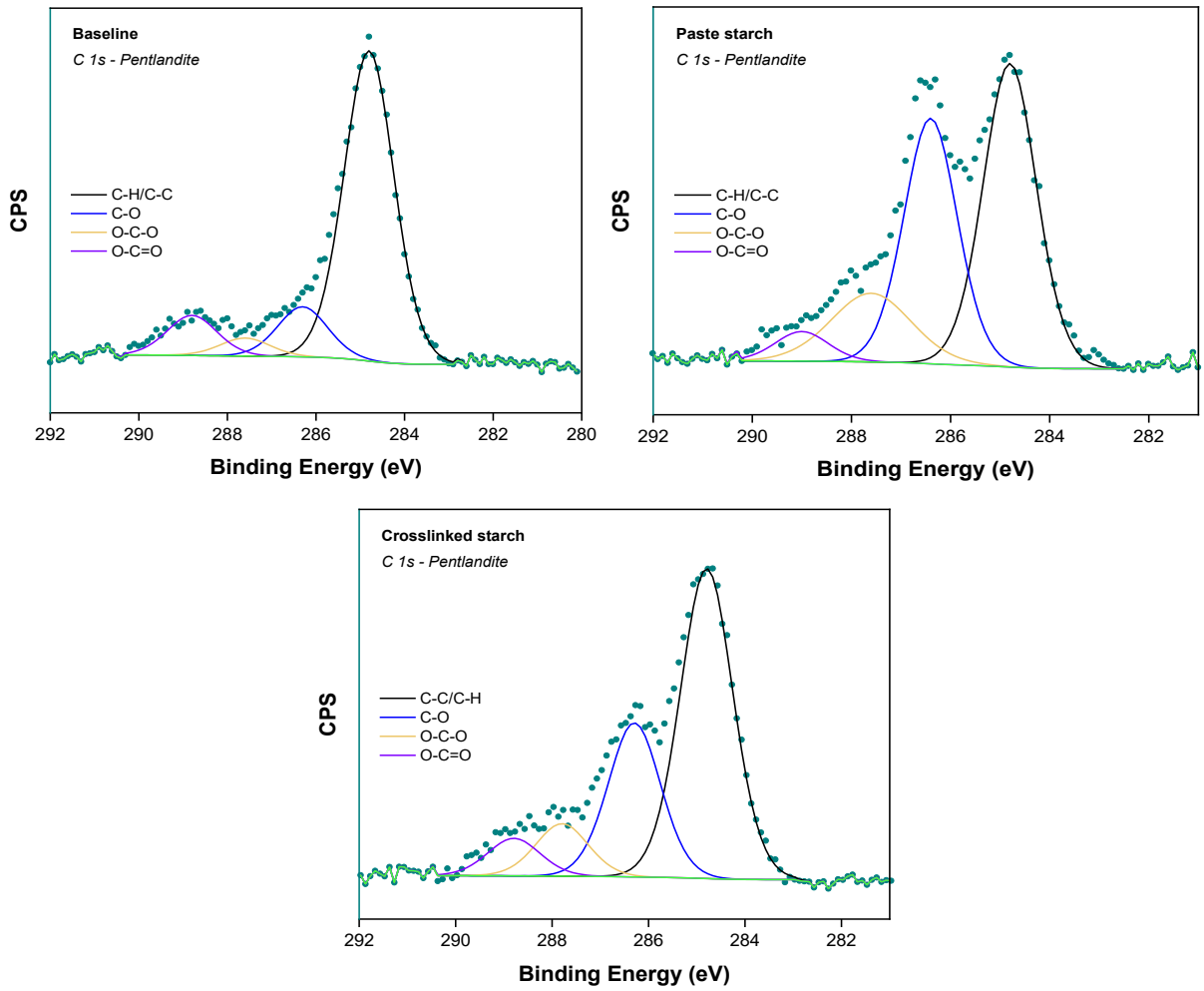

Figure 79: C 1s spectra comparison between baseline, paste starch, and crosslinked starch interactions with pentlandite surface.

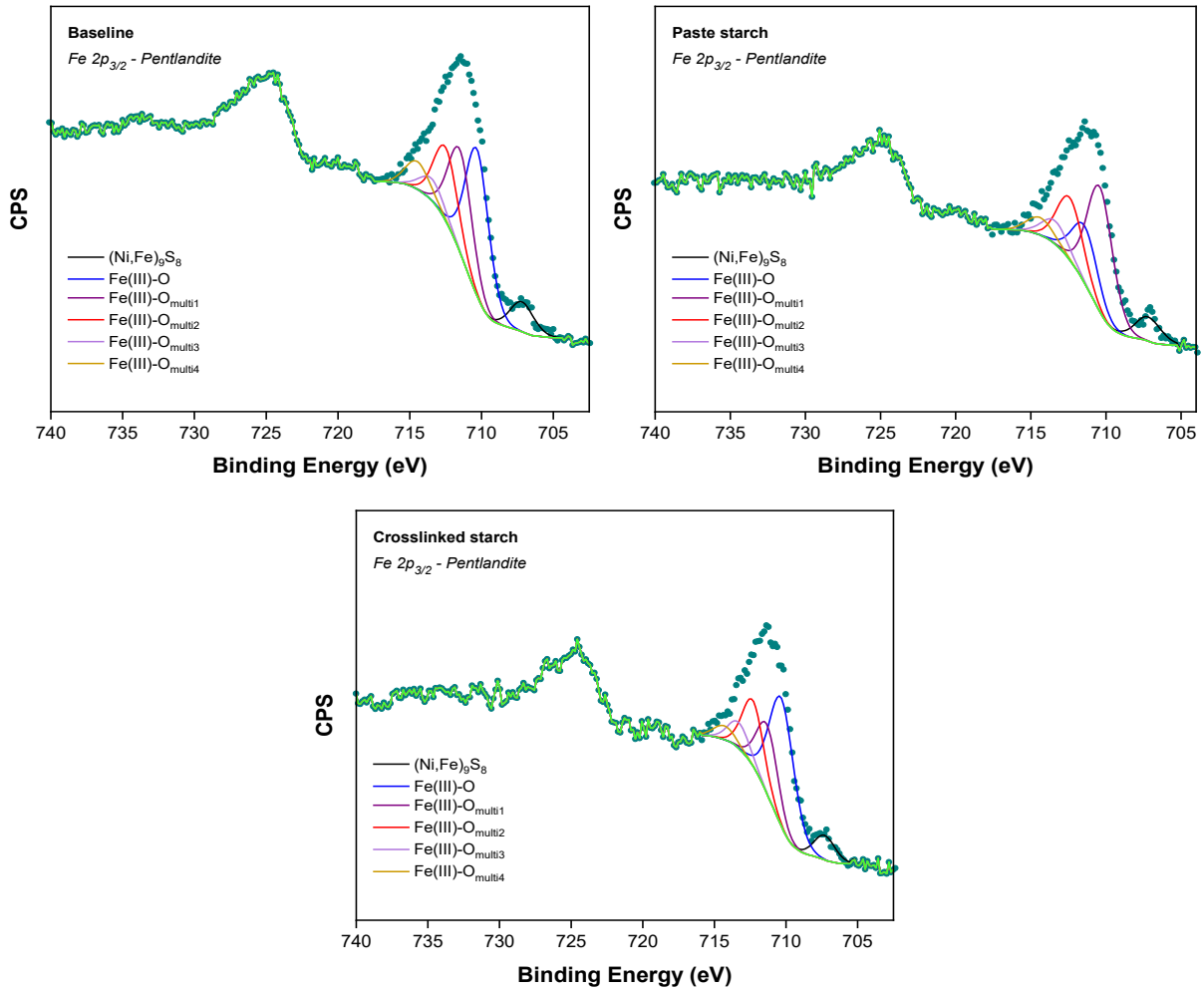

Figure 80: Fe $2p_{3/2}$ spectra comparison between baseline, paste starch, and crosslinked starch interactions with pentlandite surface.

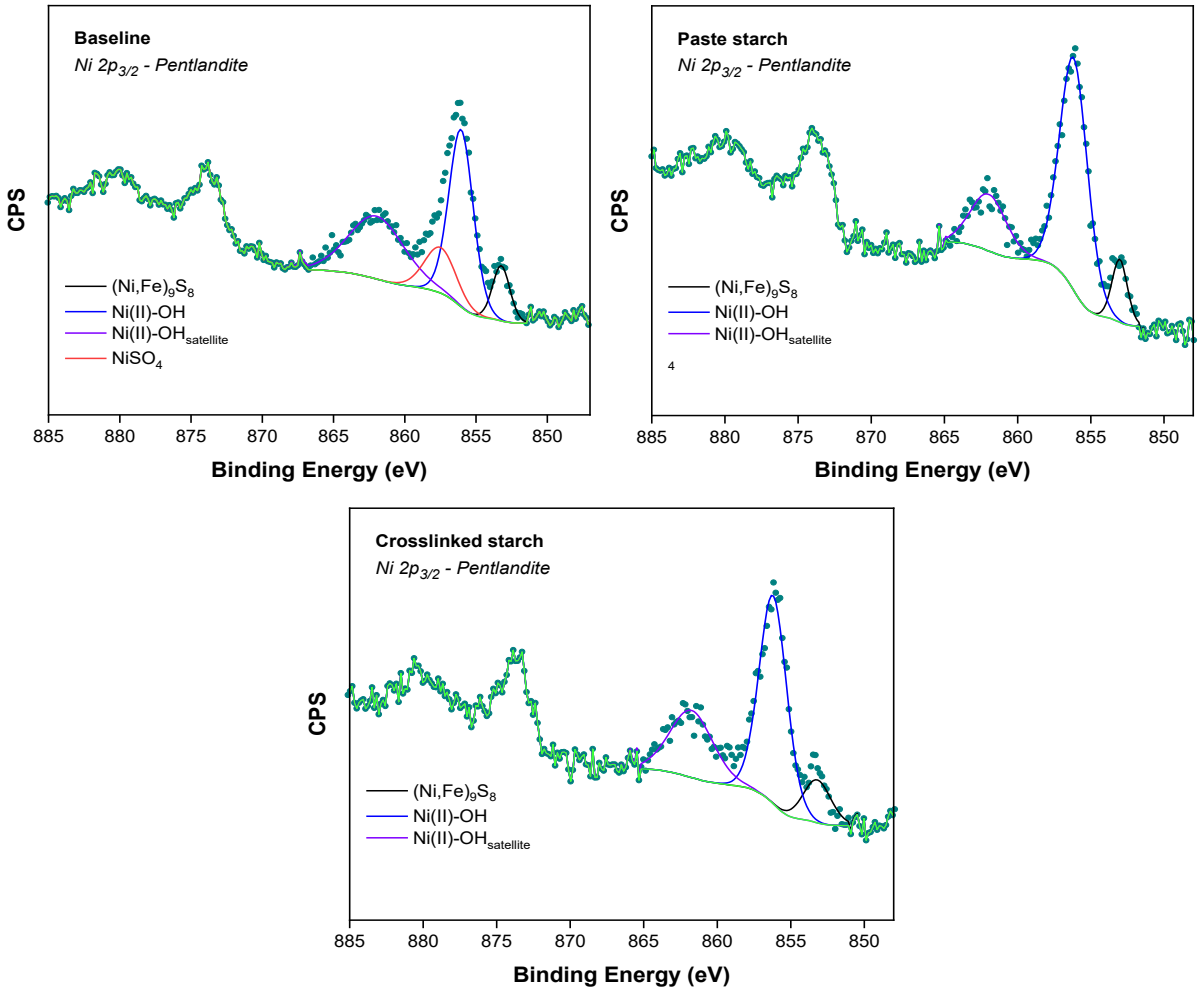

Figure 81: Ni $2p_{3/2}$ spectra comparison between baseline, paste starch, and crosslinked starch interactions with pentlandite surface.

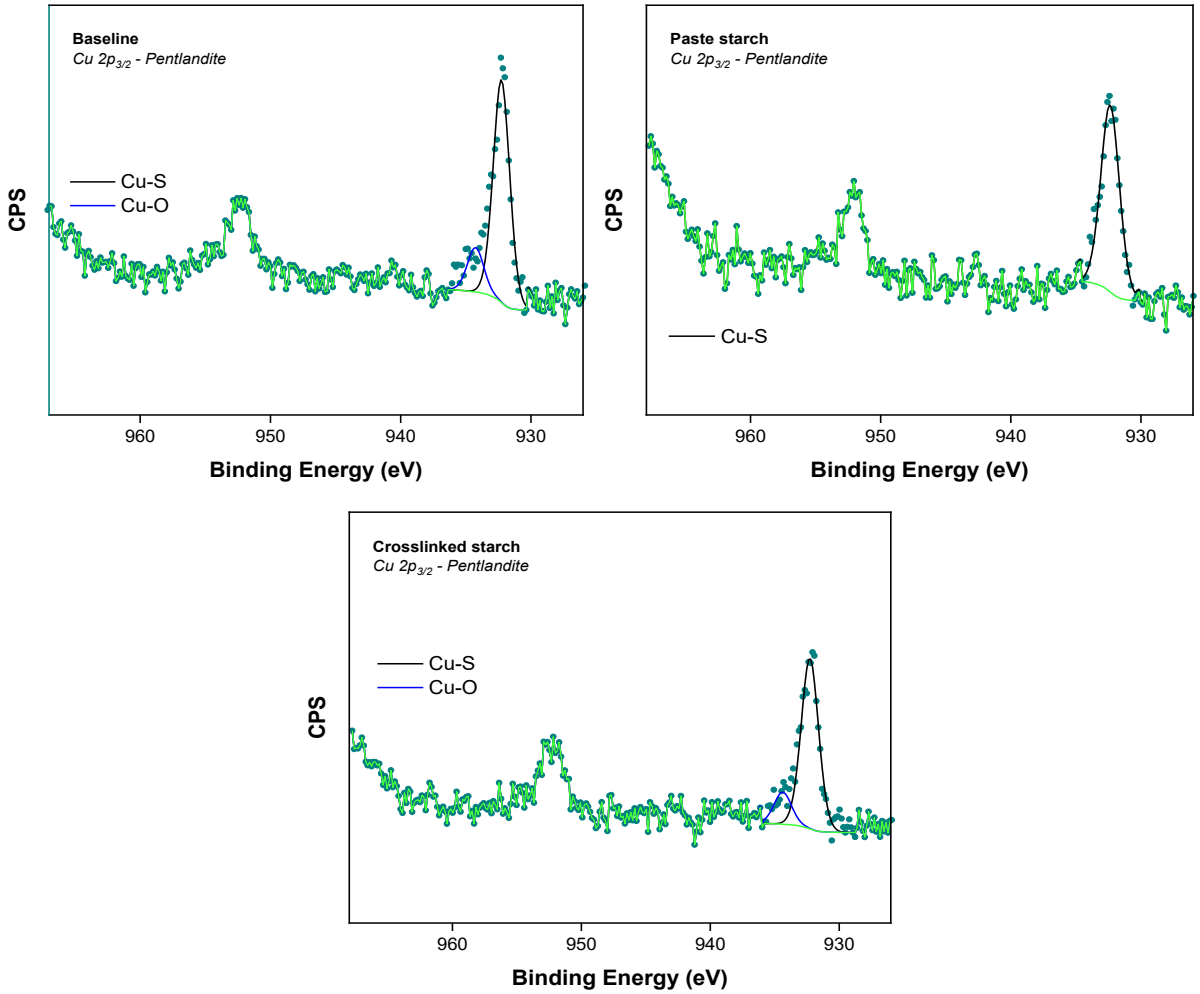

Figure 82: Cu $2p_{3/2}$ spectra comparison between baseline, paste starch, and crosslinked starch interactions with pentlandite surface.

Table 16: Residual standard deviation (STD) obtained after fitting the pentlandite data using a Shirley background.

Spectrum		STD		STD		STD
C 1s	**Baseline**	0.82	**Paste starch**	1.25	**Crosslinked starch**	1.19
O 1s		0.82		0.63		0.83
Fe $2p_{3/2}$		0.97		0.73		0.77
Ni $2p_{3/2}$		0.74		0.83		1.15
Cu $2p_{3/2}$		1.26		0.87		0.87